CONDITION ASSESSMENT OF WATER IN HIGH VISCOSITY INSULATING CABLE TERMINATION OIL

Master of Science Thesis

Done in collaboration with Prysmian Cables and Systems B.V.

Supervised by Dr. Armando Rodrigo Mor

NOVEMBER 25, 2016

JOEL YEO WEI WEN, 4393120

Faculty of Electrical Engineering, Mathematics and Computer Science

Delft University of Technology

THESIS

submitted in partial fulfilment of the

requirements for the degree of

MASTER OF SCIENCE

in

ELECTRICAL ENGINEERING

by

Joel Yeo Wei Wen, B.Eng (1st Class Honours)

The thesis is under embargo

Thesis Committee

Dr.ir. Henk Polinder	TU Delft, chair
Dr.Dipl.-Ing Marjan Popov	TU Delft, external member
Dr. Armando Rodrigo Mor	TU Delft, thesis supervisor

Acknowledgements

I would like to express my deepest gratitude to my daily postdoc, HuiFei Jin, for her valuable insights, support and patience during the work for the thesis. Her guidance has been invaluable for the completion of this thesis, especially when I broke my hand mid-way and had difficulties performing certain physical experiments.

I would also like to thank Armando Rodrigo Mor, for his supervision and reviewing of my work. I would like to thank Henk Polinder and Marjan Popov for taking part in the thesis defense committee.

Finally, I would like to thank my family for supporting me throughout my studies and their encouragement. There is a special thanks to Ulrike for always believing in me, we are going to make a gym now.

Psalm 23:4

Amen.

Abstract

Oil-filled terminations for high voltage XLPE insulated cables have been used for four decades in the Netherlands with a good service record. Prysmian would like to gain better insight into the effects of water contamination in insulating oil, to further extend the in-house experience and potential related failure mechanisms.

High voltage termination is contained within a bushing that is filled with insulating cable oil. The insulating cable oil is a containment medium for the electric field lines and should have low dielectric losses, chemical inertness against the construction material, non-flammability and stable electrical property during prolong heating. The insulating oil is also self-healing, leaving no permanent conductive path in the fluid. The containment should be well-sealed to prevent any forms of leakage from the surroundings.

The initial stages of the thesis seeks to inventory and address a few topics, mainly regarding water polluting oil. Studies will be done into the phenomena surrounding water within oil, the influence of water particles on the electrical performance of the oil, movement of water within the termination during temperature gradients and movement of water within the termination during electrical gradients.

The next step is to inventory the current on-line and off-line tools available for measurements of water contents in oil. They would be AC voltage breakdown test, dielectric loss measurement, partial discharge detection, permittivity measurement and humidity check.

Finally, the last phase would look to find mitigation techniques integrating the given inventories and observations, so as to formulate non-intrusive diagnostic methods to ascertain polluted terminations.

Table of Contents

Table of Figures

Table of Tables

1 Introduction

Oil-filled terminations for high voltage XLPE insulated cables have been used for four decades in the Netherlands with a good service record. Prysmian would like to gain better insight into the effects of water contamination in insulating oil, to further extend the in-house experience and potential related failure mechanisms.

1.1 Background Consideration

Prysmian Group is the world leader in energy and telecommunication cable systems industry. It has 140 years of experience, with approximately 19,000 employees across 55 countries. It has operations in underground and submarine cables, along with systems for power transmission and distribution.

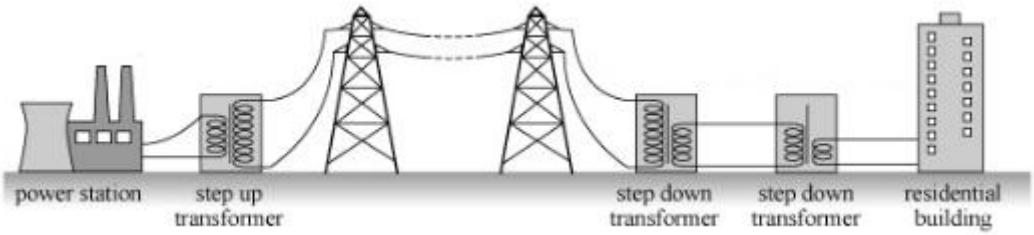

Figure 1: Classic Electrical System

As shown in Fig. 1, high voltage cable is a cable used for electrical transmissions at an elevated potential difference, it basically contains a conductor and may contain insulations. The high voltage cable is the transmission link between generation and distribution.

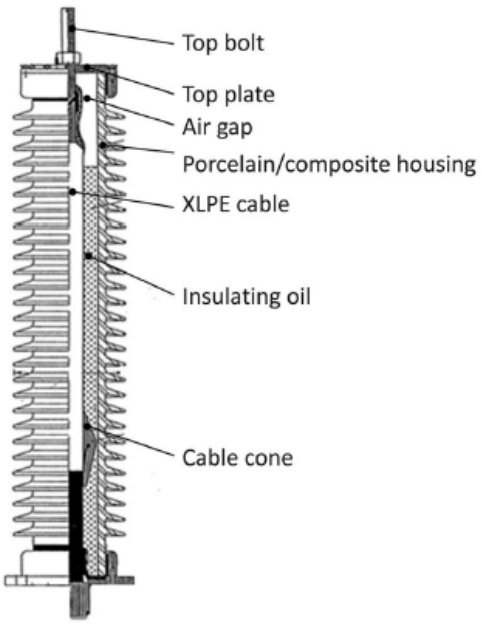

Figure 2: The anatomy of a cable termination

As shown in Fig. 2, connection from the high voltage cable is made with a cable termination. The purpose of such a setup is to reduce the field enhancement when connection is made to the conductor.

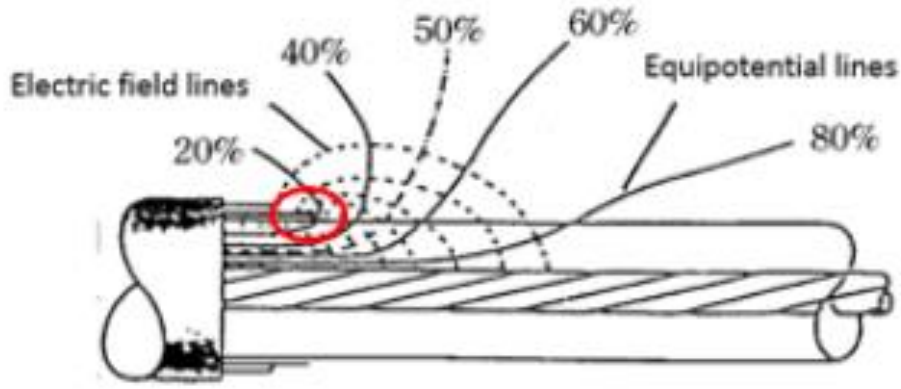

Figure 3: Sudden removal of earth shield, causing field concentration [1]

As shown in Fig. 3, the electric field lines concentrates at the end of the earth conductor (in red), when it is abruptly removed. Such a behaviour is undesirable and will lead to a breakdown.

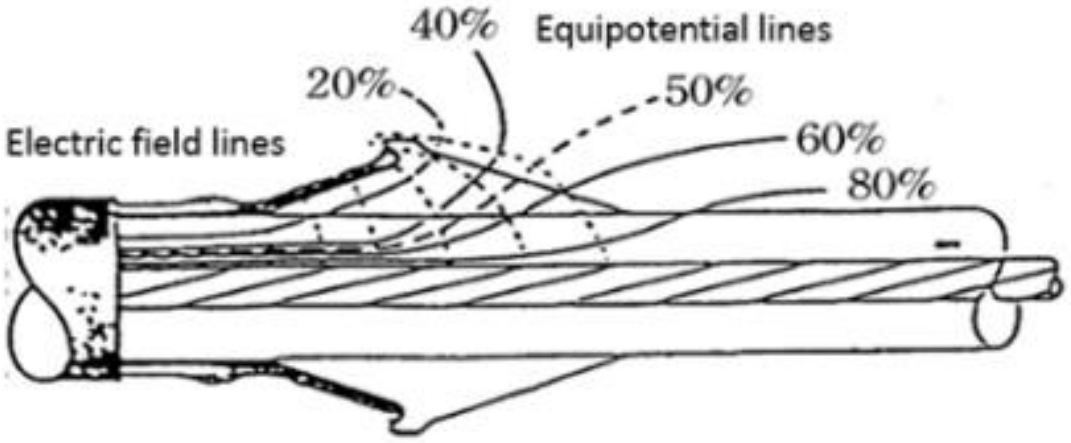

Figure 4: Stress cone placed to prevent field concentration [1]

To smoothen out and control the field lines, a stress cone is place on the termination as shown in Fig. 4. In the stress cone the field between high voltage conductor and earth screen is gradually decreased. However, in doing so, a tangential field might arise between the rubber and cable insulation interface. Mechanical pressure is applied to prevent formation of air pockets, and is applied in a form of stretching the rubber core, the original bore of the core being smaller than the cable diameter.

Figure 5: Transition joint [2]

As shown in Fig. 5, the high voltage termination is contained within a bushing that is filled with insulating cable oil. The insulating cable oil is a containment medium for the electric field lines and should have low dielectric losses, chemical inertness against the construction material, non-flammability and stable electrical property during prolong heating [3]. The insulating oil is also self-healing, leaving no permanent conductive path in the fluid. The containment should be well-sealed to prevent any forms of leakage from the surroundings [4].

Before placement into the termination, insulating oil is heated up to reduce the viscosity. The oil is then poured in and the termination is sealed to prevent unwanted introduction of moisture. Such sealing must be secure and strong as a vacuum-like effect is seen when the hot oil decreases in temperature. Faulty seals will lead to presence of undesired air and water.

1.1.1 Technology Overview on Water Content in Cable Termination

Water content in cable oil are measured either in parts per million (ppm) or percentages, when in high magnitudes, with the acceptable limit for dry oil at 20 to 30 ppm. Measurements of such precisions depend greatly on stable conditions and laboratory environments.

Water can be found in oil in three forms: dissolved state, tiny droplets mixed in oil (emulsion) and free water at the base. Coalescence occurs when small droplets add up to form bigger droplets, and could be found at the base of the container, if sufficiently heavy. Moisture content is undesired due to its inherent high permittivity, which leads to field concentration and enhancement [5].

It should be interesting to note that while dissolved water, compared to tiny droplets, does not pose as much danger to the dielectric strength of the oil, high temperature dissolved water is the coalescence cause of tiny droplets when cooled. Tiny droplets affects the dielectric strength more because a larger volume has more polarising force acting on it, and also has a lower critical breakdown strength, as shown in Eq. 3 and Eq. 5 later in the chapter.

1.1.2 Force Presented to Water Droplets in Oil under Electric Field

Prediction of electrically induced coalescence or emulsion is an arduous process due to the complexity involved [6]. Modelling of such an activity is effortful because the dynamic nature of the movement often results in an incomplete inclusion [7].

When calculating the electric field acting upon the water droplets, each droplet is usually considered as point dipoles oriented in the direction of the applied field [8]. However such simplification does not allow for multipolar interaction between droplets, which causes inaccuracies [9].

Different forces acts upon a water droplet in a fluid when exposed to an external electric field [10]. Considering a droplet of water on a base of a container under the presence of a non-uniform electric field, there is the inherent gravity force, $F_{gravity}$, pushing the droplet down, and the electric field force, $F_{electric}$, moving the droplet. When the droplet is moving, a force, F_{fluid}, creates an equilibrium and oppose the movement. As shown in Eq. 1, the summation of these three basic forces is, from Newton's second law, the acceleration of the water droplet,

$$m\,\frac{dv}{dt} = F_{gravity} + F_{electric} + F_{fluid} \quad (1)$$

where m is the mass of the droplet, v is the velocity vector of the droplet.

As shown in Eq. 2 the gravity force on a water droplet in oil is given by,

$$F_{gravity} = V(\rho_{water} - \rho_{oil})g \quad (2)$$

Where V is the volume of the droplet, g is the gravitational acceleration, ρ_{water} and ρ_{oil} are the densities of water and oil respectively.

As shown in Eq. 3, the force acting on a particle polarised by an inhomogeneous field is given by [1],

$$F = \frac{\varepsilon_0}{2} V \frac{\varepsilon_1 - \varepsilon_2}{\varepsilon_1 + \varepsilon_2} \cdot \nabla E^2 \quad (3)$$

where V is the volume of the droplet, ε_0 is the vacuum permittivity, ε_1 is the permittivity of the droplet, ε_2 is the permittivity of the oil and E is the local field strength.

As shown in Eq. 4, the friction and drag force due to movement is given by,

$$F_{drag} = -\frac{1}{2}\rho_{oil} C_d A |v| v \quad (4)$$

where C_d is the drag coefficient, A is the representative area of the droplet and v is velocity vector of the droplet.

Other than the given factors above as mentioned from [11], there are still other considerations that were not used such as, but not limited to,

1) Resonance oscillation under electric field
2) Movement inertia
3) Elongation of droplet
4) Deformation through elongation
5) Change of surrounding E-field when droplet changes shape
6) Change of surrounding E-field when droplet has partial discharge

As shown from the additional listed points, comprehensive modelling is not possible as all the parameters are intrinsically-linked and not fully defined. Quasi-static consideration is sufficient in this study as it provides ample information and understanding.

1.1.3 Instability of Water Droplets in Oil under Electric Field

An electric field will elongate a water droplet due to the electric stress on its surface, and beyond a critical field strength, the water droplet will disintegrate at the ends into smaller droplets.

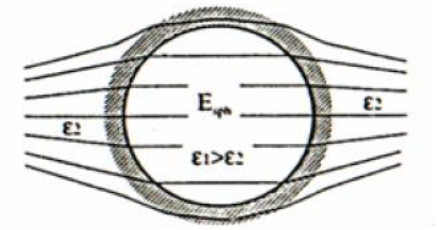

Figure 6: Distortion of field lines with the presence of sphere [1]

As shown in Fig. 6, in the presence of homogeneous field lines, inclusion of a sphere with permittivity higher than the surroundings causes the field lines to wrap around the sphere. It can be seen from the shape of the field line that a water droplet will be compressed and elongated, taking on the shape of the field lines.

The field strength, E_{sph}, in the dielectric next to the spherical inclusion is as given [1],

$$E_{sph} = \frac{3\varepsilon_1}{\varepsilon_1+\varepsilon_2}E \qquad (4)$$

where ε_1 is the permittivity of the droplet, ε_2 is the permittivity of the oil and E is the local field strength. It can be seen that if the permittivity of the droplet tends to infinity, E_{sph} becomes 3 times as large as the average field strength, similar to a metal sphere.

Without the presence of an electric field, the surface tension γ will keep the water droplet spherical with radius α. When uniform electric field is applied, the droplet will deform from the stress on its surface and elongate in the direction of the field. E_{crit} is the critical field value obtained from the electric field before deformation and is given in Eq. 5 by [9] as,

$$E_{crit} = 0.64\sqrt{\frac{\gamma}{2\varepsilon_2\alpha}} \qquad (5).$$

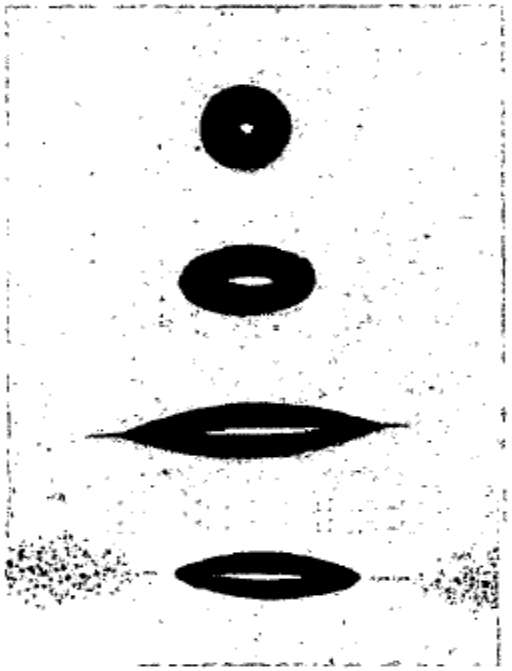

Figure 7: From top to bottom, spherical droplet undergoing elongation and degradation at the tips due to electrical stress [9]

Beyond the critical value from Eq. 5, the droplet becomes unstable at the tips and degradation occurs as shown in Fig. 7. The droplets ejected during this instability may carry charges due to polarisation of the original droplet. This model is valid for DC and frequencies below 100 Hz.

1.1.4 Short Introduction on Water Movement in Operating Termination

As mentioned previously, when seal of a termination is faulty, unwanted water is able to seep into the termination leading to contamination. As shown in Fig. 8, when a droplet of water sinks from the top, it has two basic visible motions – gravitational and electrical attraction.

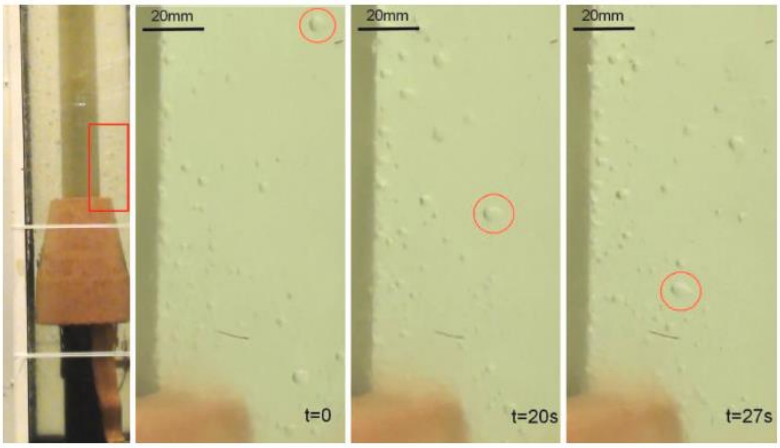

Figure 8: Water droplet with diameter of 3.3 mm moving through oil from left to right, downward attraction by gravity, leftward attraction by electric field [12]

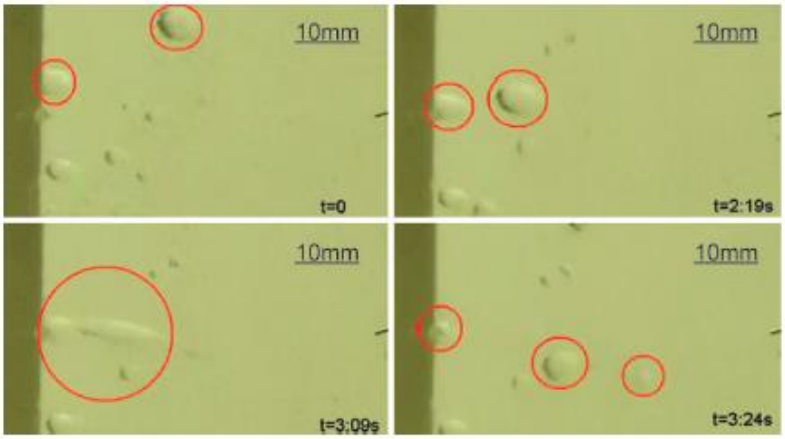

Figure 9: Two water droplets being attracted and coalesce, elongated and dispersed into three smaller droplets [12]

As shown in Fig. 9, electrical coalesce happens due to attraction forces between two charged droplets, and electrical emulsion occurs after elongation and degradation. This corresponds with Eq. 5, with the critical field strength needed for deformation lowered when the radius of the water droplet increased.

The continued action of coalesce and emulsion results in a collection of fine water content around regions of higher field strength. This is due to the tiny water droplets being charged and would naturally congregated to the origin of the electric field.

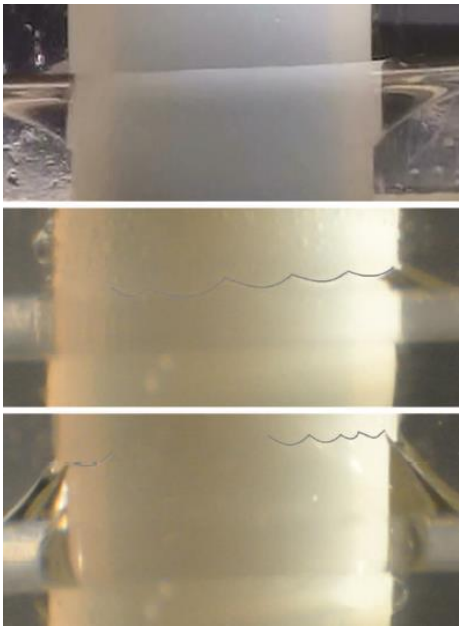

Figure 10: From top to bottom, 0 kV/mm, 1.27 kV/mm, 3.17 kV/mm [13]

As shown in Fig. 10, with the presence of accumulated water content at areas containing electric fields, tapering of the water occurs with increased field strength. The tapering of the water ripple is of concern due to further field enhancements.

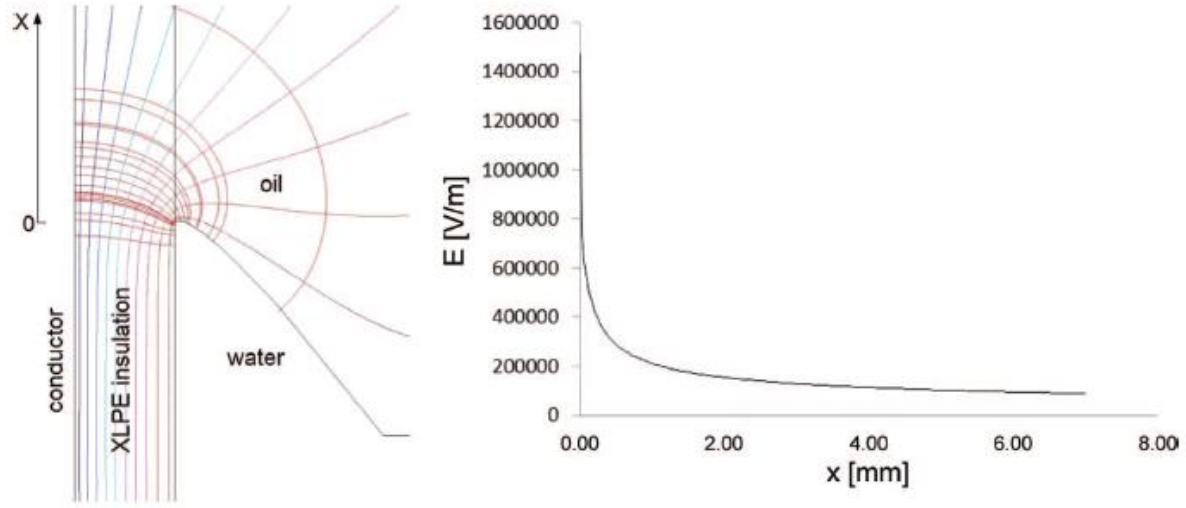

Figure 11: Electric field simulation (left), Corresponding field strength for 1 kV (right) [13]

As shown in Fig. 11, with a simulated ripple, it can be seen that the tip is a sharp point which causes unwanted field enhancements. This enhancements leads to eventual degradation at the tip, causing finer water droplets to be dispersed.

1.2 Thesis Goals

Primarily, the goal of this research is to investigate the influence of water content on the electrical properties of the insulating fluid. The secondary objective is to effectively detect water with the established diagnostic tools.

1.3 Thesis Objective

The initial stages of the thesis seeks to inventory and address a few topics, mainly regarding water polluting oil. Studies will be done into the phenomena surrounding water within oil, the influence of water particles on the electrical performance of the oil, movement of water within the termination during temperature gradients and movement of water within the termination during electrical gradients.

The next step is to inventory the current on-line and off-line tools available for measurements of water contents in oil. They would be AC voltage breakdown test, dielectric loss measurement, partial discharge detection, permittivity measurement and humidity check.

Finally, the last phase would look to find mitigation techniques integrating the given inventories and observations, so as to formulate non-intrusive diagnostic methods to ascertain polluted terminations.

1.4 Thesis Approach

In order to study the interactions between cable oil and pollutant water, methods of introducing moisture have to be formulated and verified to be true. Three types of methods were considered – 1) usage of climate chamber, which simulated external moisture content diffusion over time 2) emulsion

of water droplets through heat and ultrasonic treatment, which simulated temperature gradients and vibrations that the termination might be exposed to over time 3) amounts of free water, which simulated entries of unexpected water content.

After introduction of moisture content, observation of the mutual interaction is performed. This allows an insight into the behaviour, and guides decisions on future experiments. The humidity test is performed in tandem with permittivity, tan delta and breakdown test as all four information is required for accurate and complete portrayal of the characteristics. Prediction of partial discharge is made from initial characterisation, and results are ascertained after experimentation.

Having a better understanding of the interaction and identified the responses, relation between individual results are conducted to formulate a conclusion. The methods proposed are supported by academic and simulation results. The conclusion will endeavour to produce the goal of non-intrusive diagnostic methods.

1.5 Thesis Outline

The present thesis is organised in six chapters. Chapter 1 presents an overview of the current technological state along with the evolution of the system components. Chapter 2 begins the analysis on behaviour between oil and water with heat and electrical influence. It characterises the mutual interaction, which aims to detail the interplay between the two components.

Chapter 3 and 4 characterises the influence of water within oil and aims to describe the extent of effect water has when found in oil. Chapter 5 further analyses the effect through partial discharge test and verifies the result on an actual setup.

Chapter 6 marks the close of the thesis, with formulation of a non-intrusive diagnostic method, conclusion and future works.

2 Behaviour of Water Movement in Oil

Before any form of experiment could be performed, it was necessary to understand the characteristic of the given material.

2.1 Temperature Influence

The oil was considerably viscous at 40°C, with rated value of 7200 cSt, and was 230 cSt at 100°C. The viscosity was considered to be higher than 7200 cSt at room temperature. Tests aimed to get an insight into the reaction when moisture content of various sizes were introduced at room and high temperature.

2.1.1 Various Parameters Involved

Various interchangeable parameters involved were,

1) Large droplets of water from a syringe
2) Small droplets of water from a spray
3) Fine droplets (invisible to the eye) from the climate chamber
4) Oil at room temperature
5) Oil at slightly elevated temperature
6) Oil at elevated temperature

These various permutations were considered because,

1) Accidental leakage from sealed tank
2) Seepage of water over time
3) Diffusion with surroundings
4) Cooled conditions
5) Heat generated from cable carrying load current
6) Heat from conduction and convection

Figure 12: Moisture content after 2 hours in climate chamber at 60% and 75C

Due the high viscosity of the oil at room temperature, when small droplets of water (diameter < 2 mm) from a syringe was added to the oil, it sunk at an extremely slow pace, almost remaining on the surface at times. Droplets of water that were larger (7 mm < diameter < 10 mm) gradually went down, with the rate of descend relative to the volume. The climate chamber was used as shown in Fig. 12. It can be seen that the infiltration of smaller moisture content was slow at room temperature.

2.1.2 Heating Phenomena

A phenomenon was observed during the change in temperature, when the oil sample had been polluted by moisture content that was dispersed internally.

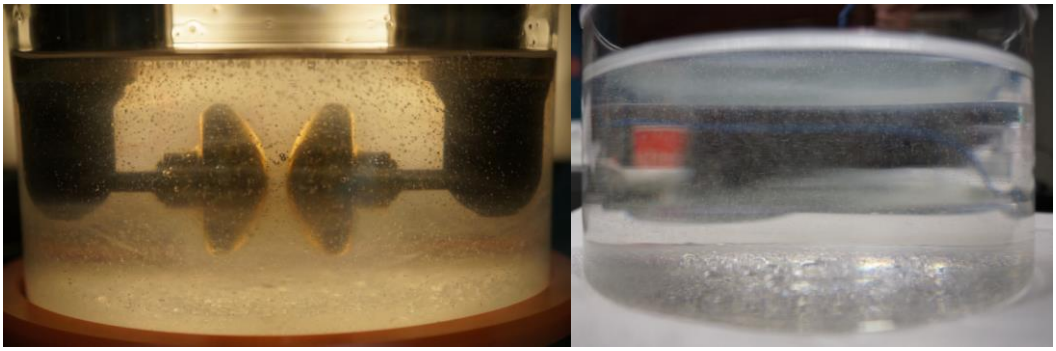

Figure 13: Approximately 120 ppm of dispersed water, Room temperature (left), 60^{o}C (right)

As shown in Fig. 13 on the left, the dispersed water was more evident at lower temperatures, and lesser at high temperatures on the right of Fig. 13. The reason for such a behaviour was due to the intrinsic link between heated water and oil viscosity.

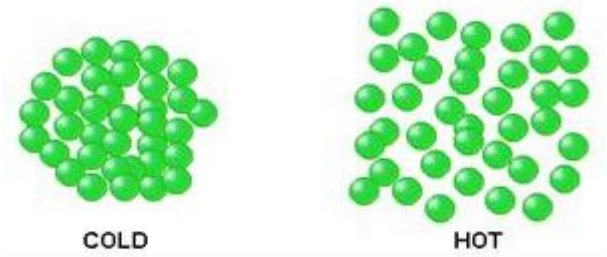

Figure 14: Liquid molecules at different temperatures [14]

During the heating of the sample, the dispersed water gains energy which causes the atoms and molecules to vibrate. The space between atoms are increased, which causes an expansion of the substance as shown in Fig. 14; the mass is not changed. The converse holds true, with contraction of the substance when cooled, due to a reduction in vibration.

The lowered viscosity meant increased mobility, and when coupled with the more active water molecules resulted in emulsion of moisture content that was previously visible to the human eye.

Similarly, when the temperature is reduced, contraction of the substance coupled with increased viscosity caused the coalescence of water droplets.

It is well-known that lower breakdown strength occurs in liquids with higher temperature due to low viscosity [1]. However, it can be said that at lower temperature for the given sample, lower breakdown strength will happen due to the presence of immobile pollutants from high viscosity.

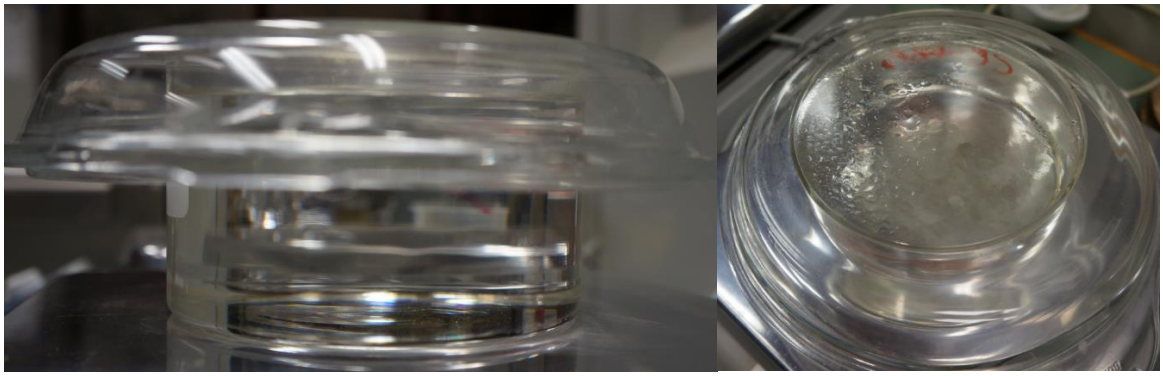

Figure 15: Oil heated up at 100ºC for 10 hours, Side view (left), Top view (right)

As shown in Fig. 15, an oil sample polluted with approximately 2 ml of dispersed water was heated up for 10 hours at 100ºC. No visible moisture content was found in the oil sample as shown on the left, and could be seen captured on the top of the plate as shown on the right. It is known that water droplets are more dense than oil which causes it to sink, but when heated are less dense than oil which causes it to rise – this behaviour is evident in Fig. 15.

Density is given as follows,

$$\text{Density} = \frac{\text{Mass}}{\text{Volume}} \qquad (6).$$

It can be seen from Eq. 6 that the density is inversely related to the volume. Taking into consideration a water of a given amount, when it is heated up, the molecules are excited with energy and expand – the volume increases. As mentioned previously, the mass will not change despite the expansion of volume. This leads to a reduction in density. Therefore, as shown in Fig. 15, when the sample is brought to elevated temperatures for a prolonged duration, this will cause the water to move upwards and eventually leave the oil.

2.2 Behaviour of Water Movement in Oil under Electrical Influence

The behaviour of water in oil had been studied in detail from [12]. Full and comprehensive modelling of such deceptively simple interaction is not possible due to the dynamic relationship [15]. Basic study will be conducted with observation of a single water droplet for simplicity. The forces faced by the water droplet are [16], but not limited to,

- Resonance oscillation under electric field present
- Drag/drift force from the medium
- Surface tension
- Inertia
- Gravity
- Elongation of droplet
- Deformation through elongation
- Change of surrounding electric field shape when droplet changes shape
- Change of surrounding electric field shape when droplet emits partial discharge

As evident from the list above, there are numerous forces acting on the water droplet under the presence of an electric field. These forces not mutually exclusive, but will cause an intertwined reaction [17]. For instance, under the presence of a homogenous electric field, a droplet will be polarised and attracted. During this attraction process, it will also elongate. However, elongation creates a non-rounded shape which causes field enhancements. As evident, the relationship is intrinsically connected [13].

To better understand the electrical relationship with a simple water droplet, a cable with similar material properties and field strength was used in COMSOL simulation and later, experiments. The purpose is to first obtain knowledge through simulating and verifying via experiments that the results of the simplifications were suitable. Further simulations are then performed on COMSOL with the same water droplet when placed in an actual termination setup and field strength. This further solidifies the effects faced by a water droplet and the results of the previous efforts. The water droplet is lastly increased in size in the termination simulation to demonstrate the effects of larger water droplets. Naturally, simplification of the forces seen by a water droplet is done.

First, knowledge of the highest field strength seen on the surface of the stress cone is obtained through COMSOL simulations of the actual termination when operating voltage is applied. Next, the same field strength is achieved on the cable in COMSOL simulations with a water droplet of 0.1 ml used and placed at a distance of 15 mm apart. An arbitrary 15 mm was chosen as it provided an assumed reasonable experimental distance from the tip of the water droplet to the cable. Simplified polarisation and critical field strength calculations are made to ascertain the simulation results. Finally, physical experiments are made to verify the results from the calculations.

2.2.1 Simplification of Forces Acting on a Water Droplet

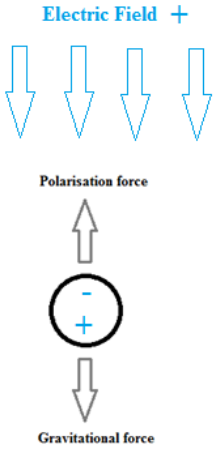

Figure 16: Simplified consideration of forces on a water droplet

Eq. 3 from the previous chapter gives the polarisation force in an inhomogeneous field. As described previously and shown in Fig. 16, for simplification purposes, consideration of forces only from the electric field and gravity will be made for the following calculations. The purpose is to ascertain if the polarisation force at a distance of 15 mm is greater than the gravitational force and will therefore attract the water droplet of 0.1 ml to areas of higher field strength, which is potentially dangerous.

2.2.2 Electric Field Plots of 70 kV Medium Voltage Cable Termination

Figure 17: Stress cone of a cable termination

As shown in Fig. 17, the stress cone smoothens the electric field lines and reduces the field enhancements faced. The simulation field plots for an applied voltage of 70 kV are as given below.

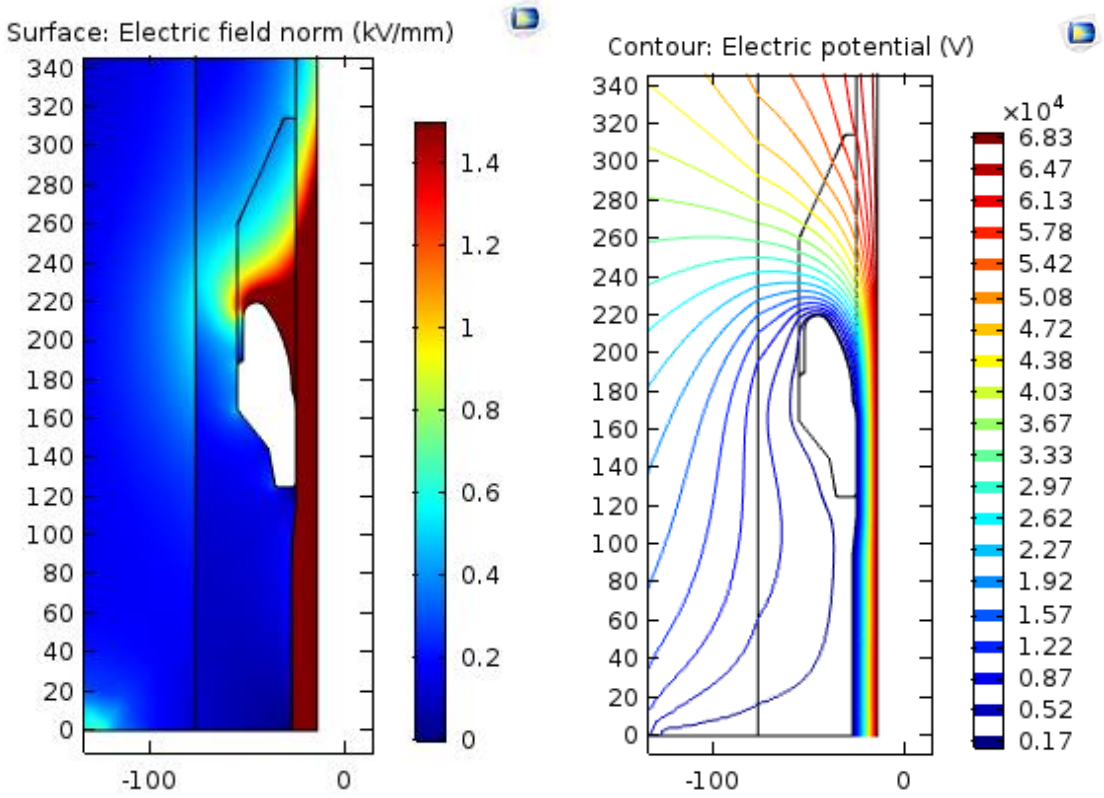

Figure 18: Electric field plot of MV cable (left), Equipotential lines of MV cable (right)

As shown on Fig. 18, the area around the stress cone had a maximum field strength of 1.4 kV/mm, and additional unwanted enhancement at the side of the termination tank.

2.2.3 Electric Field Plots of Forces Acting on a Water Droplet

The electric field plots from COMSOL provided the necessary field strength and gradient required for Eq. 3. It also provided insight into the enhancement magnitude faced by the droplet.

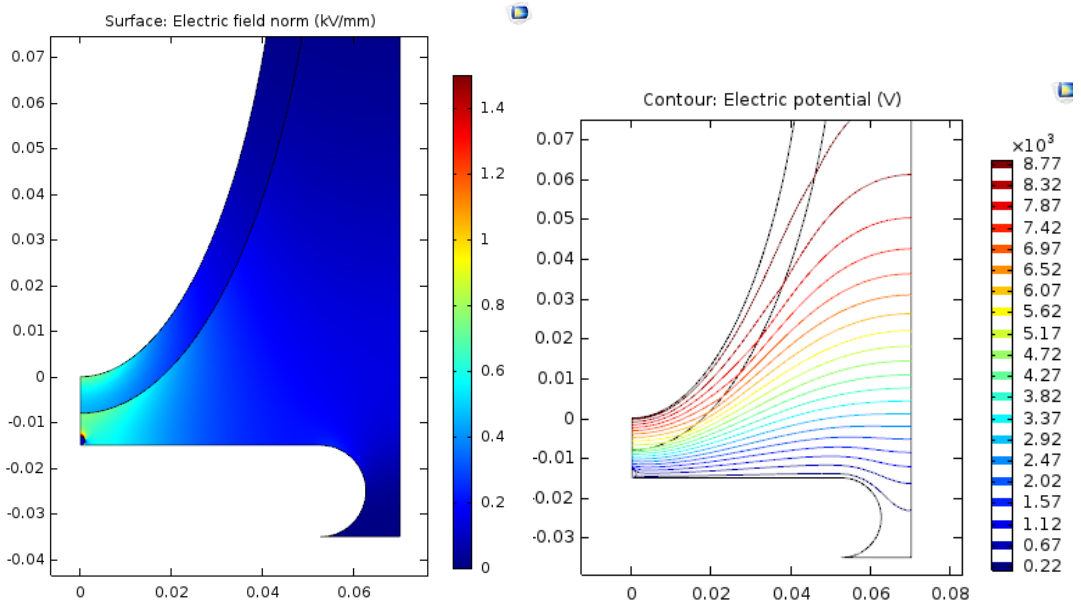

Figure 19: Cable and 0.1 ml water droplet, Electric field plot (Left), Equipotential lines (Right)

As shown in Fig. 19, consideration was made with a piece of cable of polyethylene surface. It can be seen that there was a field strength of 1.4 kV/mm, for an applied voltage of 15 kV, which is approximately similar to the field strength at the cable terminations used.

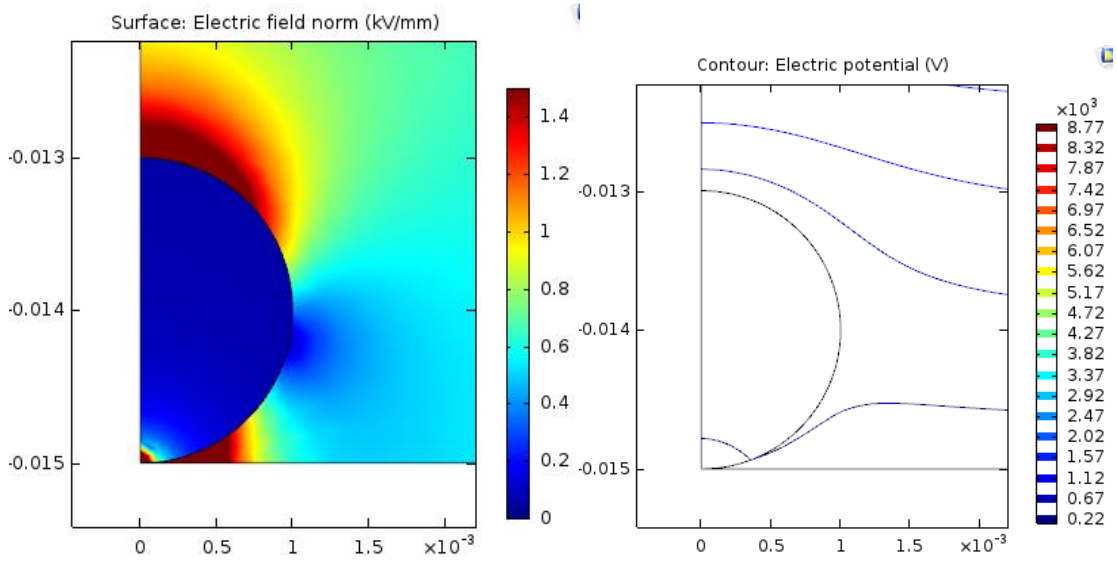

Figure 20: Field plot of water droplet (Left), Equipotential lines of water droplet (Right)

As shown in Fig. 20, water droplet of 0.1 ml was considered and placed directly under the piece of cable. It can be seen that there was a field enhancement at the top of the droplet with the same highest strength as the cable. There is a gap distance of 15 mm between the cable and the water droplet.

2.2.4 Simplified Calculation of Forces Acting on a Water Droplet

$$F = \frac{\varepsilon_0}{2} V \frac{\varepsilon_1 - \varepsilon_2}{\varepsilon_1 + \varepsilon_2} \cdot \nabla E^2 \qquad (3)$$

With the following considerations made,

$\varepsilon_0 = 8.854 \times 10^{-12}$ F/m
$\varepsilon_1 = 88 \times \varepsilon_0$ F/m
$\varepsilon_2 = 2.4 \times \varepsilon_0$ F/m
$V = 1 \times 10^{-7}$ m^3
$\nabla = 1400 \times 10^6$
$E = 1400 \times 10^6$ V/m

Placing the necessary values into Eq. 3 yields an upward acceleration of 1.15 m/s^2 and it can be seen to be lesser than the downward gravitation force of 9.81 m/s^2. For basic considerations, if a water droplet of 1 ml is 15 mm from a field strength similar to Fig. 18, it will be polarised but the complete droplet would not attracted upwards as the force is not sufficient.

Under similar conditions, the water droplet is also exposed to elongation and deformation if the electric field is greater than the critical field strength from Eq. 2.

$$E_{crit} = 0.64 \sqrt{\frac{\gamma}{2\varepsilon_2 \alpha}} \qquad (5)$$

With the following considerations made,

$\gamma = 50 \times 10^{-3}$ N/m

$\varepsilon = 2.4 \times \varepsilon_0$ F/m
$\alpha = 2.879 \times 10^{-3}$ m

Placing the necessary values into Eq. 5 yields a critical electric field strength of 409 V/mm.

It can be seen that when 0.1 ml, or 1×10^{-7} m^3, water droplet was exposed to an electric field with maximum field strength and enhancement strength of 1.4 kV/mm, that attraction force was not sufficient to pull the droplet up, but was fully capable of exceeding the critical field strength needed to deform the droplet.

2.2.5 Application of Electric Field on a Water Droplet

The cable of polyethylene surface was used, with an applied voltage of 15 kV, which gave a maximum field strength of 1.4 kV/mm as shown in the simulations. As mentioned before, such material was selected as it gave the best replication of actual conditions.

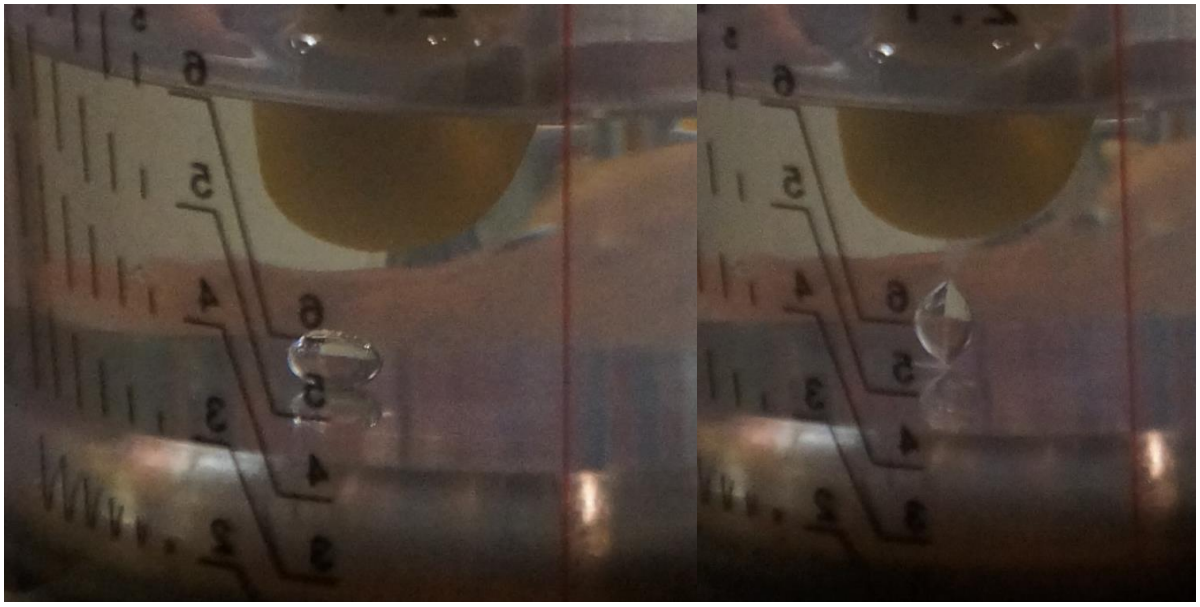

Figure 21: Water droplet under surface tension, no electric field (left), Water droplet elongated due to electric field (right)

As shown in the left of Fig. 21, a water droplet is kept at a spherical shape by surface tension from the imbalance in cohesive forces of the surface layer. When electrical field is applied as shown on the right of Fig. 21, it was attracted upwards and elongated as calculated before with Eq. 5.

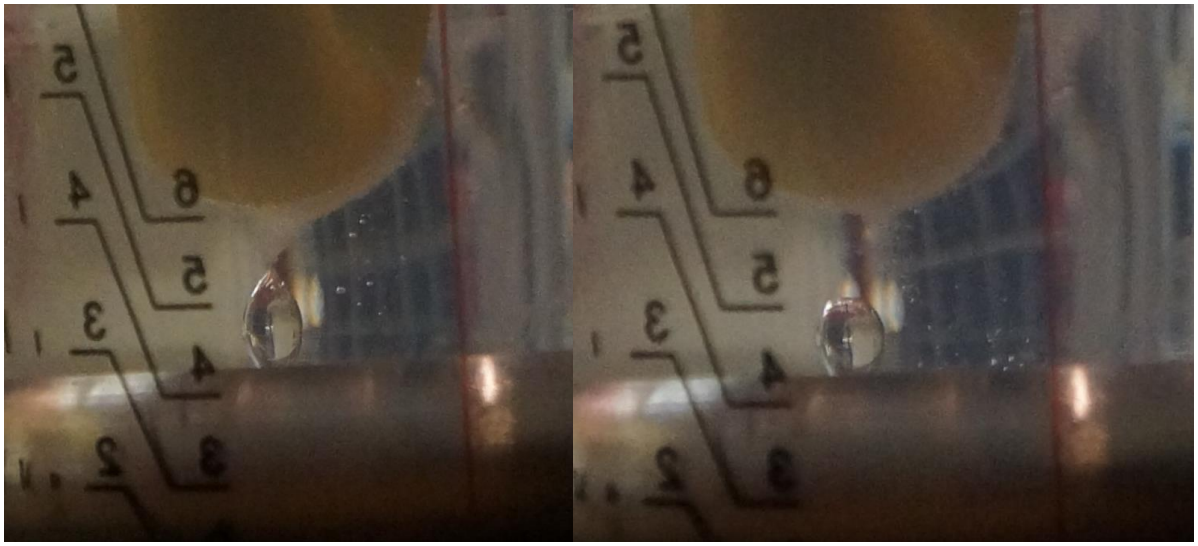

Figure 22: Water droplet elongating and dispersion at the tip (left), Water droplet not elongating (right)

As shown on the left in Fig. 22, the water droplet was elongated and dispersion occurred at the tip of the bubble where there was field enhancements. As shown on the right in Fig. 22, the water droplet faced continual degradation and reduced in volume. As shown in the inverse relation from Eq. 5, with a smaller radius, the critical field strength needed is higher.

Figure 23: Contribution to dispersion water from surrounding smaller droplets (left); Continuation of elongation of water droplet due to dispersed water field enhancement from above (right)

As shown on the left in Fig. 23, there is contribution to the dispersed water from the surroundings water droplets which had coalesced and sunk and then degraded further. As shown on the right in Fig. 23, the dispersed water droplets created additional field enhancement that was able to re-elongate the bubble.

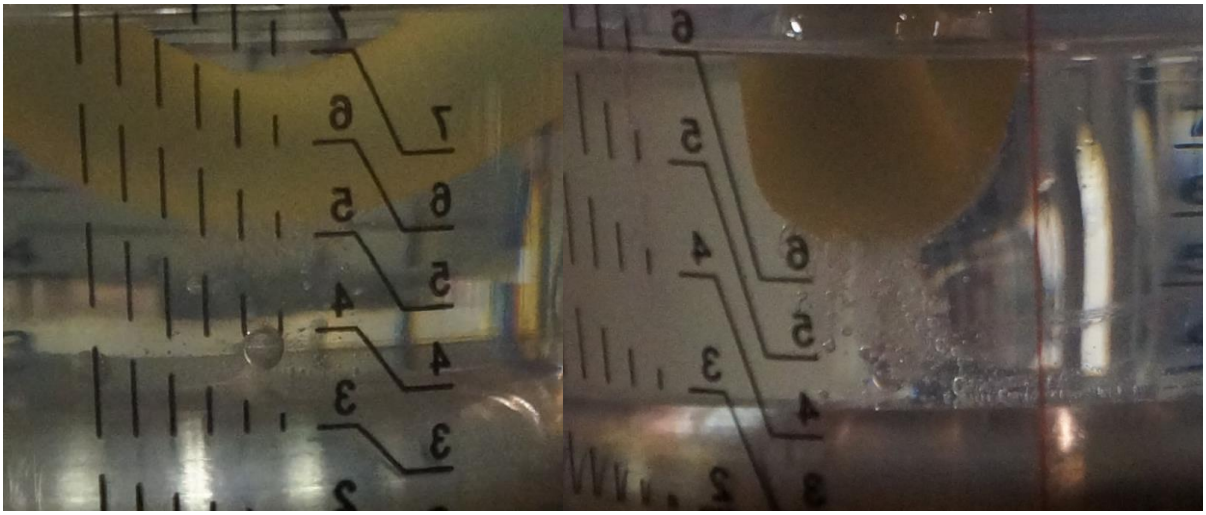

Figure 24: Greater disintegration of droplet (left), Further total disintegration of initial droplet (right)

As shown on the left in Fig. 24, the water droplet further disintegrated after continuous interaction with the increased dispersed water on the top. As shown on the left in Fig. 24, the water droplet degraded completely and was left in small droplets. This activity was expected from the runaway condition faced from elevated field enhancement, contribution to total dispersed water, gradual and continual degradation of water droplets.

2.2.6 Electric Field Plots of a Water Droplet near a Stress Cone

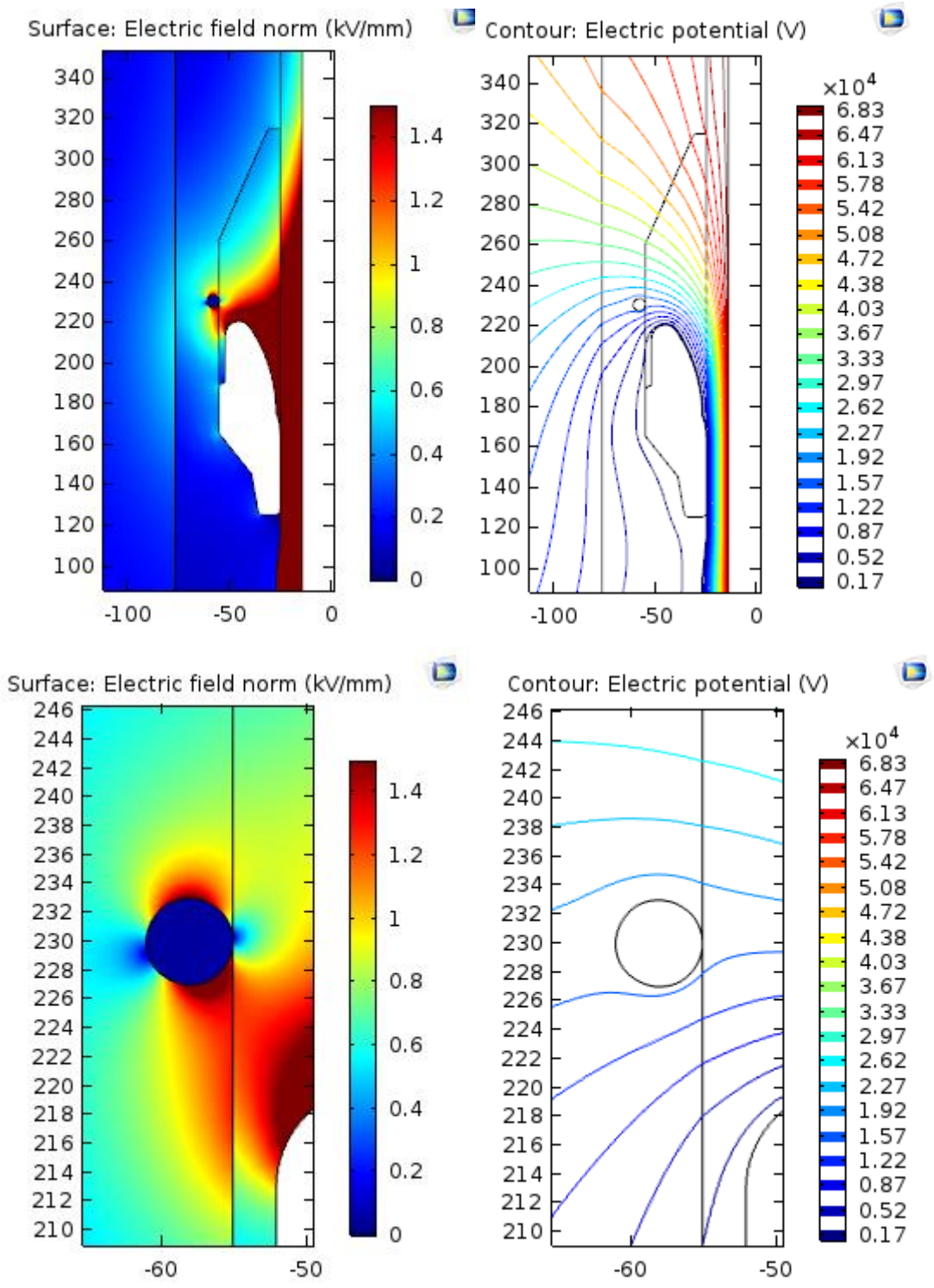

Figure 25: 0.1 ml water droplet attached to stress cone

As shown on Fig. 25, a 0.1 ml conductive water droplet was placed directly beside the stress cone and 70 kV was applied. This caused field enhancements on the water droplet that was equally as large as the highest magnitude seen by the stress cone. Enhancements of this value will cause dispersion and disintegration to the water droplet and possibly attraction around that region.

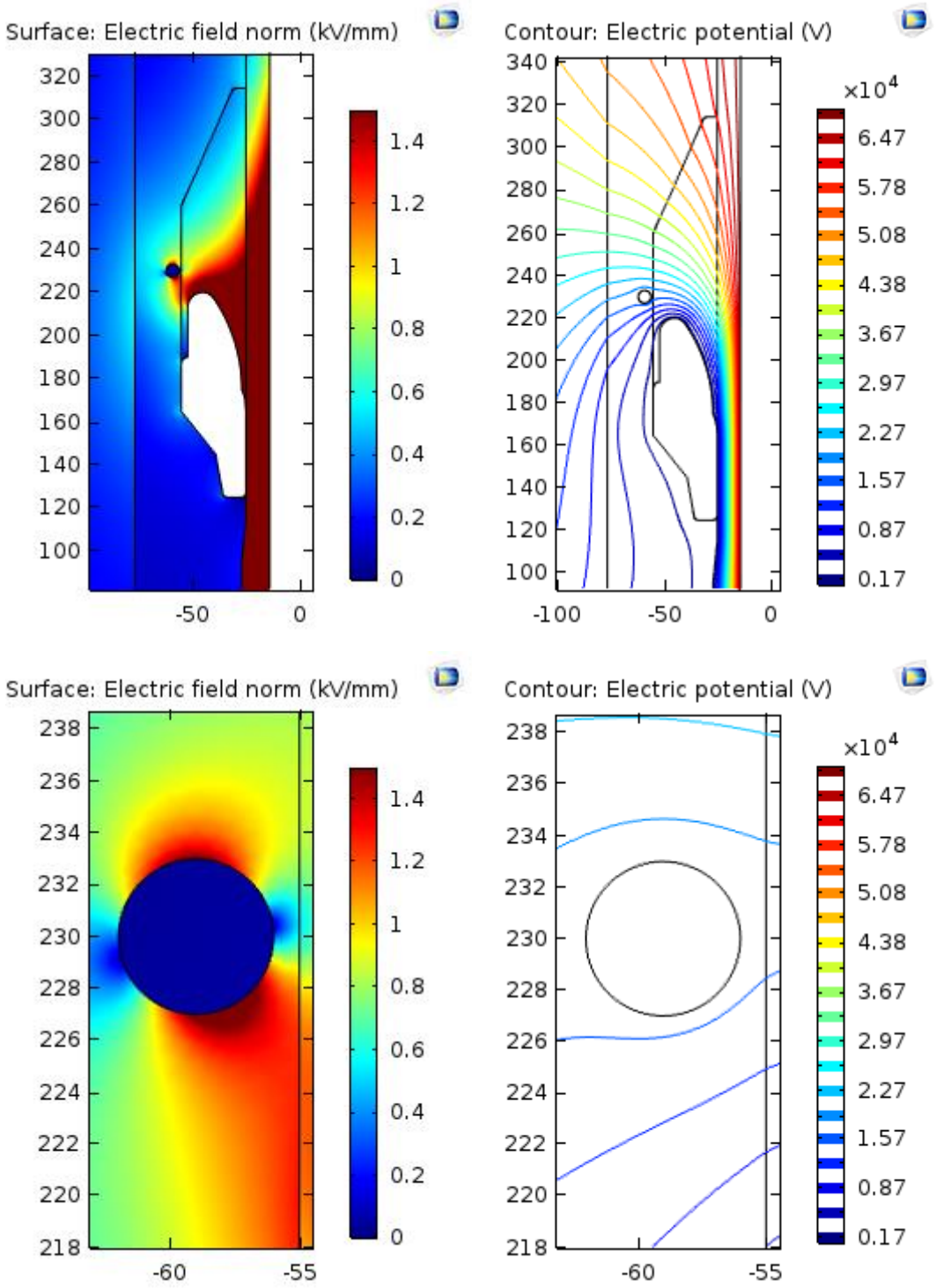

Figure 26: 0.1 ml water droplet 1 mm from the stress cone

As shown in Fig. 26, displacement of 1 mm did not reduce the enhancements faced by the droplet. The droplet was exposed to equally as high magnitude as attached to the surface of the stress cone.

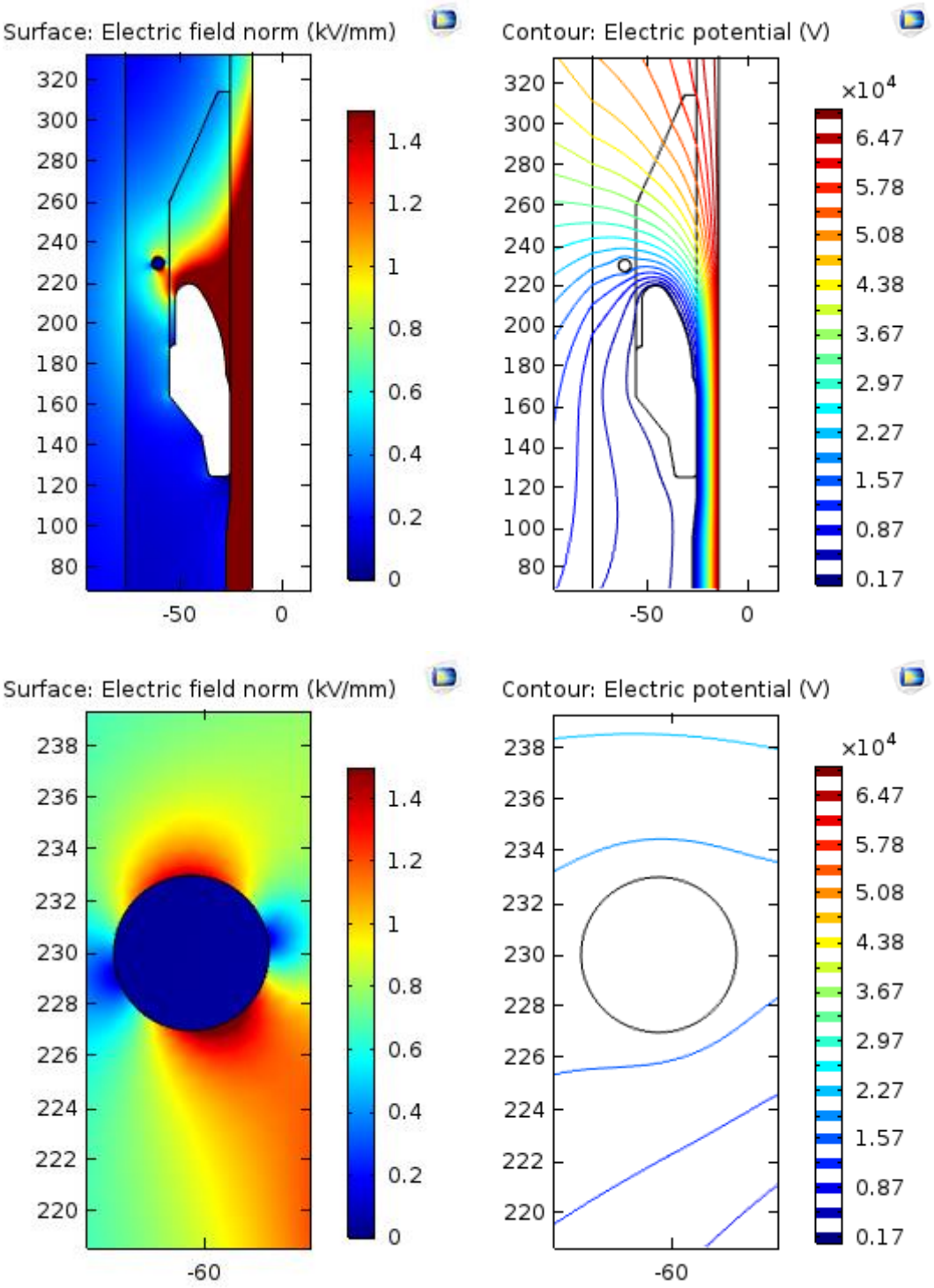

Figure 27: 0.1 ml water droplet 2.5 mm from the stress cone

As shown in Fig. 27, the water droplet was displaced by 2.5 mm with reduction of amplification observed, but enhancement of 1.4 kV/mm was still seen.

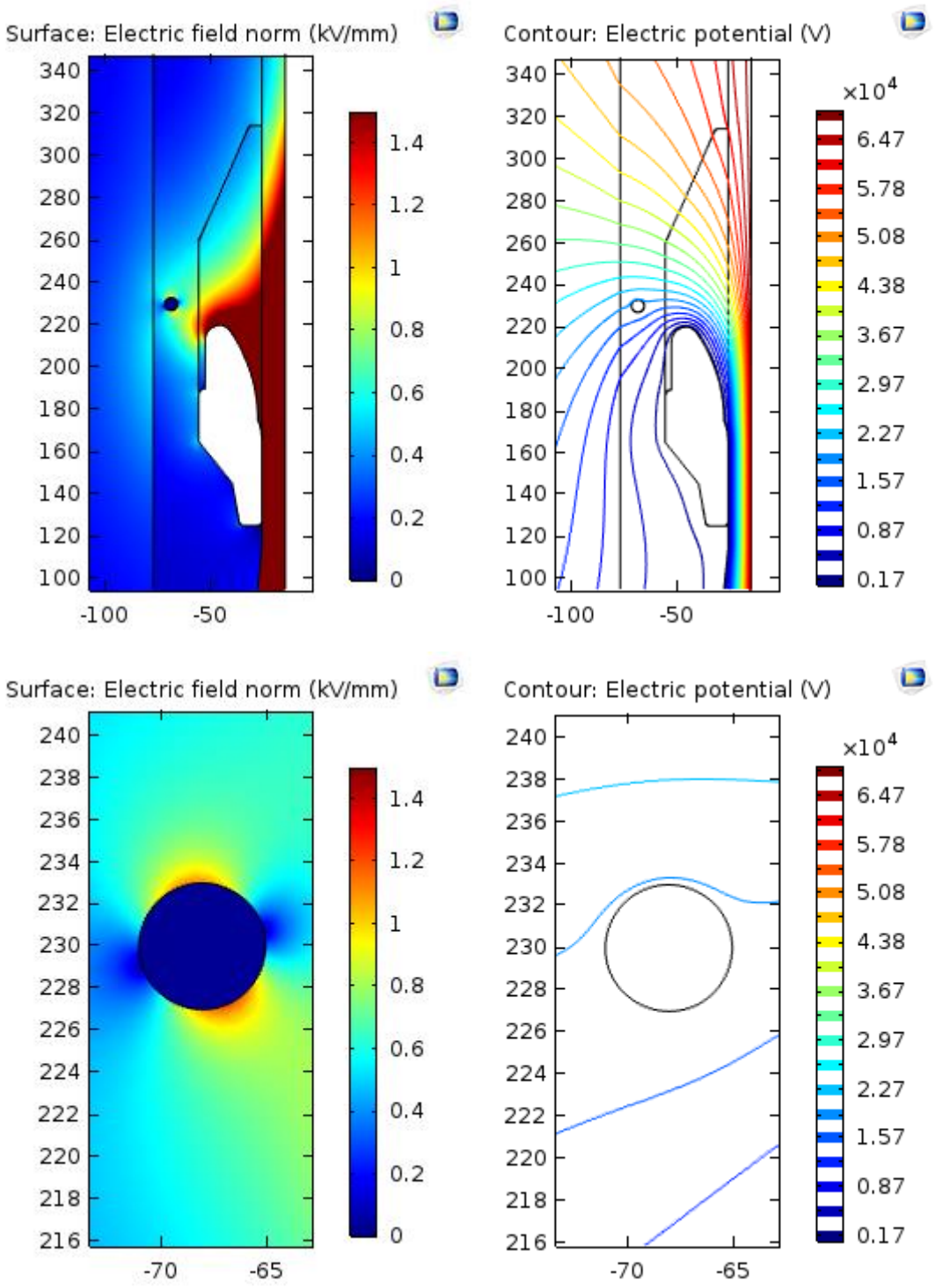

Figure 28: 0.1 ml water droplet 5 mm from the stress cone

As shown in Fig. 28, the water droplet was displaced by 5 mm and consideration reduction in enhancement was observed.

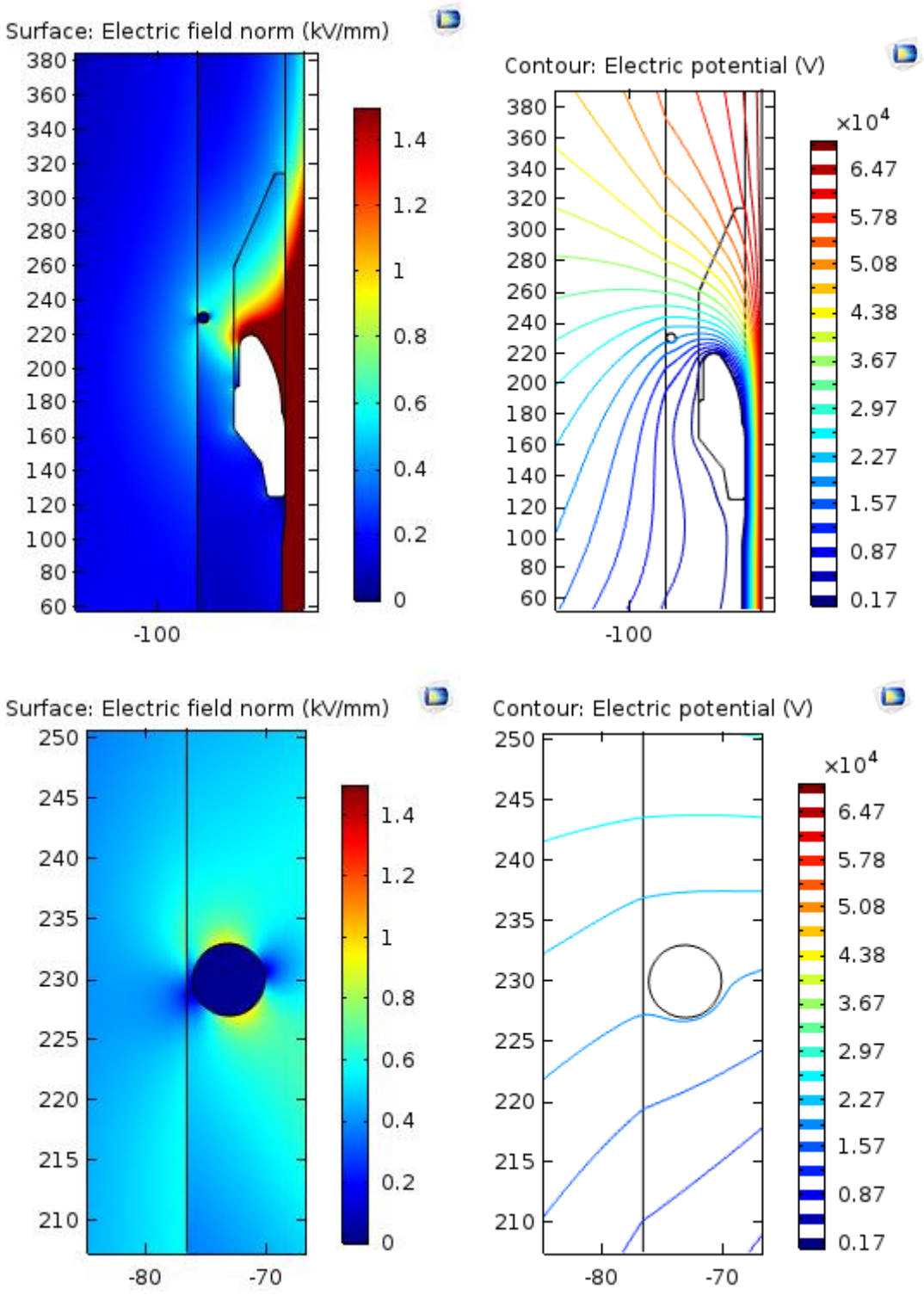

Figure 29: 0.1 ml water droplet 15 mm from the stress cone

As shown in Fig. 29, the water droplet was displaced by 15 mm and even further reduction in enhancement was observed.

2.2.7 Observation for Electric Field Plots of a Water Droplet near a Stress Cone

As clearly shown on the numerous simulations, field enhancement will be faced by the water droplet if within the regions of electric fields and the magnitude of amplification is greater as the droplet is closer to the stress cone – such a result is expected.

The simulation, coupled with the experiment performed before, proved a small 0.1 ml water droplet will be deformed when it is at least 15 mm from the stress cone. A larger water droplet will be even more affected as it has a bigger radius which results in a lower critical field strength.

Further simulations were performed with a larger droplet, with the same distances, to differentiate the effects due to size and can be found in the appendix.

2.3 Preparation Steps for Moisture Introduction in Samples

There were 3 different methods of sample preparation, methods 1 and 2 are for dispersed water and method 3 is for free water

1. Conditioning process involving heating and ultrasonic bath (oil samples with 80 ppm, 120 ppm and 600 ppm were prepared in this manner)
2. Usage of climate chamber (oil samples with 40 ppm and 60 ppm)
3. Direct injection of free water (oil samples with free water droplet for only AC breakdown tests)

Figure 30: Heat and vacuum chamber

All samples were first degassed and heated to 75ºC with the machine shown in Fig. 30 for removal of air bubbles and lowering viscosity, as samples might have increased amount of air bubbles through diffusion after prolonged storage duration. The use of vacuum would not remove all the air bubbles in the sample, but reduced a significant amount.

The moisture content of all the oil samples were measured with Karl Fischer titration in Prysmian.

2.3.1 Conditioning Process Involving Ultrasonic Bath and Heating

Figure 31: Hot oil with droplets added on surface

As shown in Fig. 31, demineralised water was dripped and allowed to sink after the sample was removed from the heated vacuum chamber. As shown in Fig 32, introduced water droplets had

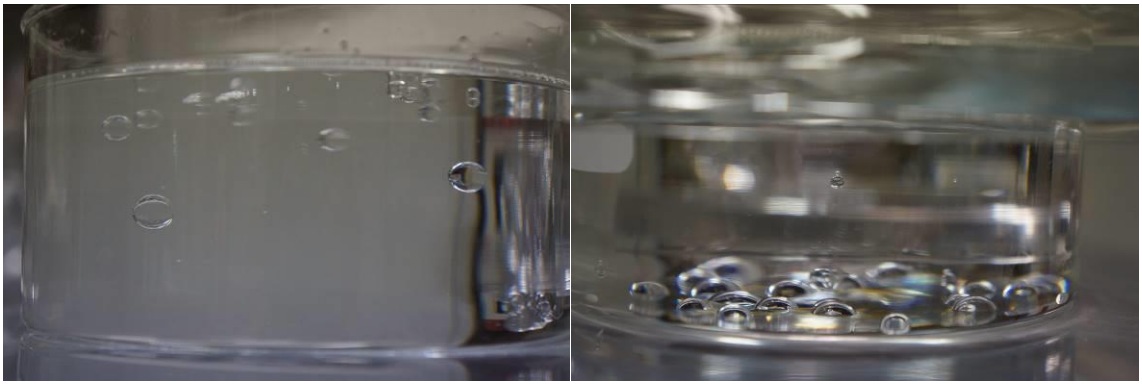

Figure 32: Hot oil with droplets sinking

to be large enough to sink, smaller water droplets remained on the surface of the sample, which was undesired.

After a large majority of the water droplets had sunk to the base, the container was placed on a hot plate at 130ºC for 30 minutes to heat up introduced water content.

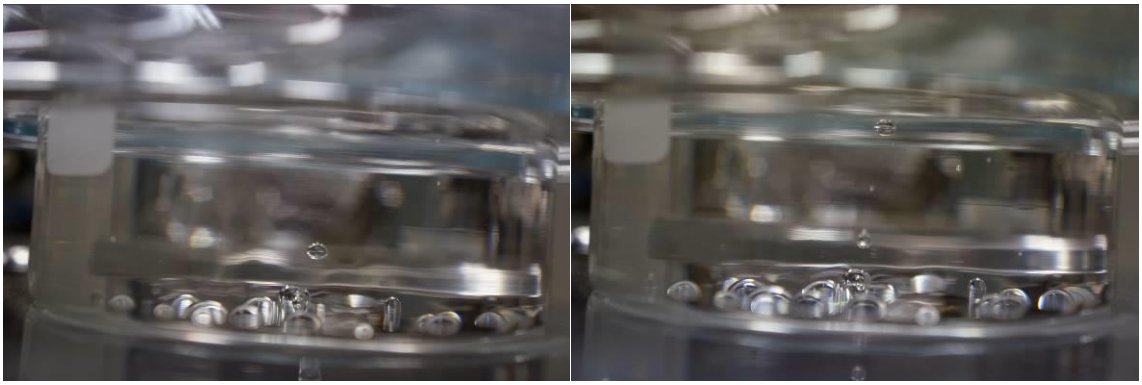

Figure 33: Small heated water bubble floating

As shown in Fig 33, smaller water bubbles resulted from the heated water and floated upwards. This is due to the water molecules moving more rapidly and bouncing off each other, taking up lesser space – the heated up water is less dense than the cool one which causes the rise.

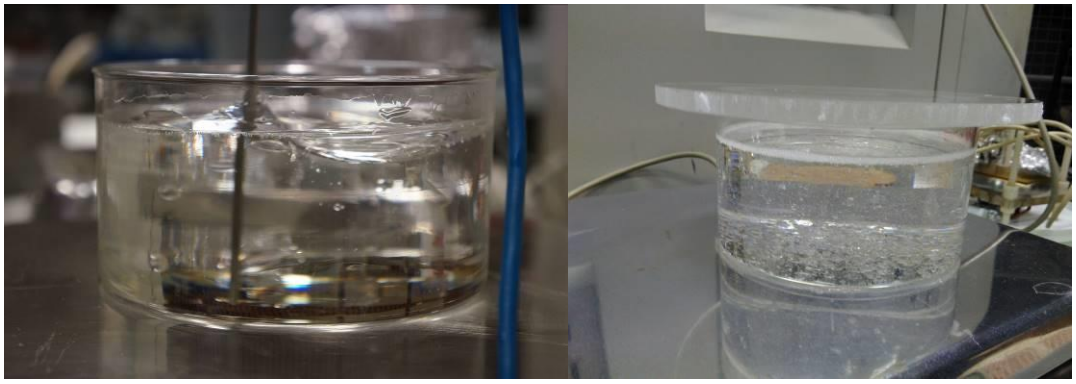

Figure 34: Slightly dispersed water droplets

As shown in Fig. 34, the larger water droplets were provoked to disintegrate, encouraging dispersion. This result is essential for further dispersions. As the next step of disintegration involves ultrasonic waves, smaller water molecules that are heated up were needed. Smaller water molecules allows easier introduction of heat.

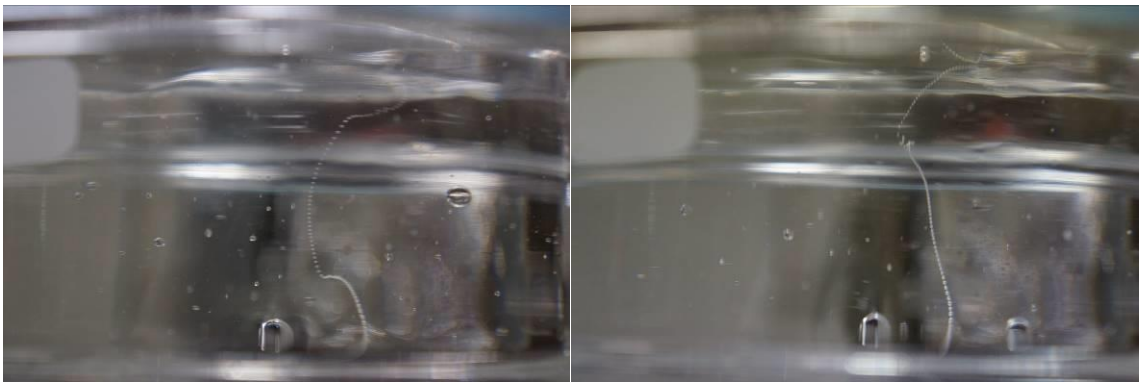

Figure 35: Air bubble trail in hot oil

Air bubble reactions as shown in Fig 35 were observed in one of the preparation procedures, there was no water reservoir at the origin.

Figure 36: Ultrasonic bath (left), End result (right)

As shown in Fig 36, after visual inspection to determine if the sample was suitable, the sample is placed in the ultrasonic bath and kept at approximately 50^{o}C via an external heater. It was crucial to retain elevated temperatures in order to reduce the viscosity of the oil, allowing for water movement. During the initial stages, the same preparation was performed without ensuring careful retention of heightened temperatures and resulted in water droplets not dispersing. It can be seen that the final result was complete dispersion of water droplets that created a misty look.

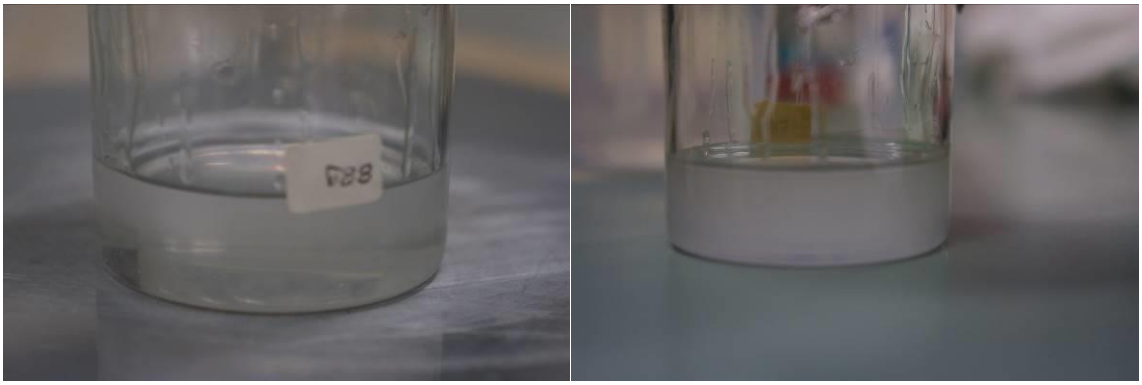

Figure 37: Heating of dispersed water mixture (left), Cooling down of heated mixture (right)

As shown on the left of Fig. 37, upon heating of the oil either via the hot plate or oven, the dispersed water droplets reduced; cooling down of the oil creates dispersion similar to the before heating and can be seen on the right of Fig. 37. This form of preparation allowed for dispersion of visually fine water droplets and was able to achieve ppm levels up to 600 ppm within the oil, with free water present at the base. An aluminum foil and lid is kept over the container at all times to cover the sample, in order to prevent loss of moisture content.

2.3.2 Usage of climate chamber

Figure 38: Climate chamber

As shown in Fig. 38, the climate chamber used demineralised water for the humidifying process. The temperature and humidity level of the machine could be adjusted. The settings used in preparing the samples was at 75ºC for two main reasons – at a higher temperature the oil is less viscous, and AC breakdown tests was performed at a higher temperature, also due to viscosity reasons.

Samples were placed into the climate chamber after removal and varying humidity settings were used for achieving different moisture content within the sample.

Figure 39: 40 ppm (left), 60 ppm (right)

It was observed that at duration of 16 hours, 25% humidity level resulted in 40 ppm of moisture content as shown on the left of Fig. 39, whilst 40% resulted in 60 ppm of moisture content as shown on the right of Fig. 39. As shown in Fig. 39, there was no observable visual differences at low moisture content.

The method which utilised the climate chamber under exposure of a short duration, was able to produce an assumed homogenous dispersion of the water in lower ppm values of approximately 60 ppm without the presence of free water content.

2.3.3 Direct Injection of Free Water

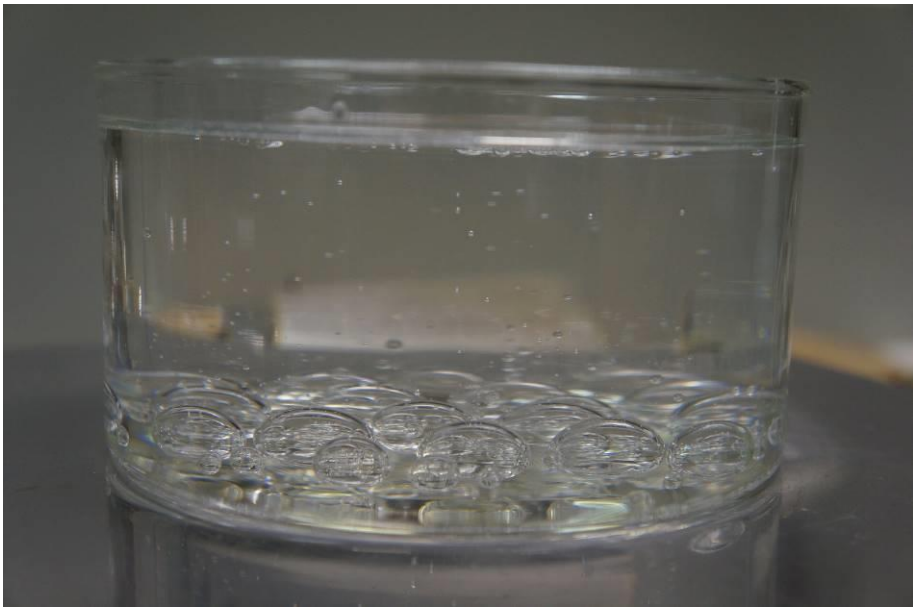

Figure 40: 15 ml of free water added

Water is dripped and allowed to sink after sample was removed from heated vacuum chamber, as shown in Fig. 40.

2.3.4 Karl Fischer Titration

Karl Fischer titration was invented by the German chemist Karl Fischer, and uses coulometric or volumetric titration to determine the amount of water content within a given sample. The popularity of the method could be attributed to the numerous practical advantages it has over other methods in accuracy, selectivity, speed and minimal sample requirement.

Despite being of destructive nature, Karl Fischer is preferred for water samples because the titration reaction consumes water, whilst measuring mass loss on drying considers loss of total combusted material. However, external leaked water input can hinder measurements and called, "drift". In order to produce accurate results, a dry run is done to obtain the rate of drift for the given duration and is subtracted from the results of following tests.

The volumetry method is used for high water content samples. The iodine-containing solution works as a titrating agent, calculating the water content of the sample by using titration volume and titer of the titrating agent.

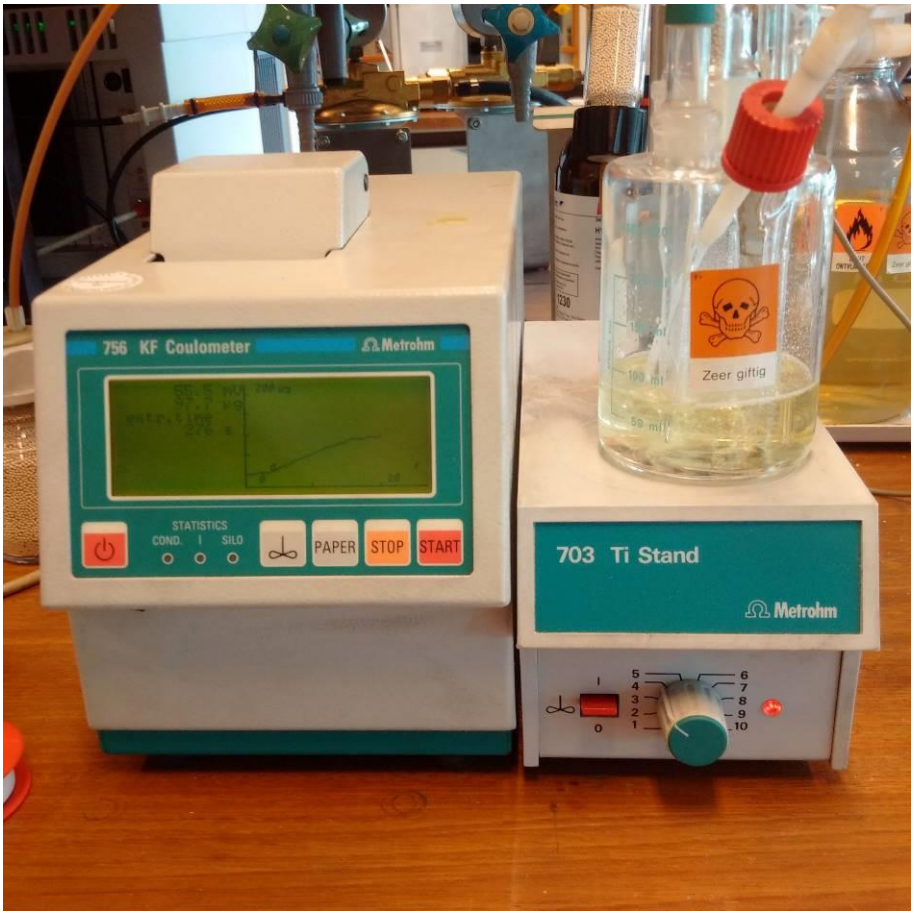

Figure 41: Karl Fischer titration

The coulometry titration is a micro-method and is most commonly used for samples with low water content, this method was used in the thesis and is as shown in Fig. 41. The required iodine is produced electrochemically in the titration vessel by anodic oxidation from iodide obtained in the coulometric reagents. The amount of water in the sample is determined by calculating the consumption of iodine, which represents the consumed electric charge.

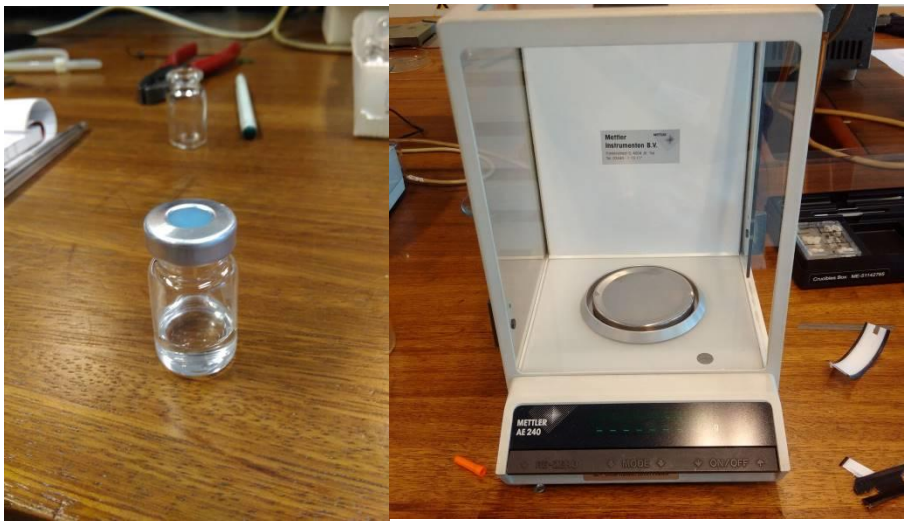

Figure 42: Sample bottle (left), Industrial weighing scale (right)

As shown on the left of Fig. 42, samples were placed into the given bottle, sealed and was weighed on the Mettler 240 scale shown on the right. The Mettler had an accuracy of 0.01 mg, and was critical in the process.

Figure 43: Full titration setup

Finally, the samples were placed in a holder and penetrated with a syringe as shown in Fig. 43. The sample was then heated up, extracting and determining the water content.

2.4 Discussion for Behaviour of Water Movement in Oil

Paramount in this chapter would be the influence of heat and electric field on water content in oil.

2.4.1 Discussion for Heat Influence

As shown at the start of this chapter, a phenomenon was observed with an oil sample containing large amounts of visible dispersed water at a lower temperature. When heated up, the visible dispersed water cleared up and an originally milky texture became largely clear. This is because of two reasons – 1) the presence of heat reduced the viscosity enabling mobility within the material, 2) the water molecules gained energy from the heat and expanded, causing separation of once larger droplets.

While it is true that low viscosity causes lower breakdown strength, with extremely viscous oil as studied in the experiment, high viscosity does not increase the breakdown strength due to the presence of immobile pollutants.

2.4.2 Discussion for Electrical Influence

As shown in the middle of this chapter, moisture content is affected by two visible forces – polarisation force and a critical electric field strength before deformation.

Through the simplified experiments, it can be seen that despite the polarisation force from the electric field not being high enough to attract a water droplet, the electric field can be greater than the critical electric field strength, causing it to deform and disintegrate. This disintegration causes smaller droplets which goes through the same process. Continuous electron activity will lead to degradation and eventual breakdown.

3 Permittivity and Tan Delta Test

Permittivity, ε, is the quantification of resistance from a medium, when exposed to an electric field, which will provide information on the dielectric constant. Dielectric constant, ε_r, indicates the polarisation ability of a material when exposed to an electric field and is defined as,

$$\varepsilon_r(\omega) = \frac{\varepsilon(\omega)}{\varepsilon_0} \qquad (7).$$

Relative permittivity, ε_r, is dimensionless and complex-valued, with its real and imaginary parts defined as,

$$\varepsilon_r(\omega) = \varepsilon'_r(\omega) - i\varepsilon''_r(\omega) \qquad (8).$$

$\varepsilon'_r(\omega)$ is what we know as the relative permittivity, it is a measure of the amount of polarization (quantifying the capability of the material to store energy). The imaginary part $\varepsilon''_r(\omega)$ represents the loss component, it is a measure of the losses involved in the polarization processes. The behaviour of the permittivity as a function of frequency and temperature is sensitive to material changes, such as aging processes, absorbed moisture or the addition of fillers [18]. Any change of the molecular structure of a dielectric will show up if the related polarization phenomena are occurring in the measured frequency range.

Tangent Delta indicates the loss angle of a material, with the real component referring to the resistive losses and the imaginary component referring to the reactive losses. Dielectric losses can be catergorised under the loss angle Delta or loss tangent Tan Delta. In an ideal capacitor, the current and voltage are shifted by 90° which is indicative of a capacitive current. Presence of impurities will cause an increase of resistive current through the insulation.

The goal is to determine, when moisture content is introduced, the dielectric constant and tangent delta of the oil samples. This is to ascertain the dielectric quality and amount of loss incurred.

3.1 Test setup and procedure

Figure 44: Novocontrol Alpha-A Series [19]

As shown in Fig. 44, the complex permittivity of all the samples was determined with the use of a fully automated Alpha-A dielectric analyser from Novocontrol. The permittivity was measured as a function of frequency (0.01 Hz to 1 MHz) and temperature (20°C to 80°C). The temperature ramp was 20°C to 80°C to 20°C to 80°C to 20°C, with the temperature change rate of steps of 20°C. Temperature ramp was performed due to significant change in oil viscosity with respect to temperature (7200 cSt at 40°C and 230 cSt at 100°C) was observed, and an insight to behaviour was desired. The change in temperature and viscosity had a great influence on the water activity within the oil [20].

3.2 Redesign of Test Cell

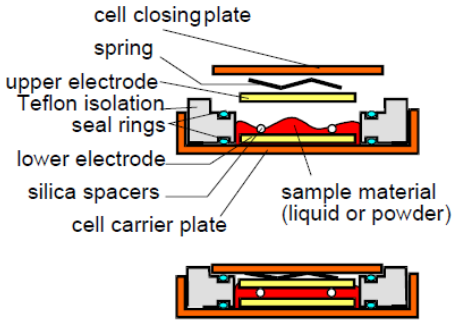

Figure 45: Illustration of standard liquid sample holder from Novocontrol [19]

As shown in Fig. 45, the standard liquid sample holder was used initially for measurements. It contain a closing plate, spring for retention of tension, top electrode, two 50 µm straight silicon spacers and a bottom electrode. It is surrounded by a Teflon ring with rubber rings on the top and bottom and a holding cell. The oil sample is placed between the top and bottom electrode, with the space between them regulated by the silicon spacers. To achieve high sensitivity, minimal space between electrodes are needed.

Due to heat, the viscosity of the oil changed with the temperature, which resulted in unwanted content movement between the top and bottom electrode. The change in viscosity, coupled with the presence of moisture content, caused erroneous results.

The problem was found to be in the initial loading stages and attributed to the uneven spread of oil sample between the electrodes due to high viscosity and displacement of silicon spacer.

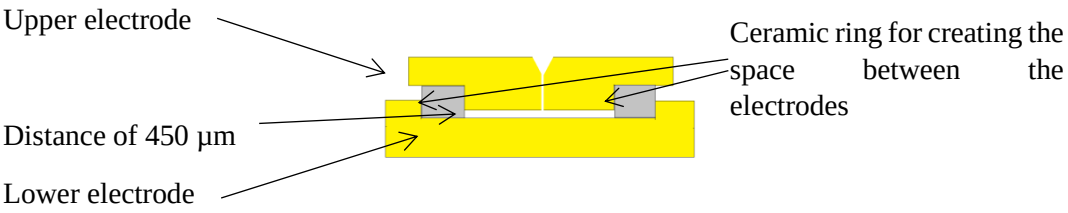

Figure 46: Illustration of the designed sample holder

The proposed solution was to apply even pressure across the sample and regulate the space between electrodes in a more reliable manner. As shown in Fig. 46, the minimal distance between electrodes was achieved by creating a difference between the new upper electrode and ceramic ring.

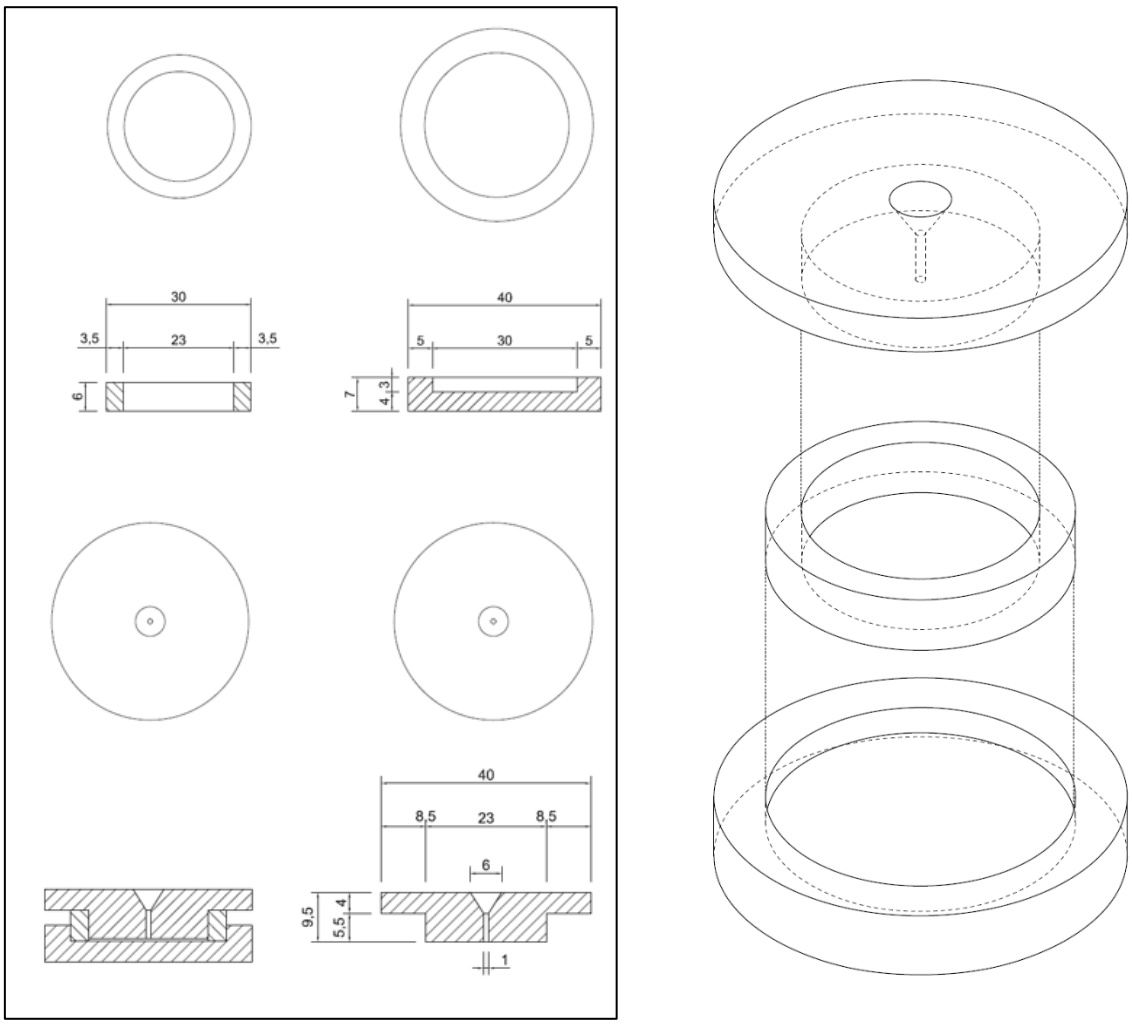

Figure 47: Clockwise from top left (in mm), Ceramic spacer, Bottom holder, Top holder, Complete holder (left), Exploded view of sample holder (right)

As shown in Fig. 47, the evenly applied pressure was achieved with the same method, and allowed residual oil sample to escape at the top. This cavity ensured that the sample space was completely filled, along with a reservoir for excess contents, to prevent contamination with the test electrode of the machine.

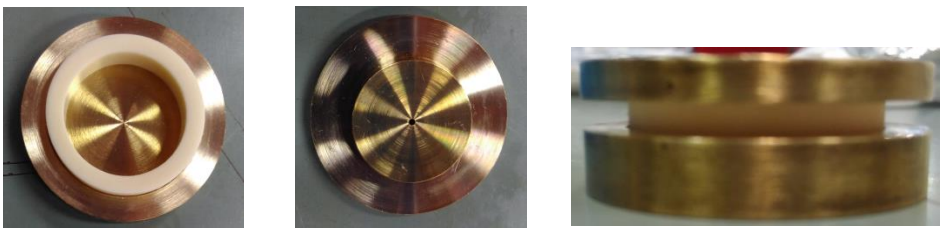

Figure 48: Lower electrode with ceramic ring (left), Upper electrode bottom view (centre), Complete sample holder (right)

The complete sample holder is as shown in Fig. 48.

3.3 Relative Permittivity Measurement Results

The low frequencies are of interest because at higher frequencies, the particles within the medium does not polarise due to the rapid change in electric field. Thus for a sample with suspected moisture content, it would be useful to observe the lower frequencies as the water molecules of high permittivity would be polarise and alter the characteristics of the oil.

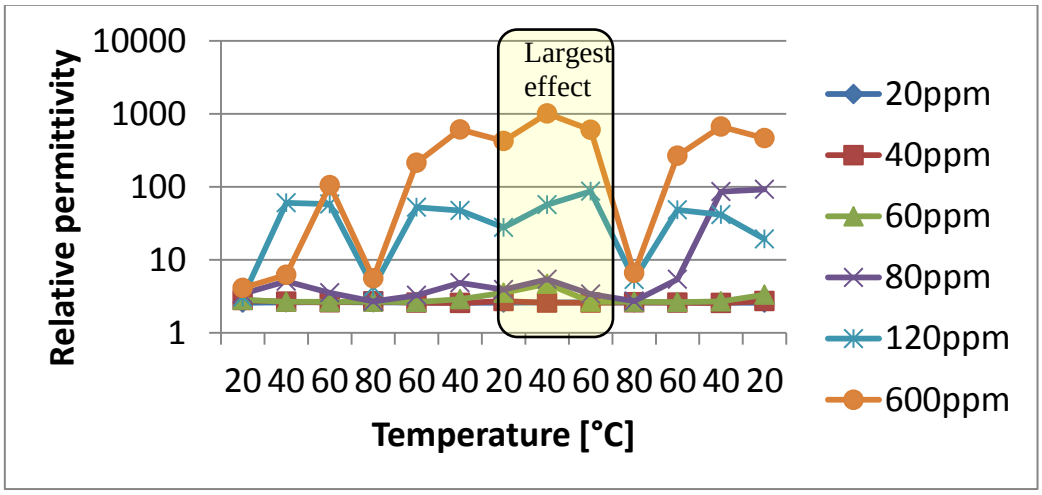

Figure 49: Relative permittivity of the oil samples as a function of temperature at 0.01 Hz

As shown in Fig. 49 considering 0.01 Hz, the temperature ramp performed showed unexpected results and had the largest effect on the second ascend. It was concluded that the first descend increased the viscosity of the oil, which coalesced moisture content, a phenomenon explained in the earlier chapter. The heating process from the second ascend gave the water molecules energy and lower the viscosity, which allowed the moisture content to diffuse. The selected segment in yellow was felt to be the more accurate representation of actual conditions which had temperature cycling.

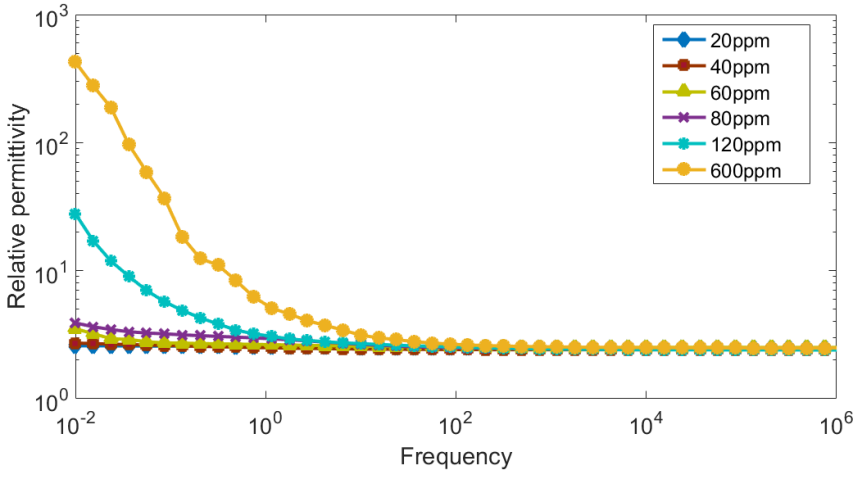

Figure 50: Relative permittivity of the oil samples at 20°C

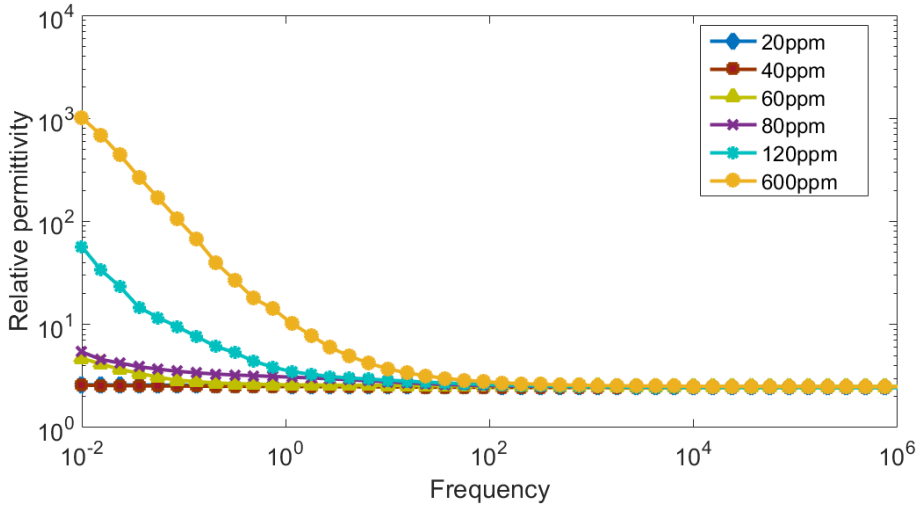

Figure 51: Relative permittivity of the oil samples at 40°C

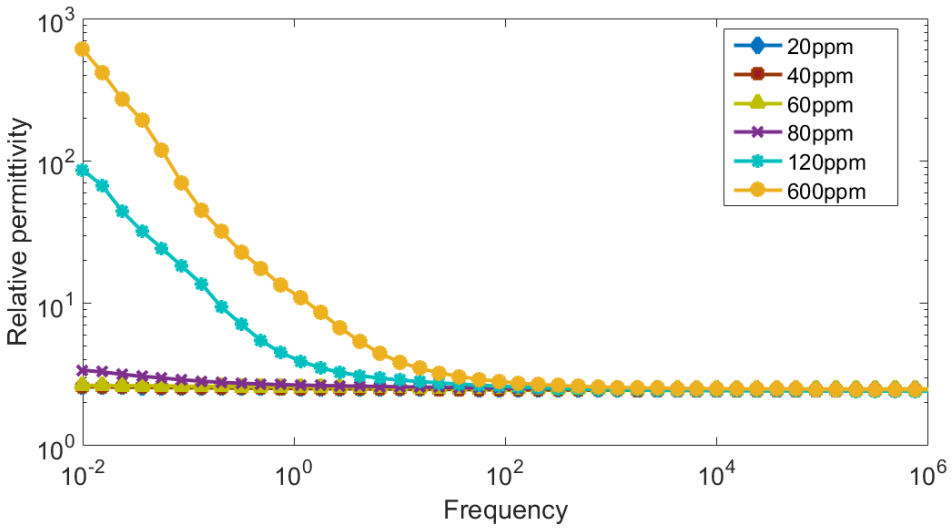

Figure 52: Relative permittivity of the oil samples at 60°C

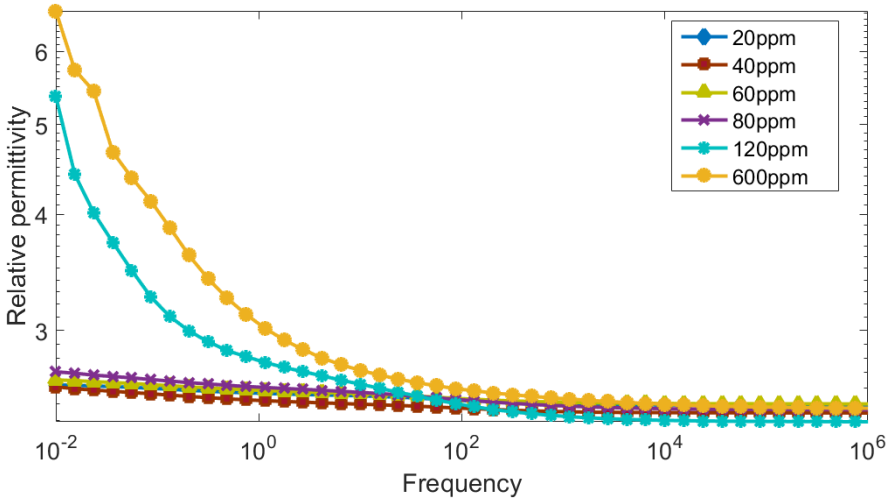

Figure 53: Relative permittivity of the oil samples at 80°C

As shown in Fig. 50 to 53, with higher moisture content such as 600 ppm the highest relative permittivity was approximately 1000, and with dry oil the lowest relative permittivity was approximately 2.4, which was roughly the dielectric constant of the oil. The general maximum permitted levels of ppm in real termination is around 100 ppm.

3.3.1 Observation for Results of Relative Permittivity

As shown in Fig. 50 to 53, moisture content had an effect on the dielectric constant of the oil at the lower frequencies, with a more pronounced effect at 0.01 Hz. Most uncertainties occurred at 40°C and 60°C. Further observation was done in Table 1 below at 50 Hz as that is the operating frequency.

	20°C	40°C	60°C	80°C
20 ppm	2.43	2.46	2.49	2.49
40 ppm	2.52	2.52	2.53	2.53
60 ppm	2.54	2.54	2.54	2.54
80 ppm	2.52	2.58	2.55	2.54
120 ppm	2.56	2.63	2.60	2.52
600 ppm	2.72	2.88	2.93	2.61

Table 1: Relative permittivity at 50 Hz

As shown in Table 1, the dielectric constant of the oil at operating conditions of 50 Hz was affected by the increased moisture content. The dielectric constant of a material is the ability to transmit electrical potential energy, with the purpose of the oil to hold a charge under an applied electric field. Evidently, the presence of a conducting contaminant like water ($\varepsilon_r \sim 80$) will elevate the permittivity because it reduces the insulating abilities.

It could be concluded that the presence of moisture content increased the permittivity of the material.

3.4 Tan Delta Measurement Results

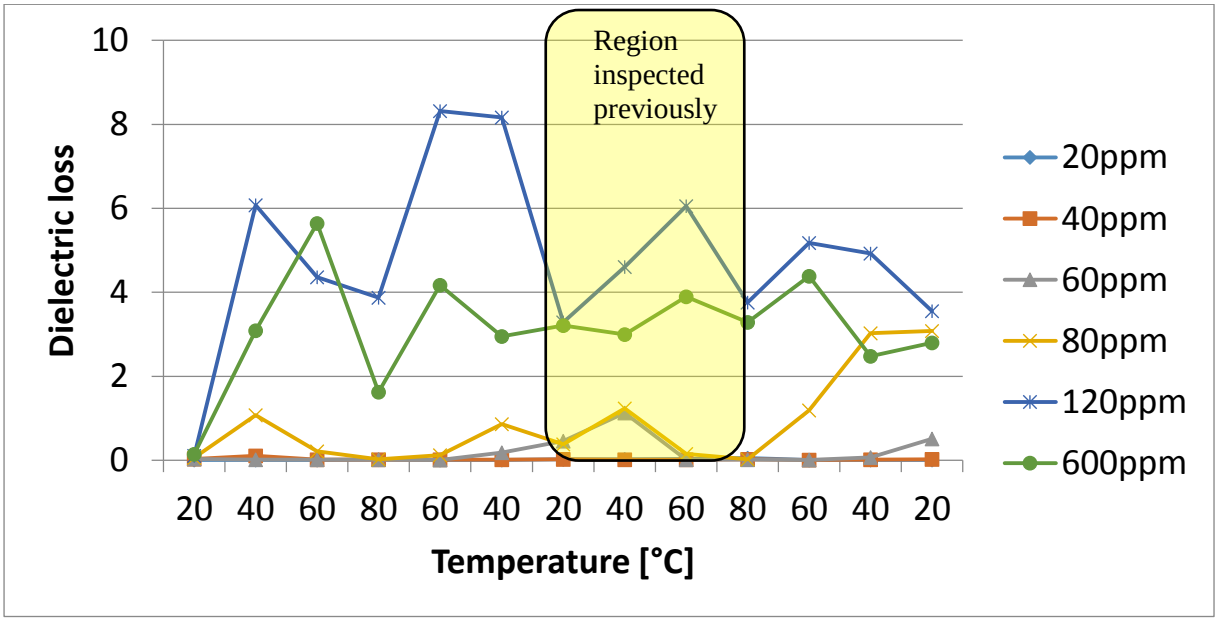

Figure 54: Dielectric loss of the oil samples as a function of temperature at 0.01 Hz

Similarly for the tangent delta measurements, which represented dielectric losses, unexpected activity occurred during temperature cycling. Observation was performed in the yellow segment as shown in Fig. 54 as it was the similar duration as relative permittivity.

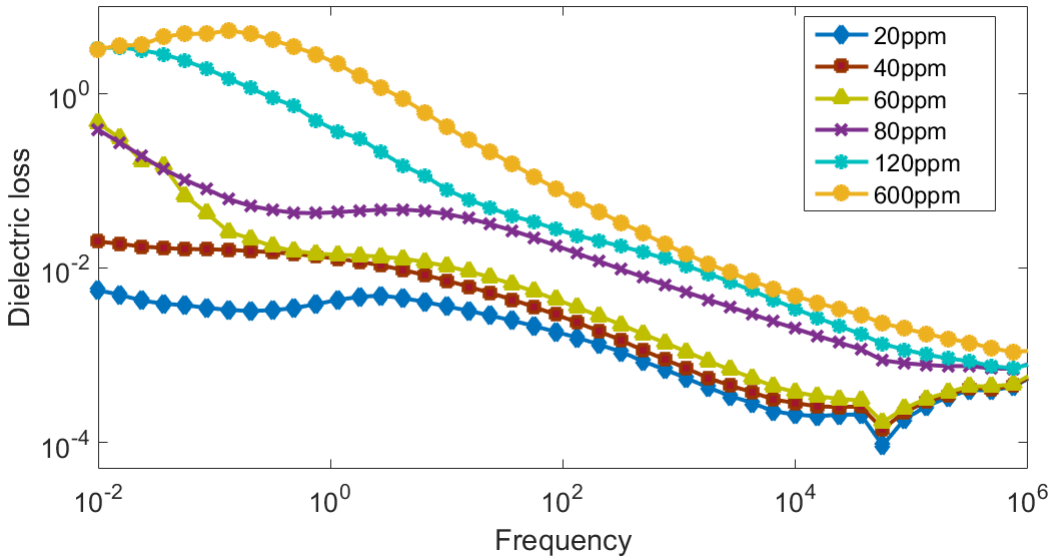

Figure 55: Dielectric loss of the oil samples at 20°C

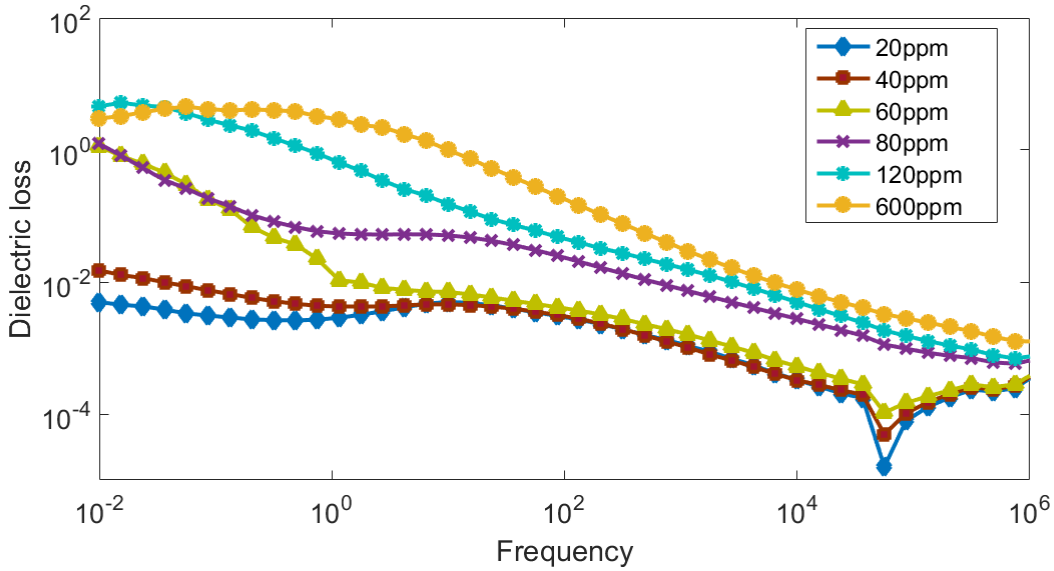

Figure 56: Dielectric loss of the oil samples at 40°C

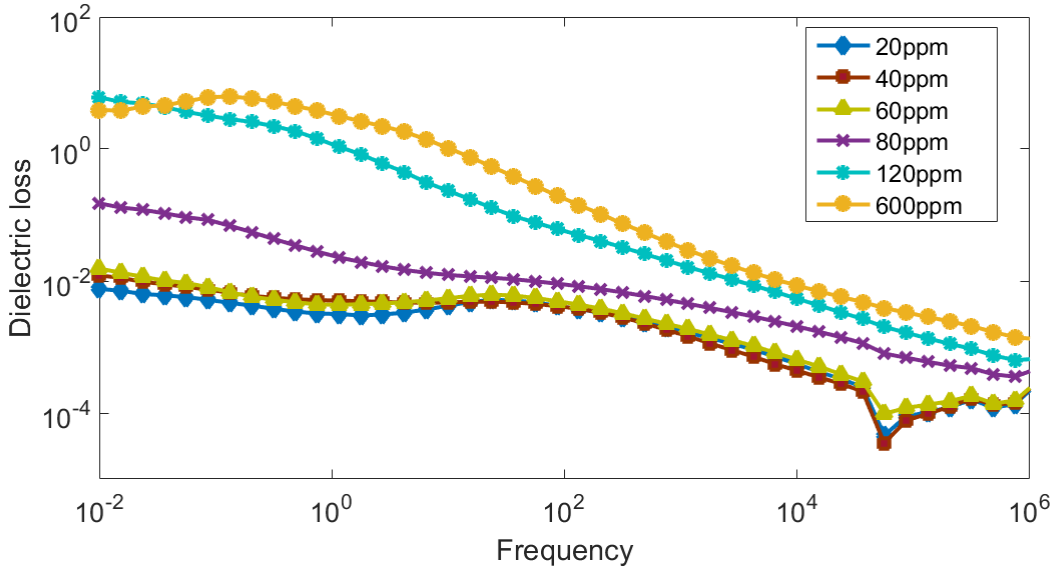

Figure 57: Dielectric loss of the oil samples at 60°C

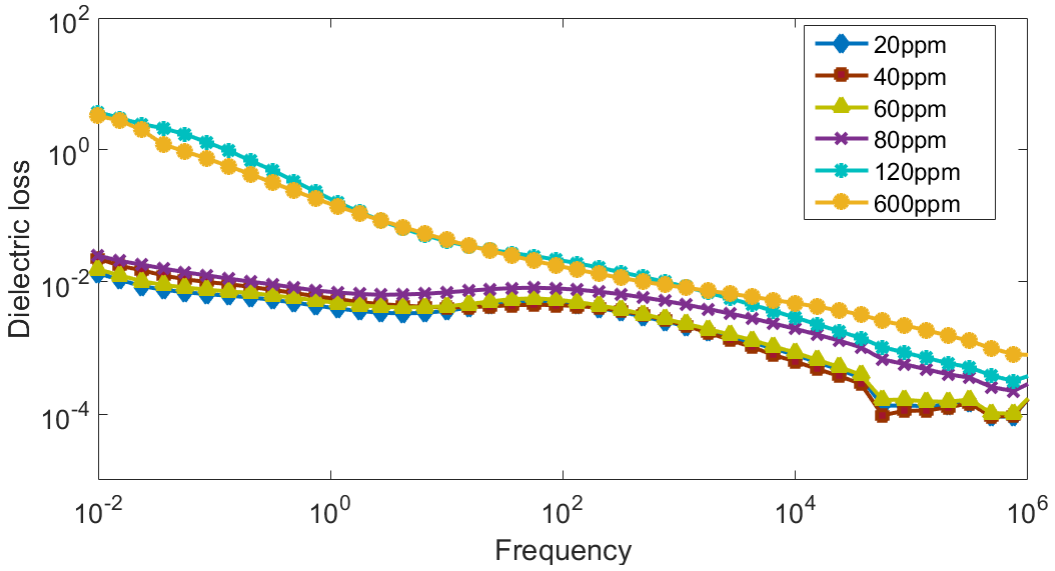

Figure 58: Dielectric loss of the oil samples at 80°C

As shown in Fig. 55 to 58, the highest tangent delta was 0.279 and the lowest was 2.16×10^{-3}.

3.4.1 Observation for Results of Tan Delta

As shown in Fig. 55 to 58, moisture content had an effect on the dielectric losses of the oil at the lower frequencies, with a more pronounced effect at 0.01 Hz. Further observation was done in Table 2 below at 50 Hz as that is the operating frequency.

	20°C	40°C	60°C	80°C
20 ppm	2.16×10^{-3}	3.47×10^{-3}	4.72×10^{-3}	5.21×10^{-3}
40 ppm	3.58×10^{-3}	3.56×10^{-3}	4.49×10^{-3}	4.52×10^{-3}
60 ppm	5.38×10^{-3}	4.65×10^{-3}	5.53×10^{-3}	5.65×10^{-3}
80 ppm	2.22×10^{-2},	3.05×10^{-2}	9.89×10^{-3}	8.19×10^{-3}
120 ppm	3.38×10^{-2}	5.40×10^{-2}	3.87×10^{-2}	2.47×10^{-2}
600 ppm	1.12×10^{-1}	2.79×10^{-1}	2.75×10^{-1}	2.10×10^{-2}

Table 2: Dielectric losses at 50 Hz

As shown in Table 2, the dielectric loss of the oil at operating conditions of 50 Hz was affected by the increased moisture content. The highest value was approximately 0.279 while the lowest was 9.89E-3. It could be concluded that the presence of moisture content produced unwanted degradation to the insulating properties desired.

3.5 Discussion of Permittivity and Tan Delta Test

As shown from the results of the dielectric constant and loss, it is clear that with increased moisture content, the Tan Delta test had more reaction. The dielectric, when contaminated with moisture, shown a more prominent resistive behaviour.

For moisture content detection purposes, the Tan Delta test would produce more conclusive results, compared to the real permittivity test, as the Tan Delta difference differed by 2 decades, whilst the real permittivity differed by 0.3.

4 Breakdown Test

The goal is to verify and observe the effect of moisture content and free water on the AC breakdown strength of the oil and to determine the critical moisture level in the oil. Dielectric quality is crucial to safe operations as the presence of dust, fibres, particles, tiny air bubbles and water bubbles can all lead to polarisation and unwanted field enhancement.

When the moisture content in oil is low [21], the water particles have a form as a monomer and possess a high dipole moment. As the moisture content is increased, the dipole moment reduces and the mobility of the electrons increases.

When the temperature increases, there is usually an increase in molecular interchange due to increased movements in higher temperatures. In liquids, there are substantial attracting cohesive forces between liquid molecules, where both cohesion and molecular interchange contribute to liquid viscosity. The result of increased temperature is the reduction in cohesive forces, while increasing the rate of molecular interchange. This causes a reduction in viscosity with an increment in temperature.

Also, with the rise in temperature, water molecules become more conductive due to ionic mobility as well as solubility of salts and minerals. This creates an eventual decrease in the dielectric strength in oil and reduces the breakdown strength.

4.1 Test Setup and Procedure

Figure 59: OPG-100A insulating oil tester [22]

As shown in Fig. 59, the AC breakdown voltage was measured with an OPG-100A insulating oil tester according to the IEC60156 standard. The electrode configuration consisted of two spherical brass electrodes with gap distance of 2.5 mm and a rate of voltage rise of 2 kV/s.

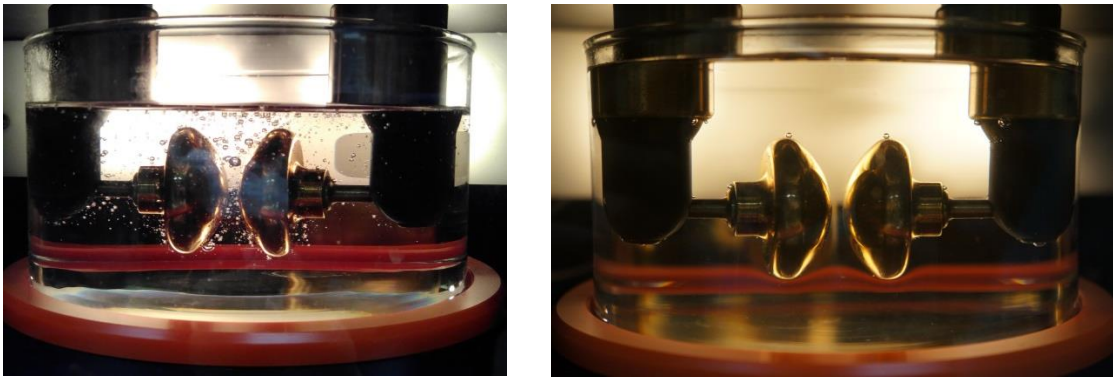

Figure 60: Air bubbles in 20 ppm oil (left), 20 ppm oil at 60°C (right)

It is well known that higher temperatures create lower breakdown voltage due to the decrease in viscosity [1], but as shown on the left of Fig. 60, due to the high viscosity of the oil, introduction of undesirable large air bubbles was made when the sample was fitted for testing. The oil was then heated to 60°C as shown on the right of Fig. 60 and tested. The test was performed at 60°C and finished at 50°C.

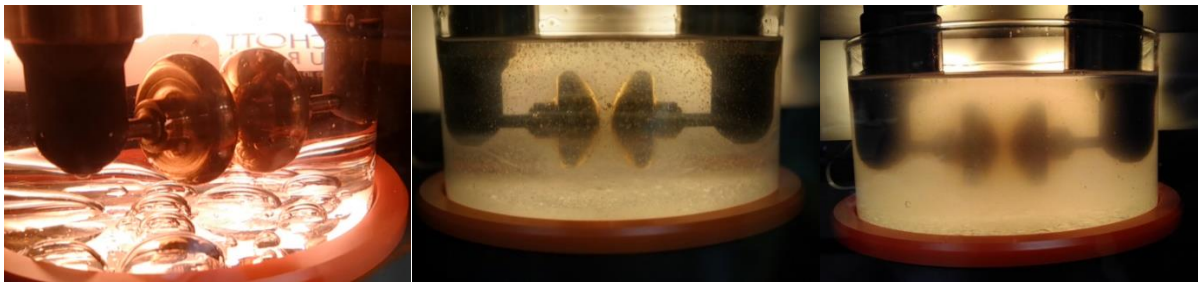

Figure 61: Oil with 15 ml free water (left); Oil with 120 ppm of water content (centre); Oil with 600 ppm of water content (right)

The tests performed were in two categories – dispersed water and free water, both categories contained different degrees of moisture content. As shown in the centre and right picture of Fig. 61, dispersed water is the water that is finely distributed in the oil. As shown on the left of Fig. 61, free water are the water droplets on the base of the holder.

4.2 Dispersed Water Breakdown Results

Moisture Content	20 ppm	40 ppm	60 ppm	80 ppm	120 ppm	600 ppm
Breakdown Voltage (kV)	80	56	30	22	25	5
	57	80	40	27	7	7
	99	65	47	31	18	7
	100	77	49	25	12	9
	99	74	58	27	17	6
	95	72	31	29	22	8
	87	71	61	19	6	7
	83	71	47	30	12	7
	101	63	46	31	18	7
	101	56	58	25	22	7
	99	64	44	20	19	7
	73	52	50	25	9	7
Average Voltage (kV)	89.5	66.75	46.75	25.92	15.58	7

Table 3: Breakdown voltage of dispersed water

As shown in Table 3, breakdown voltage test was conducted for dry oil, and 5 other samples that had moisture introduced.

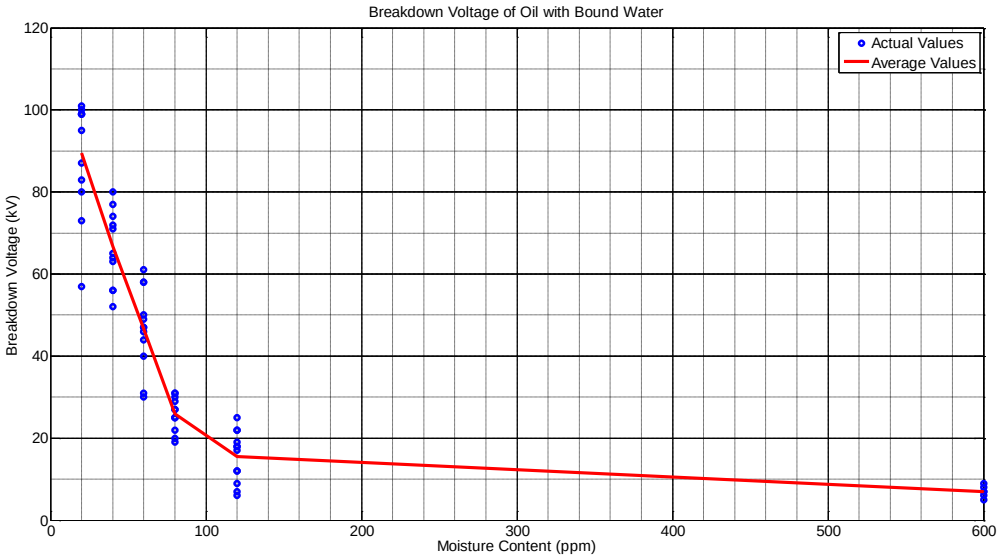

Figure 62: Breakdown voltage for dispersed water

As shown in Fig. 62, increased moisture content decreased breakdown strength, which was expected. The highest breakdown field strength was 36 kV/mm and the lowest was 2 kV/mm.

4.3 Observation for Dispersed Water Breakdown Test

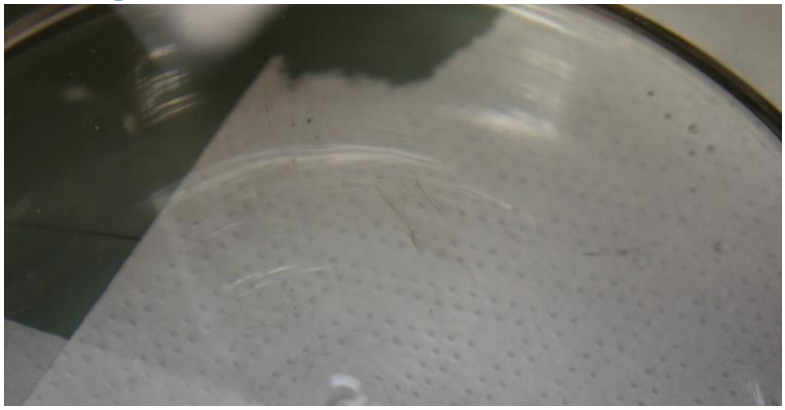

Figure 63: Oil with 60 ppm moisture content, burnt oil remnants

The addition of moisture content led to more particles with field concentration. This allowed the electrons to accelerate and ionised molecules on collision, which created current concentration that led instability. Rise of temperature and decrement of viscosity followed, which caused local breakdown and evaporation of the liquid. The breakdown path was between the electrodes and highly luminescent. It was succeeded by gas bubbles, pressure waves and traces of burnt oil could also be seen, as shown in Fig. 63.

It could be concluded that increasing moisture content within a sample leads to lower breakdown strength and is unfavourable. This is clearly shown as the breakdown strength was reduced by half when the moisture content increased to 60 ppm from 20 ppm.

4.4 Free Water Breakdown Results

Figure 64: Breakdown path in free water

As shown in Fig. 64, when the breakdown strength between electrodes is higher than the breakdown strength at the base of the electrodes, breakdown occurs through the free water instead.

Moisture Content	1 ml Free Water	2 ml free water	15 ml Free Water
Breakdown Voltage (kV)	18	22	15
	47	33	18
	25	28	12
	30	34	14
	37	32	17
	39	32	17
	38	30	18
	38		18
	21		16
	31		17
Average Value (kV)	32.4	30.14	16.2

Table 4: Breakdown voltage of free water

As shown in Table 4, breakdown voltage test was conducted for dry oil, and 2 other samples that had moisture introduced. Test of 2 ml of free water was from 80 ppm dispersed water sample, as the sample contained both dispersed water and free water.

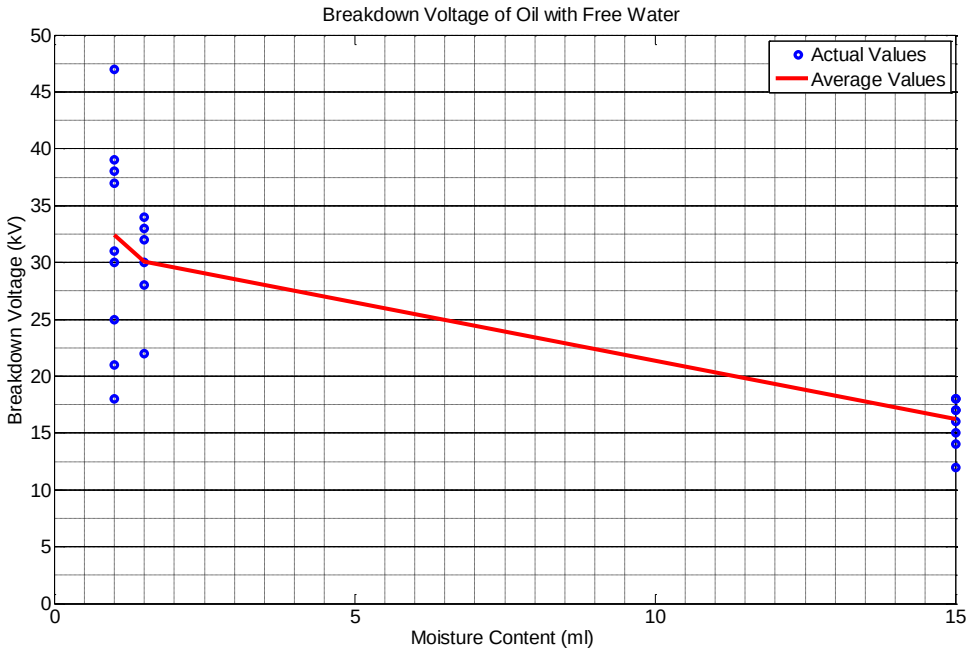

Figure 65: Breakdown voltage for free water

As shown in Fig. 65, increased moisture content decreased breakdown strength, which was expected. The highest breakdown field strength was 13 kV/mm and the lowest was 6.5 kV/mm.

4.5 Observation for Free Water Breakdown Test

The breakdown for free water differed from dispersed water with breakdown in free water being a closed circuit between the bottom of the electrodes and water droplets at the base of the holder. Breakdown occurred there because the breakdown strength between the electrodes was higher than the aforementioned location.

The size of the water droplet played an important role as droplets with bigger volume might be higher, which brought it closer to the electrodes.

4.6 Discussion of Breakdown between Dispersed Water and Free Water

As evident in the results gathered from dispersed water and free water, the presence of dispersed water beyond 60 ppm is undesired as it caused the breakdown strength to decrease by half. Also large amounts of free water is undesired as it reduced the breakdown strength by half due smaller critical strength and a smaller distance between water droplet and electrode.

Considering a condition where there is approximately 20 to 60 ppm of homogenous moisture content around the container and a large amount of free water at the base. Assumption of a higher breakdown strength would be made when a general moisture content test is performed and results obtained were 20 to 60 ppm. However, this condition could prove to be dangerous as breakdown could still occur through the base of the container under the false belief of safety.

5 Partial Discharge Test

The goal of this study is to understand partial discharge behaviour of the given oil sample when exposed to different levels of voltage, humidity and temperature. The small scale setup was chosen to allow for initial uncomplicated manipulation of various parameters, mainly moisture content, temperature and voltage. The small scale setup also provides insight into expectations for the full scale setup, which will be used next.

5.1 Partial Discharge

Partial discharges are breakdown phenomena that do not fully bridge the insulation between electrodes and are defined in [23]. They cause a slow erosion of the material and are generally distinguished as,

- Internal discharges
- Surface discharges
- Corona discharges

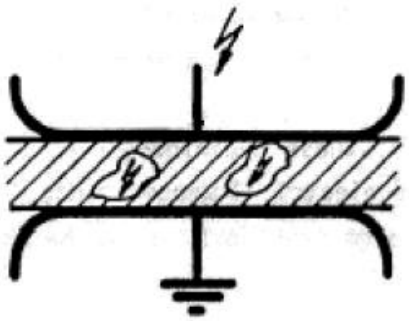

Figure 66: Internal discharge [20]

As shown in Fig. 66, internal discharges occur in cavities in a solid dielectric and are usually gas-filled. It can lead to electrical treeing and enhancement of the field from carbonisation of the material.

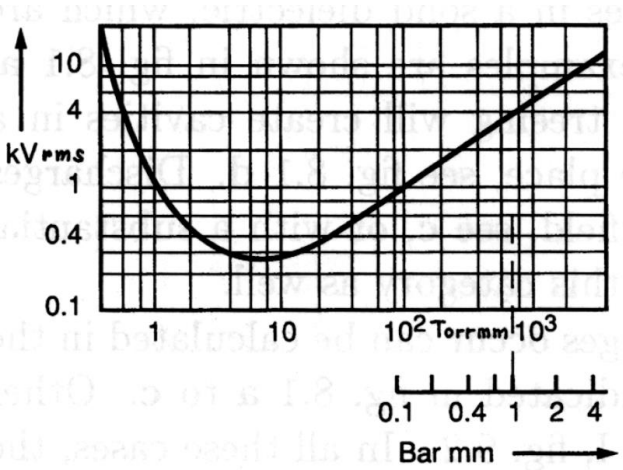

Figure 67: Paschen curve [1]

It is well known from experiments [20], that the dielectric strength of the gas in such cavities is reasonably well represented by the Paschen curve, as shown in Fig. 67.

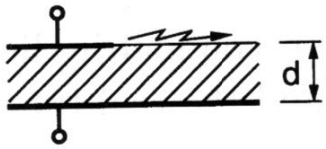

Figure 68: Surface discharge at the edge [20]

As shown in Fig. 68, surface discharges can occur along dielectric interfaces when sufficient tangential field strength is present, with the interface being gas or liquid-bounded.

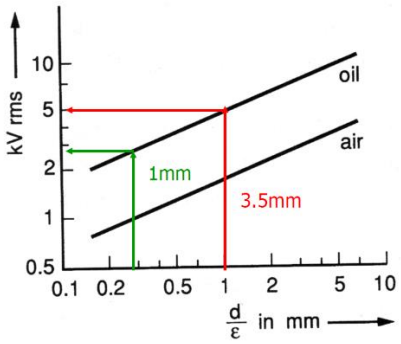

Figure 69: Inception voltage as function of distance and permittivity

As shown in Fig. 69, the inception voltage is shown as a function of distance and permittivity and the inception voltage in the dielectric is fairly low.

Figure 70: Corona [1]

Corona discharges are found at the sharp metallic points as shown in Fig. 70 in an electric field and could be found on the high voltage electrode, earthed side or in between electrodes.

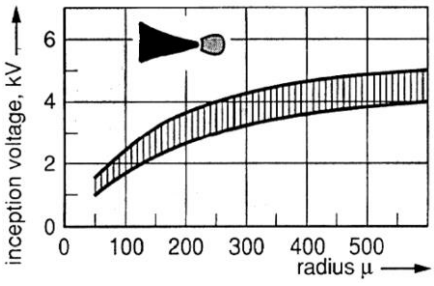

Figure 71: Corona inception voltage in small gaps [20]

The corona inception voltage is as shown in Fig. 71. Corona is a source of interference and the test area must be free of sharp edges, pointed wire or thin connection wires on the HV and earth side.

5.2 Partial Discharge Test Circuit

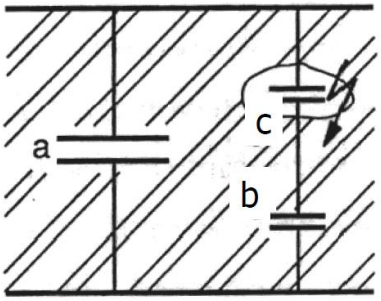

Figure 72: Partial Discharge Equivalent Circuit [20]

As shown in Fig. 72, the model of a partial discharge could be considered to be a capacitive voltage divider, “c” and “b”, placed in parallel with another capacitor, “a”. Capacitor “c” is the void, while “b” is capacitance in series and “a” the unvoided capacitance of the sample.

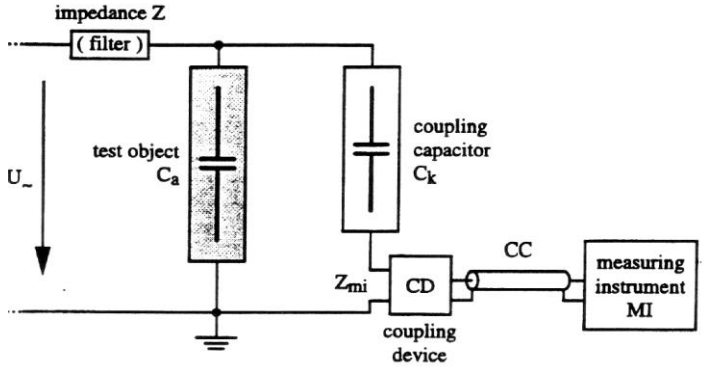

Figure 73: Basic test circuit [20]

As shown in Fig. 73, the object under test is place in parallel with a coupling capacitor and a filter. This is to enable circulating of charge within predetermined closed circuit. Calibration of the measuring instrument with a calibration is needed to ensure that the circuit is working accurately and able to be calibrated in pC.

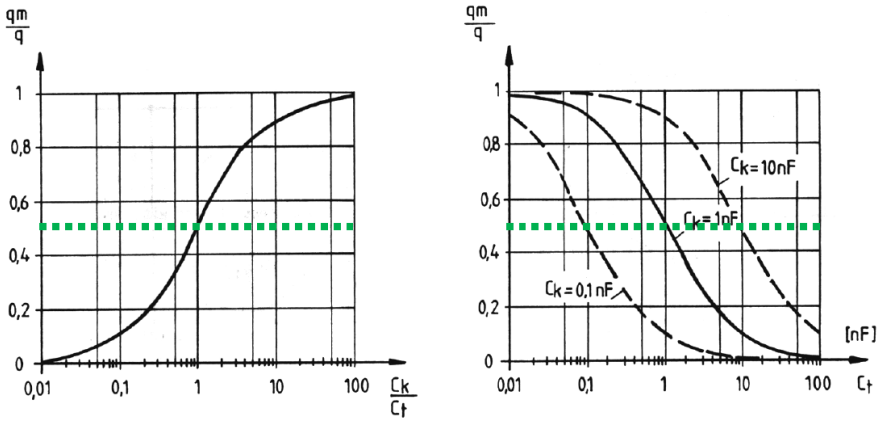

Figure 74: Influence of couple capacitor C_k [20]

As shown in Fig. 74, the coupling capacitor needs to be much larger than the test object in order to produce better sensitivity and not affect the results of the test.

5.3 Preparation of Small Scale Test

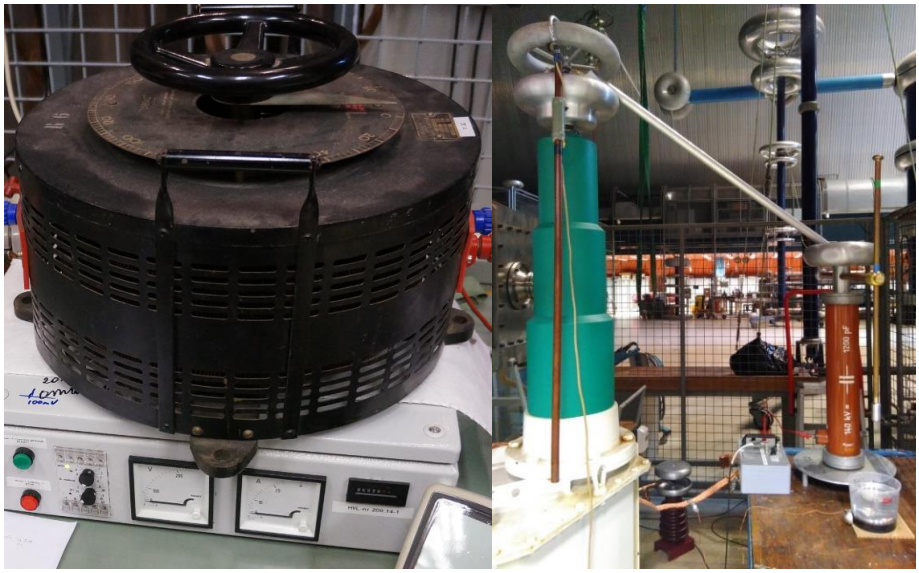

Figure 75: Small scale PD test setup

As shown in Fig. 75, preparation for the partial discharge (PD) test, had a few main components. In Fig. 75, the low voltage AC generator is on the left, the high voltage AC transformer in green, the coupling capacitor in brown, the test electrode slightly to the right and the sample below it.

To calibrate the setup, verification of the transformer turns ratio was performed with two voltmeters as shown on the left in Fig. 76, and with the box shown on the right of Fig. 76. The highest voltage possible on this setup was 40 kV, which was suitably sufficient for the pre-calculated tests of up to 30 kV.

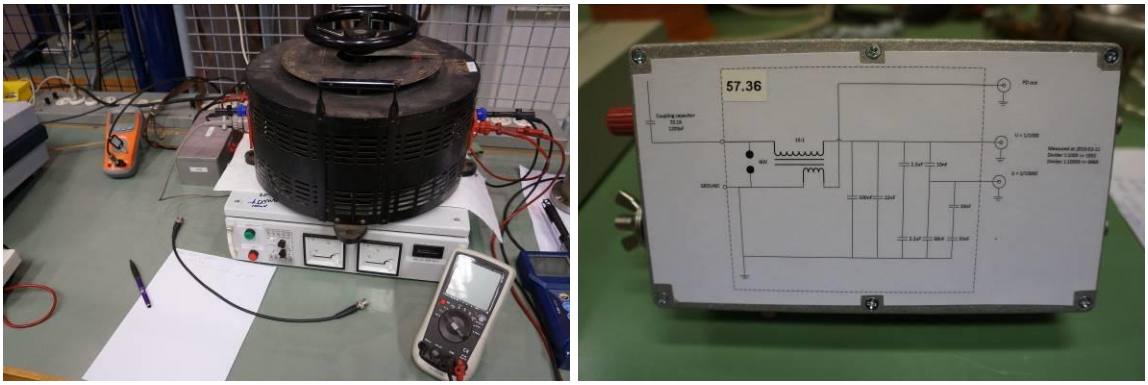

Figure 76: Small scale voltage calibration

When a known input is entered and seen on the white voltmeter, there is an expected output value on the orange voltmeter. Deviation from the expected output value indicates the behaviour of the system is not correct. Once the system is verified to be sound, verification for the PD setup can be done.

Figure 77: Small scale PD calibration

The setup for PD calibration used a Haefely DDX-9101 PD sensor as shown on the right of Fig. 77, and a communication box on the left of Fig. 77. A calibrator is used, producing known amount of charge, and the PD sensor is adjusted accordingly to different levels.

5.4 Electrodes in Small Scale Test Setup

Two different types of electrodes were used in this test. The diameter used in the electrode shown on the left in Fig. 78 is 25 mm, and is made out of a cylindrical body with a semi-spherical tip. The cable used on the right of Fig. 5 had a diameter of 20 mm. The ground electrode is flat, and the distance between the ground and the electrode is 15 mm.

Figure 78: Electrode (left), cable replicate (right)

The electrode on the left of Fig. 78 was chosen because of simplicity and produced a point-plane electric field that was neutral and general. The electrode on the right was chosen as it provided reproduction of the conductor-polyethylene interface found in actual conditions.

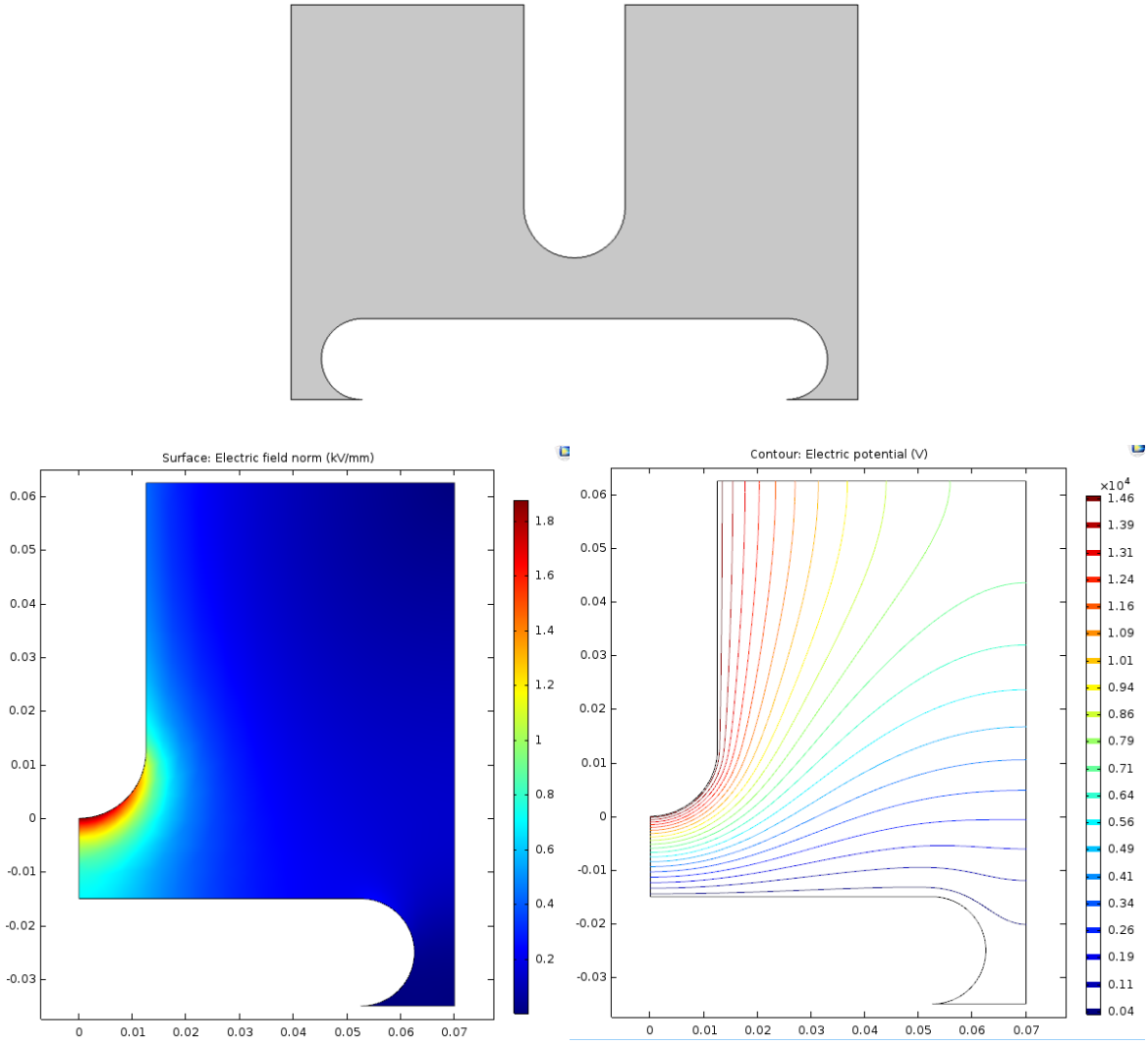

Figure 79: Clockwise from top left, Simulation geometry, Equipotential lines at 15 kV, Electric field strength at 15 kV

As shown in Fig. 79, the electrode used was composed of a cylindrical body and a semi-spherical tip, all shape edges had been smoothen out to reduce unwanted field enhancement. Applied voltage of 15 kV generated a maximum electric field strength of 1.8 kV/mm, which was approximately similar to the 1.4 kV/mm peak field strength on the actual setup. The distance between the two electrodes were 15 mm. The purpose of this setup was to achieve comparable interchange of the field strength from the electrode to the actual setup.

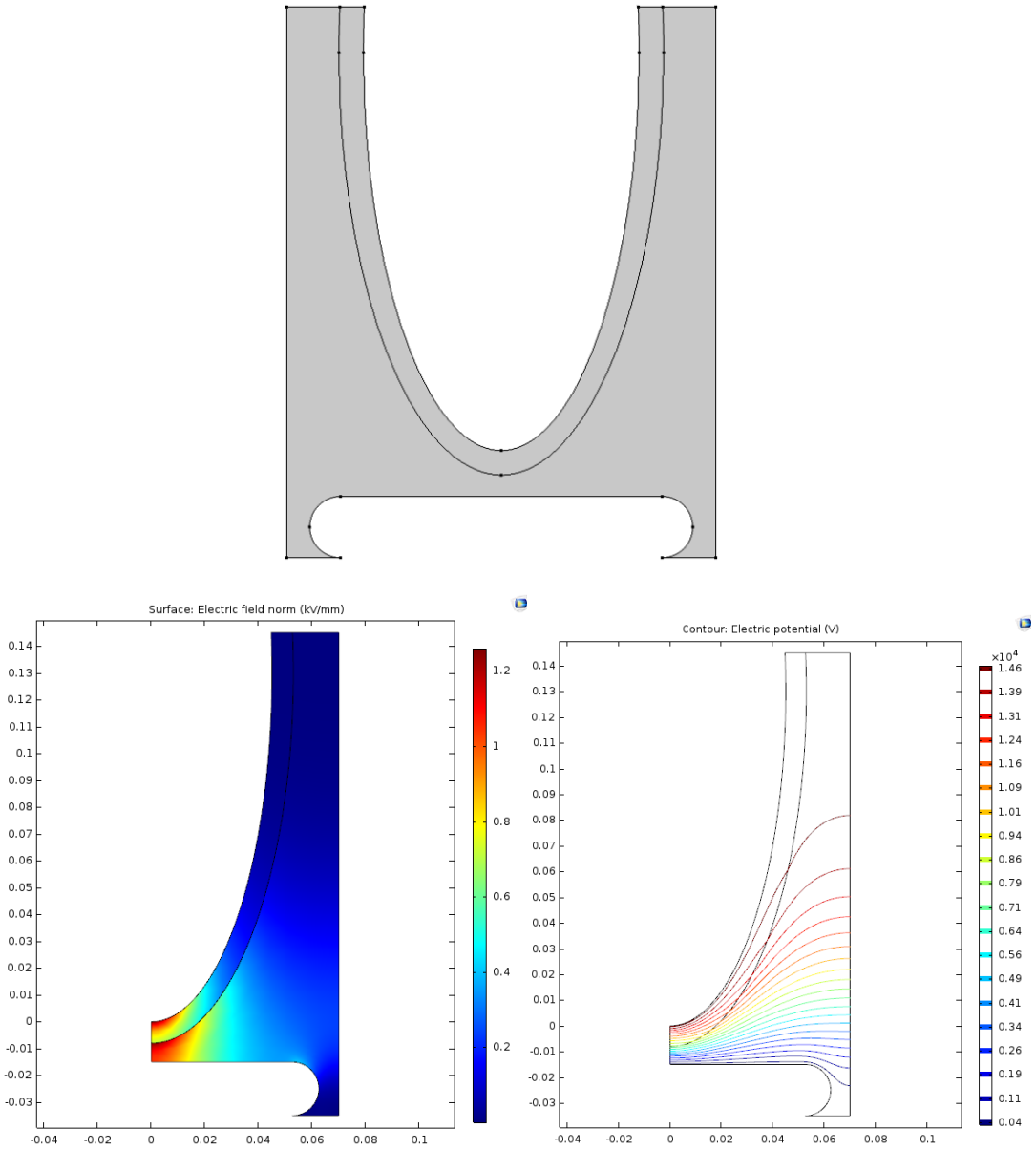

Figure 80: Clockwise from top left, Simulation geometry, Equipotential lines at 15 kV, Electric field strength at 15 kV

As shown in Fig. 80, the cable setup was used to emulate the electric field behaviour coupled with an insulating interface. Applied voltage of 15 kV generated a maximum electric field strength of 1.2 kV/mm, which is approximately similar to the 1.4 kV/mm peak field strength on the actual setup. The distance between two electrodes were 15 mm. The purpose of this setup was to have an insight into a setup that had similar field strength and interface to the actual setup.

5.5 Small Scale Test Conditions

As mentioned in the previous section, voltage, moisture content and temperature were varied in this test.

Voltage: 0 to 30 kV

Electric field: 0 to 2 kV/mm

Moisture content: Dry oil, oil in climate chamber for 16 hours at 40% humidity and 75ºC (60 ppm), oil in climate chamber for 32 hours at 40% humidity and 75ºC (120 ppm), 1 ml of free water in random small drops.

Temperature: 30 ºC to 60 ºC

Breakdown was found previously to have a ceiling value of around 36 kV/mm for dry oil, floor value of 2.8 kV/mm for oil containing 600 ppm of moisture and it was decided that 2 kV/mm was sufficiently safe enough for the test.

The electrode and cable setup was tested to be free of PD in air for 30 minutes at 30 kV.

5.6 Small Scale Test Procedure

The sample was heated up to 60ºC and tested at different voltages whilst decreasing in temperature. Durations of interest were evaluated with NQP analysis, to observe the number, charge and phase. NQP analysis overlaps time frames of 5 seconds, producing the total charge magnitude and phase for a given duration.

5.7 Dry Oil

Dry oil that was degasified and heated up was tested for PD at 30 kV, 30 minutes and 60ºC.

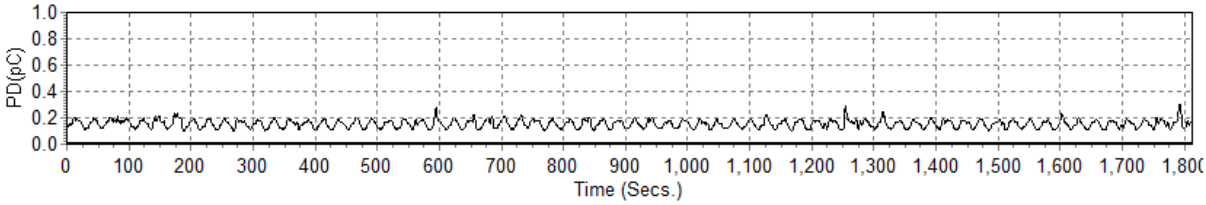

Figure 81: PD results of dry oil, electrode

As shown in Fig. 81, there was no PD detected at 30 kV, 30 minutes, 60ºC with the electrode configuration. The sample was deemed PD-free at those conditions.

5.8 Oil with Added Moisture Content

The goal is to observe the effects of dispersed and free water during PD detections. It has been seen from permittivity, tan delta and breakdown tests in previous chapters that increased moisture content altered the original characteristic of the oil. Knowledge coupled with previous results predicted PD activity in the presence of increased moisture content and decreasing temperature.

Oil sample was deemed PD-free for 60 ppm of moisture content, at 30 kV, 30 minutes, 60°C, with the electrode configuration.

5.8.1 Oil with 120 ppm Moisture Content, 60°C ,15 kV, Electrode

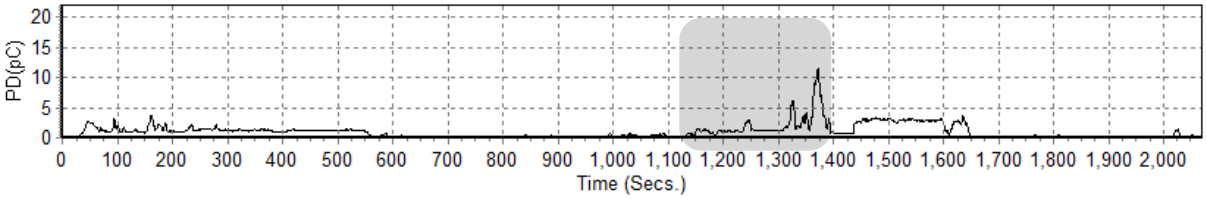

Figure 82: PD results of 60°C oil in climate chamber for 32 hours, 15 kV, electrode

As shown in Fig. 82, there was noticeable PD activity after approximately 20 minutes of observation, with several peaks. Further analysis of approximately 5 minutes was conducted on the period of interest and is as given below from Fig. 83 to 87. In that observed period, there was an average of 10 pC of charge, equally on both the positive and negative cycle, peaking at 90°.

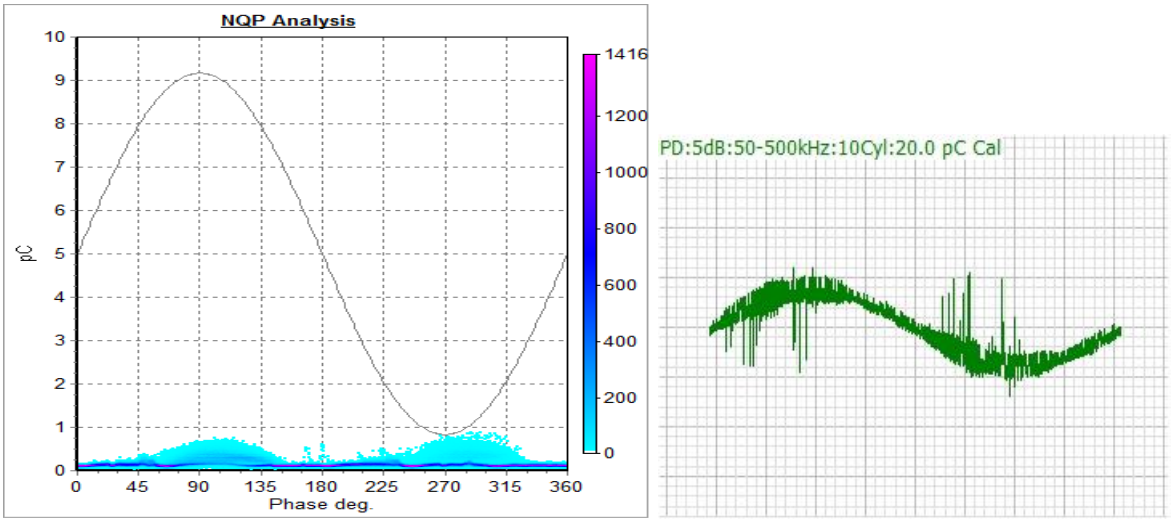

Figure 83: PD activity at 20 seconds

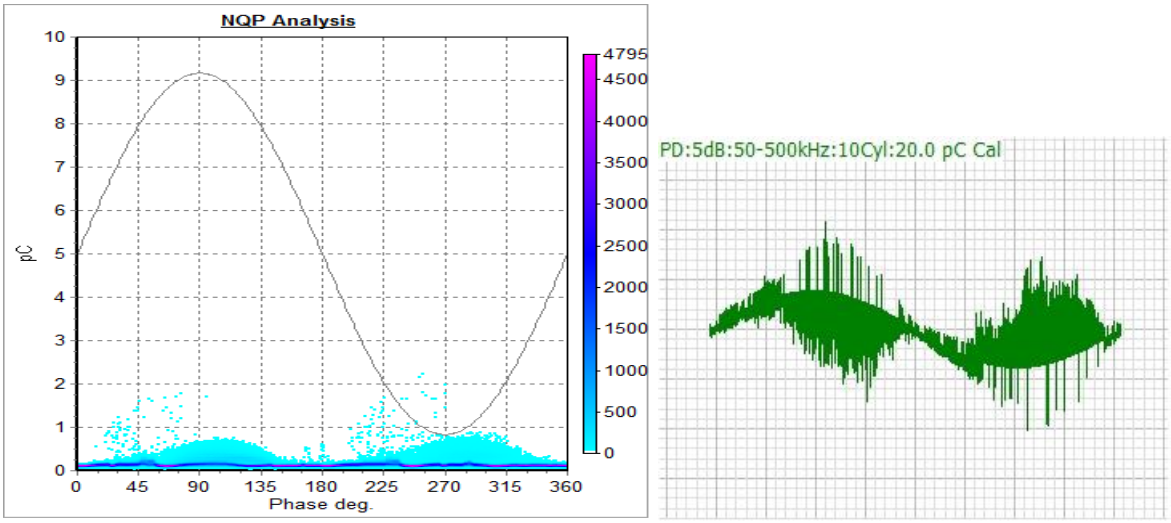

Figure 84: PD activity at 70 seconds

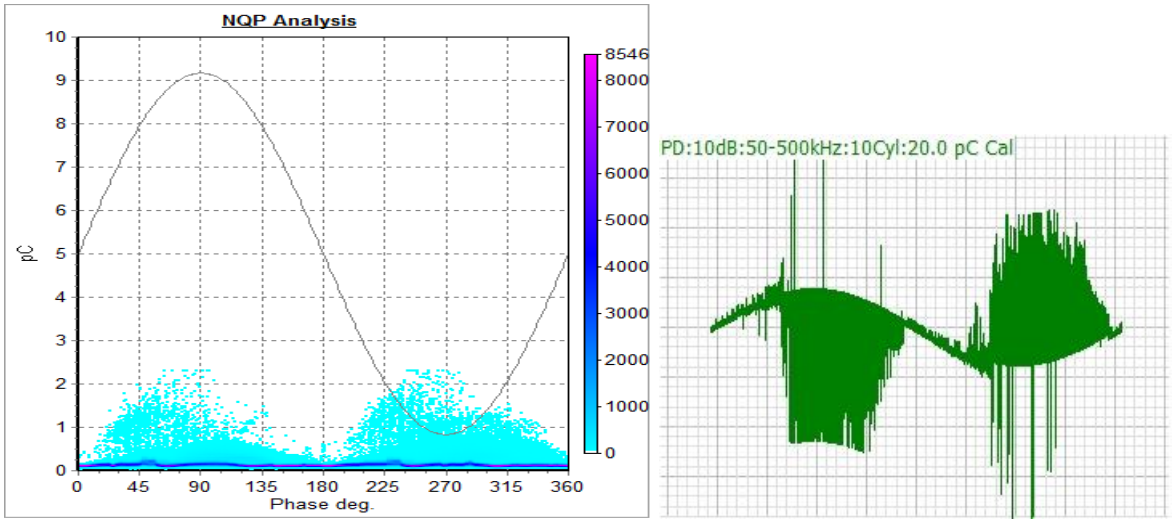

Figure 85: PD activity at 125 seconds

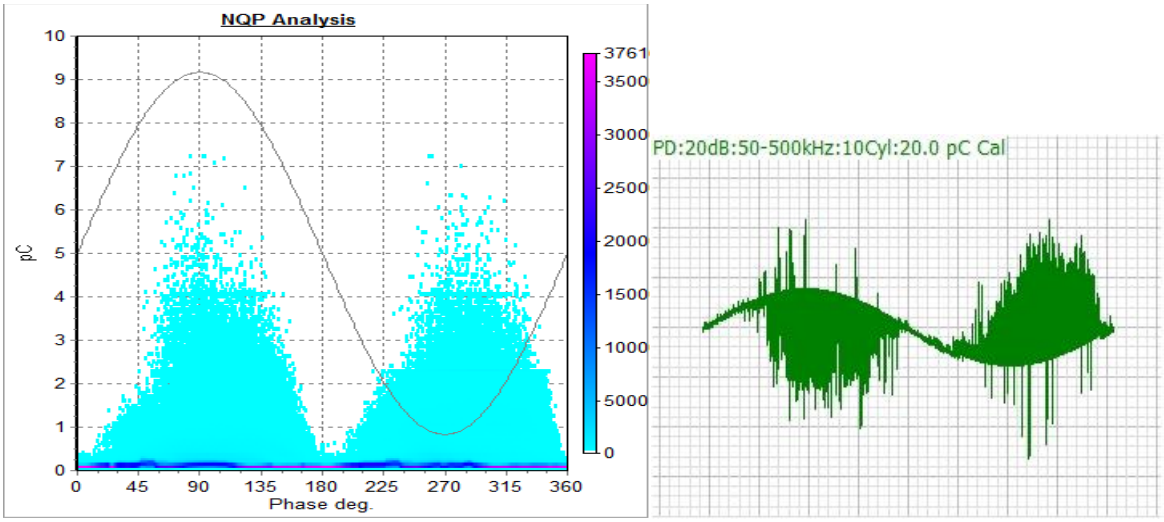

Figure 86: PD activity at 420 seconds

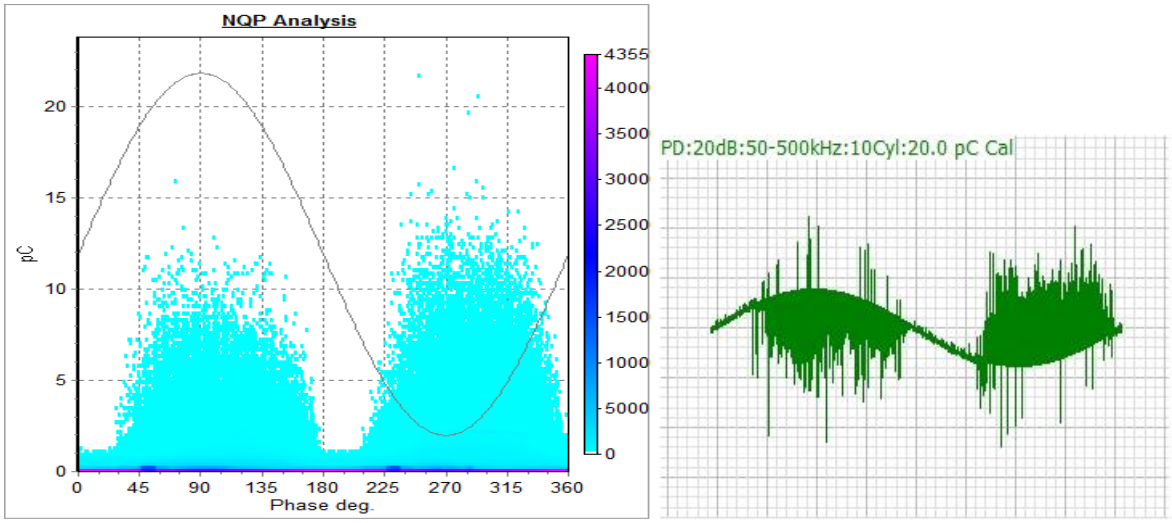

Figure 87: PD activity at 310 seconds (peak value)

5.8.2 Oil with 120 ppm Moisture Content, 50°C ,10 kV, Electrode

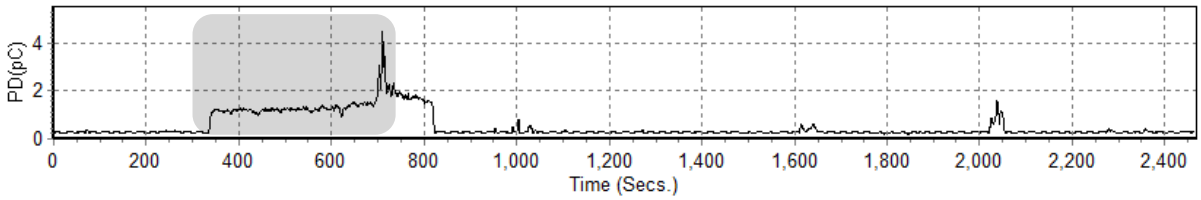

Figure 88: PD results of 50°C oil in climate chamber for 32 hours, 10 kV, electrode

As shown in Fig. 88, there was noticeable PD activity after approximately 5 minutes of observation, with several peaks. Further analysis of approximately 7 minutes was conducted on the period of interest and is as given below from Fig. 89 to 91. In that observed period, there was an average of 2 pC of charge, equally on both the positive and negative cycle, peaking at 90°. There was also over-excitation of the sensor in Fig. 91, as the sensor registered only slightly above 2 pC and constant throughout the phase.

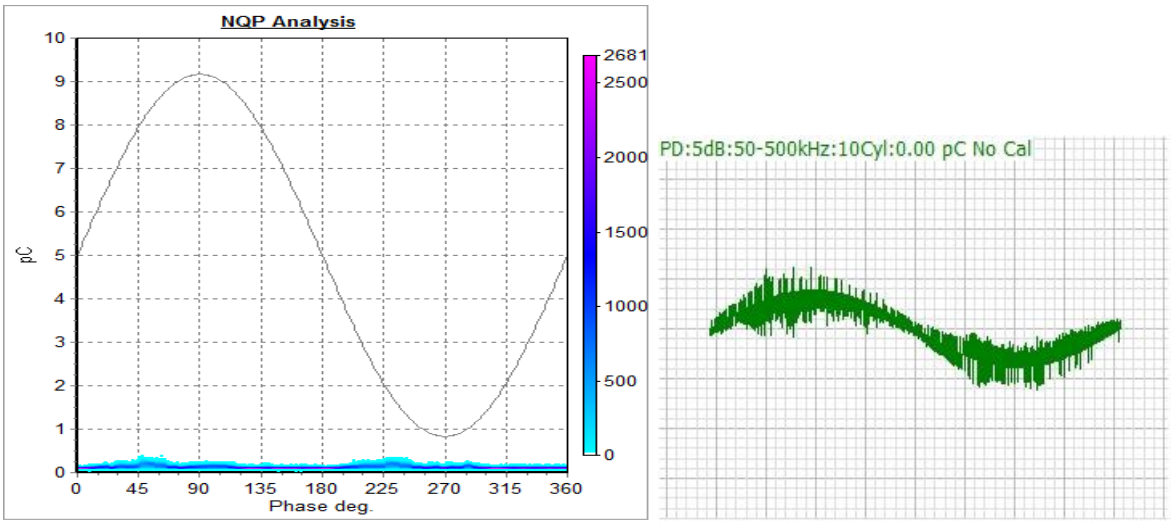

Figure 89: PD activity at 60 seconds

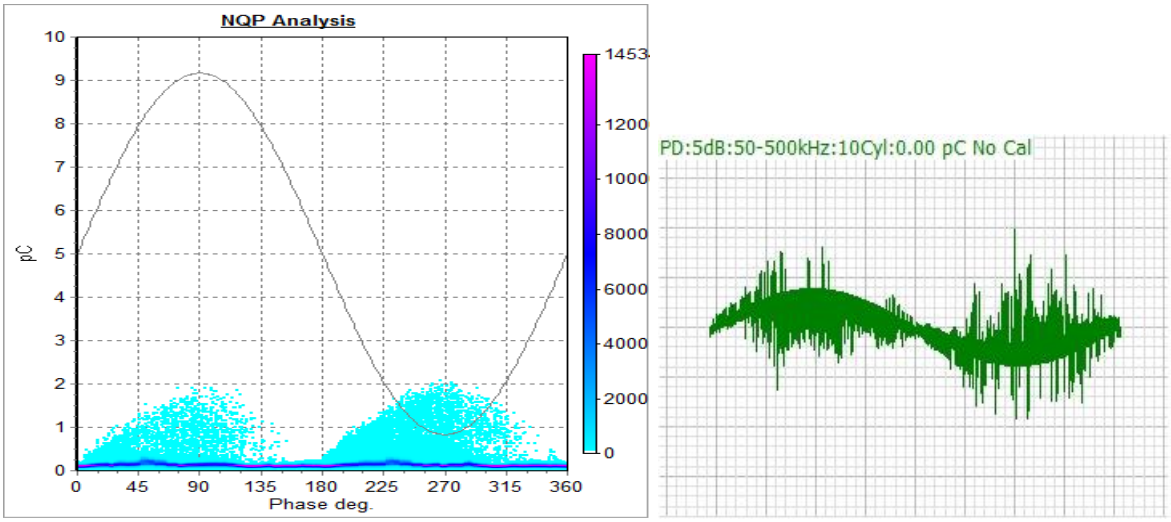

Figure 90: PD activity at 240 seconds

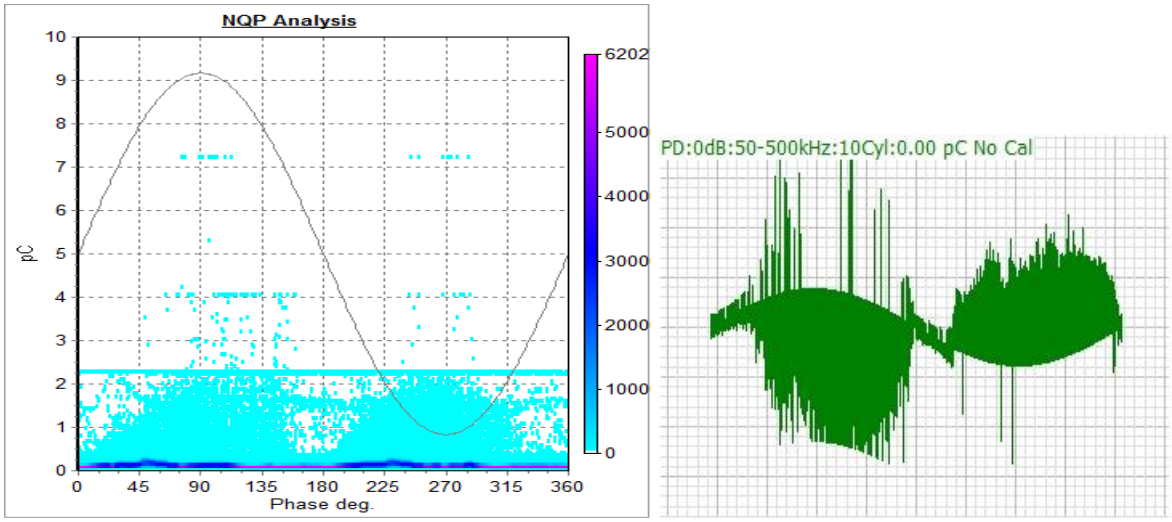

Figure 91: PD activity at 430 seconds (peak value)

5.8.3 Oil with 120 ppm Moisture Content, 40°C ,5 kV, Electrode

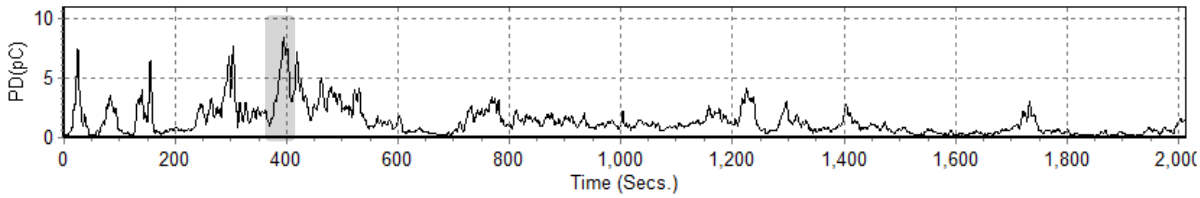

Figure 92: PD results of 40oC oil in climate chamber for 32 hours, 5 kV, electrode

As shown in Fig. 92, there was noticeable PD activity after approximately 5 minutes of observation, with several peaks. Further analysis of approximately a minutes was conducted on the period of interest and is as given below from Fig. 93 to 95. In that observed period, there was an average of 3 pC of charge, equally on both the positive and negative cycle, peaking at 90°.

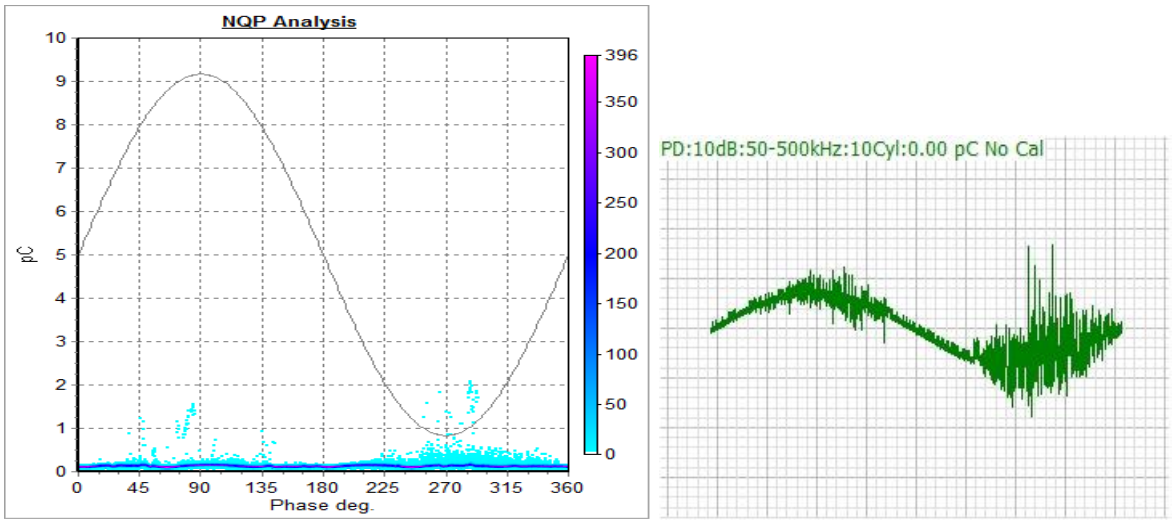

Figure 93: PD activity at 5 seconds

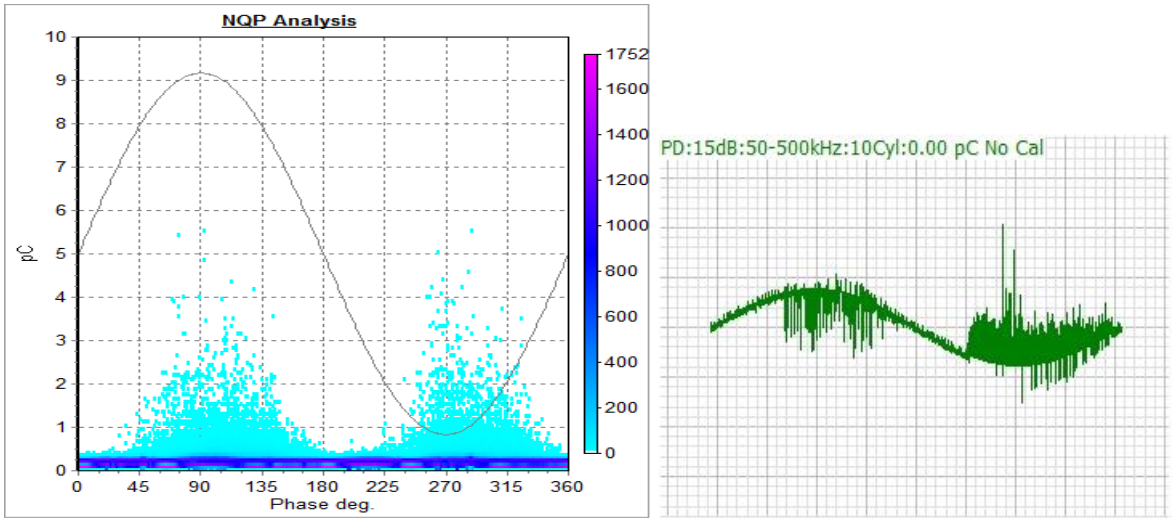

Figure 94: PD activity at 30 seconds

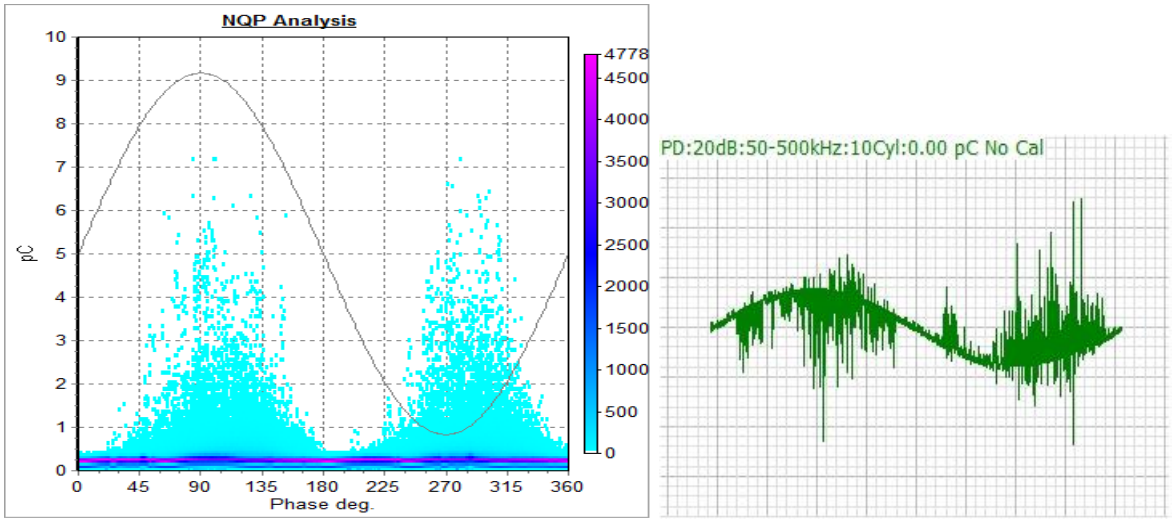

Figure 95: PD activity at 70 seconds (peak value)

5.9 Oil with 1 ml of Sprayed Free Water, Electrode

Figure 96: 60°C Oil with 1 ml free water, electrode

As shown in Fig. 96, free water was sprayed on the oil to simulate conditions of free water droplets. Approximately 1 ml of demineralised water was used and allowed to sink. Even though 15 kV provided the field strength that was similar to the actual setup, it was too high and caused breakdown. 5 kV was chosen instead.

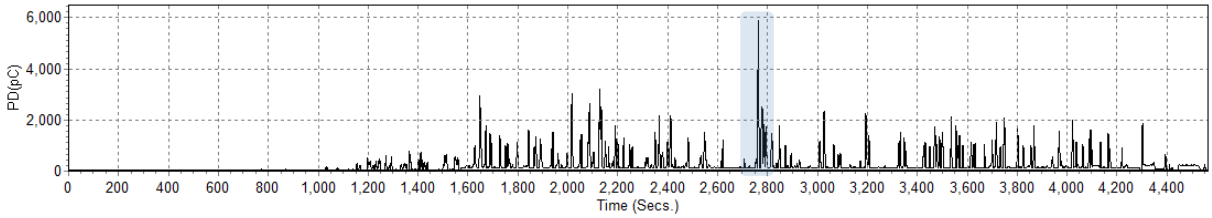

Figure 97: PD results of oil with 1 ml of sprayed free water, electrode 5 kV

As shown in Fig. 97, with a start point of 1200 seconds considered, there was noticeable PD activity after approximately 25 minutes of observation, with numerous peaks. The delayed start of the observation was to allow the water droplets to sink. Further analysis of approximately 2 minutes was conducted on the period of interest and is as given below from Fig. 98 to 99.

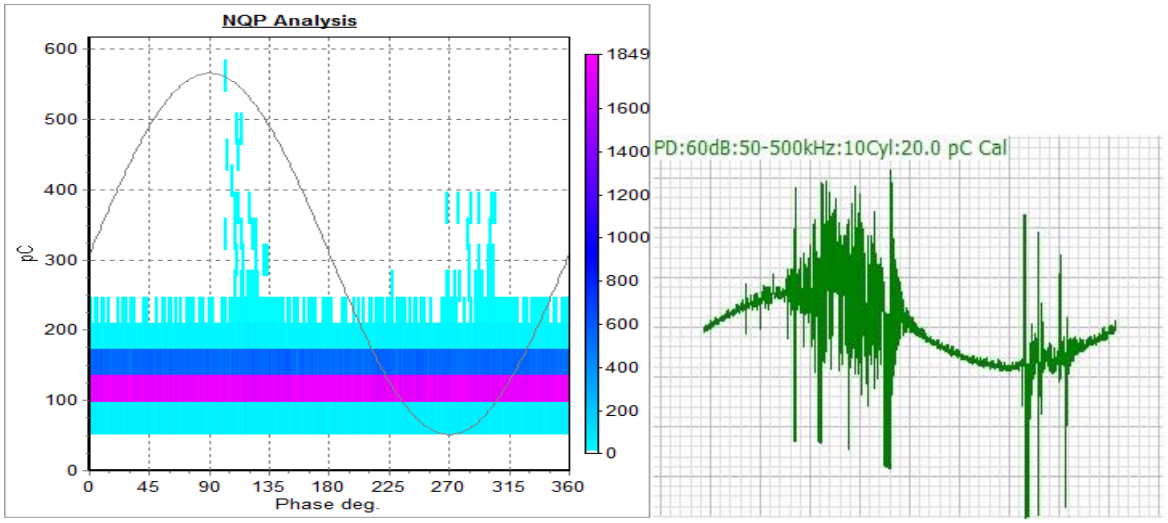

Figure 98: PD activity at 15 seconds

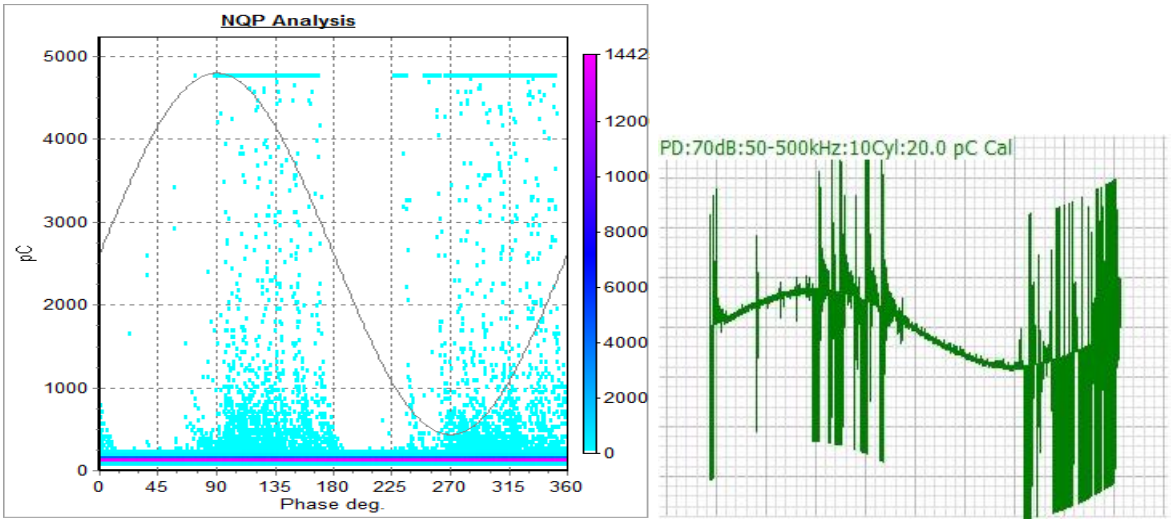

Figure 99: PD activity at 120 seconds (peak value)

5.9.1 PD Results, 1 ml Sprayed Free Water, Electrode

Water droplets were attracted to the electrode at 5 kV, which created a water channel between the electrode and ground. As evident from Fig. 98 to 99, with the presence of physically larger free water droplets, there was much higher PD activity.

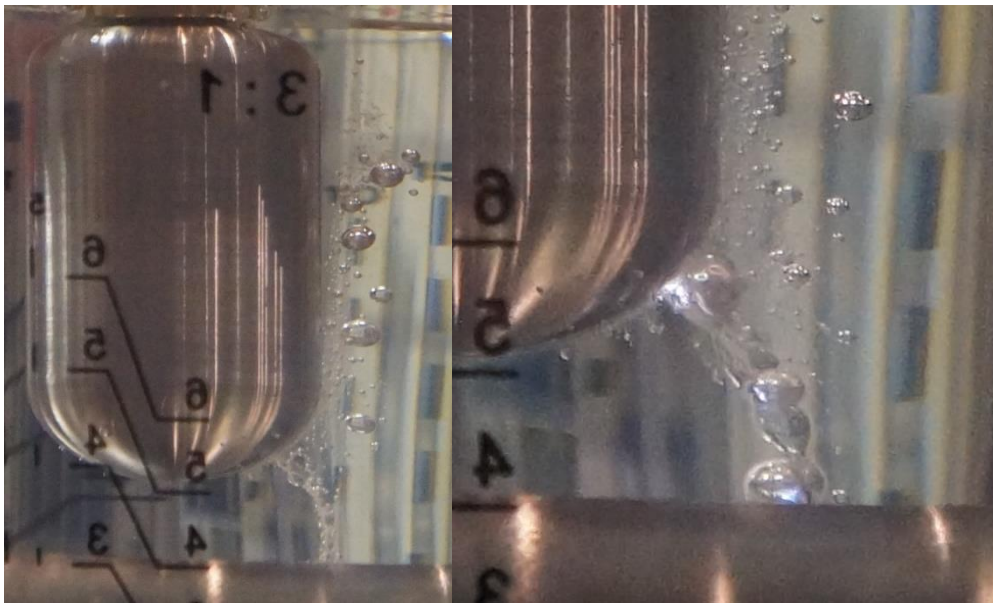

Figure 100: Water droplets attracted (left); Water channel between the two electrodes (right)

As shown on the left in Fig. 100, water droplets were attracted to the area of highest field strength. The water channel clearly showed the electric field line it followed. During the test, there was constant visible electron movement, as shown on the right in Fig. 100. This movement, when strong enough, would provide the conductive path needed for breakdown. It could be said that droplets of free water are potentially more dangerous than dispersed water.

5.10 Oil with 1 ml Sprayed Free Water, Cable

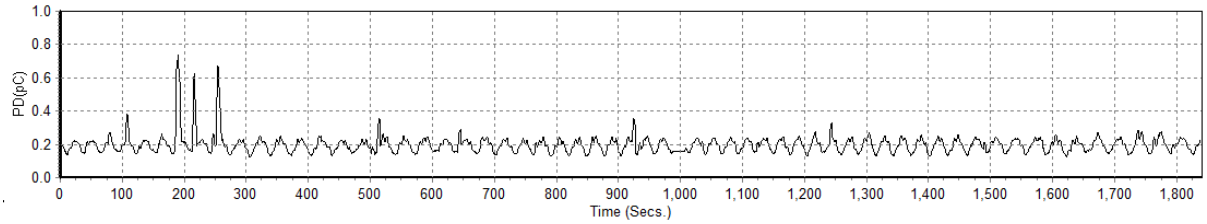

Figure 101: PD result of dry oil, cable

As shown in Fig. 101, there was no PD detected at 30 kV, 30 minutes, 60ºC with the cable configuration. The discharge at around 200 seconds was from air bubbles attached to the cable. The sample was deemed PD-free. 15 kV was used for the test because it provided similar field strength to the actual setup.

Figure 102: 60°C Oil with 1 ml free water, cable

As shown in Fig. 102, free water was sprayed on the oil to simulate conditions of free water droplets. Approximately 1 ml of demineralised water was used and allowed to sink.

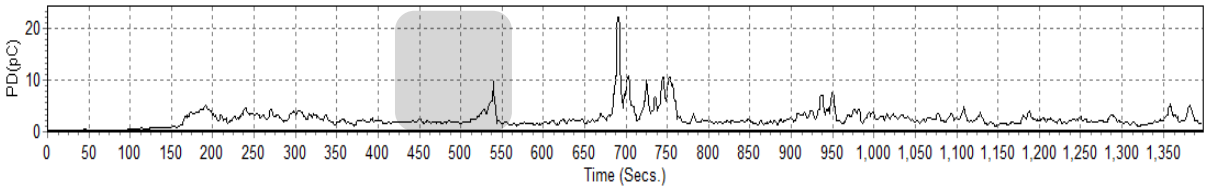

Figure 103: PD results of oil with 1 ml of sprayed free water, cable, 15 kV

As shown in Fig. 103, there was noticeable PD activity after approximately 2.5 minutes of observation, with several peaks. Further analysis of approximately 2.5 minutes was conducted on the period of interest and is as given below from Fig. 104 to 106. There was an unexpected stop of the NQP analysis at 950 seconds.

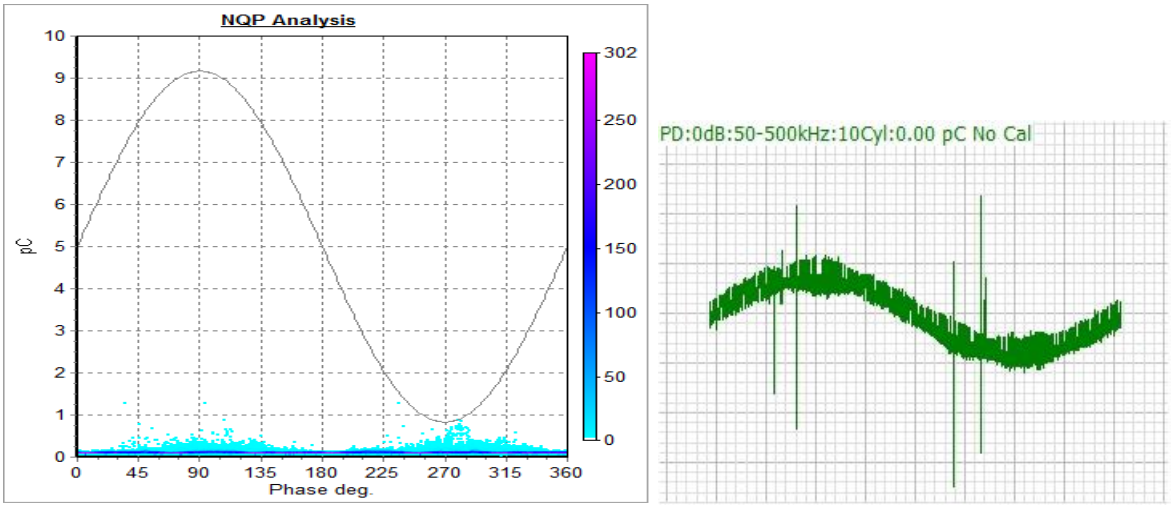

Figure 104: PD activity at 5 seconds

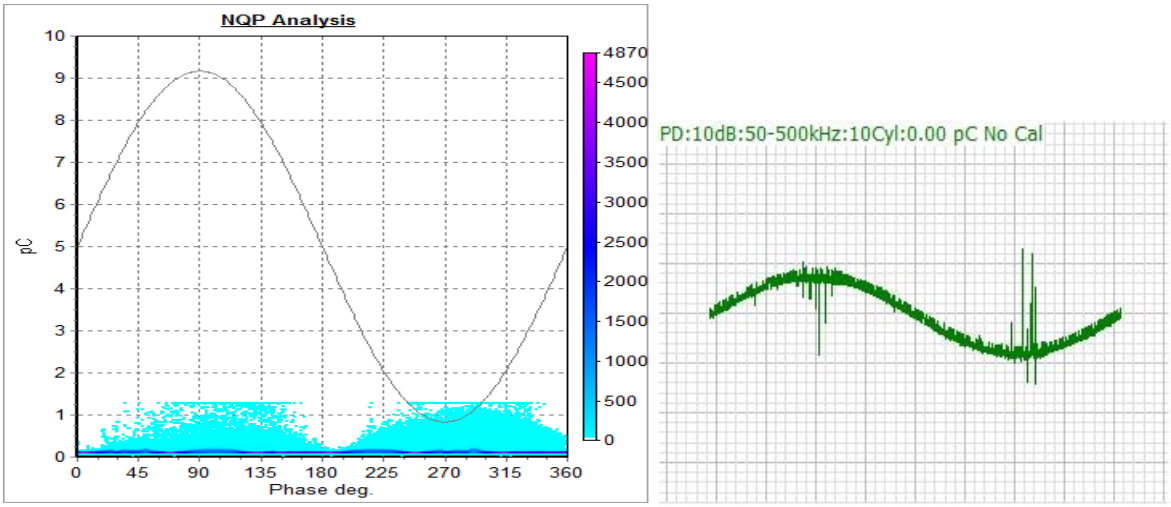

Figure 105: PD activity at 90 seconds

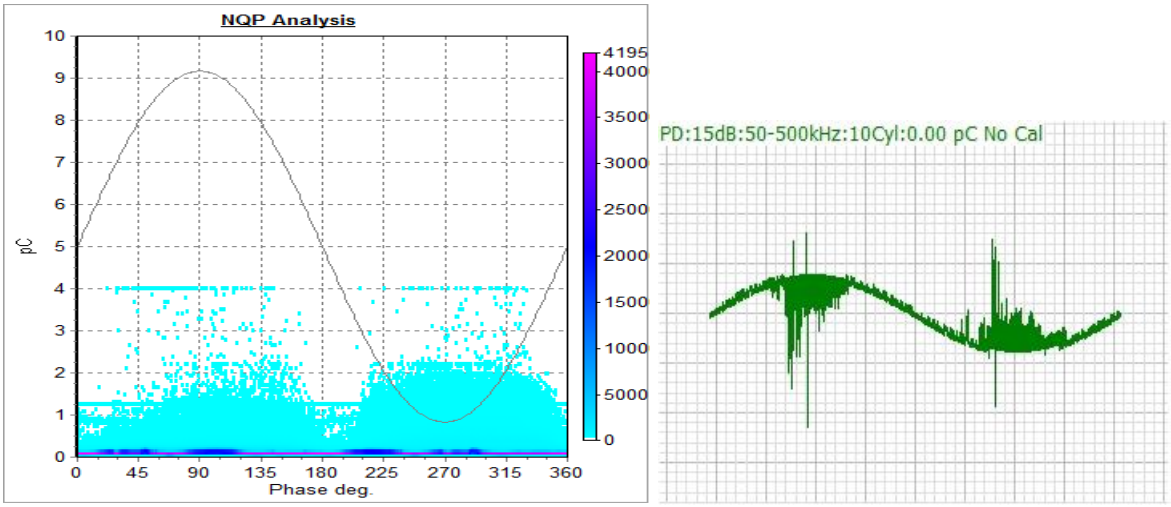

Figure 106: PD activity at 140 seconds (peak value)

5.10.1 PD Results, 1 ml Sprayed Free Water, Cable

In the first two minutes after an steady state electric field was establish, water droplets spread out randomly on the surface were attracted downwards.

Under the influence of the electric field, the water droplets were elongated and disintegration occurred at the tip of the droplet, where the field strength is the highest. During these periods of moderately active elongation and disintegration, heighten PD activity was observed, as highlighted in the grey box in Fig. 103.

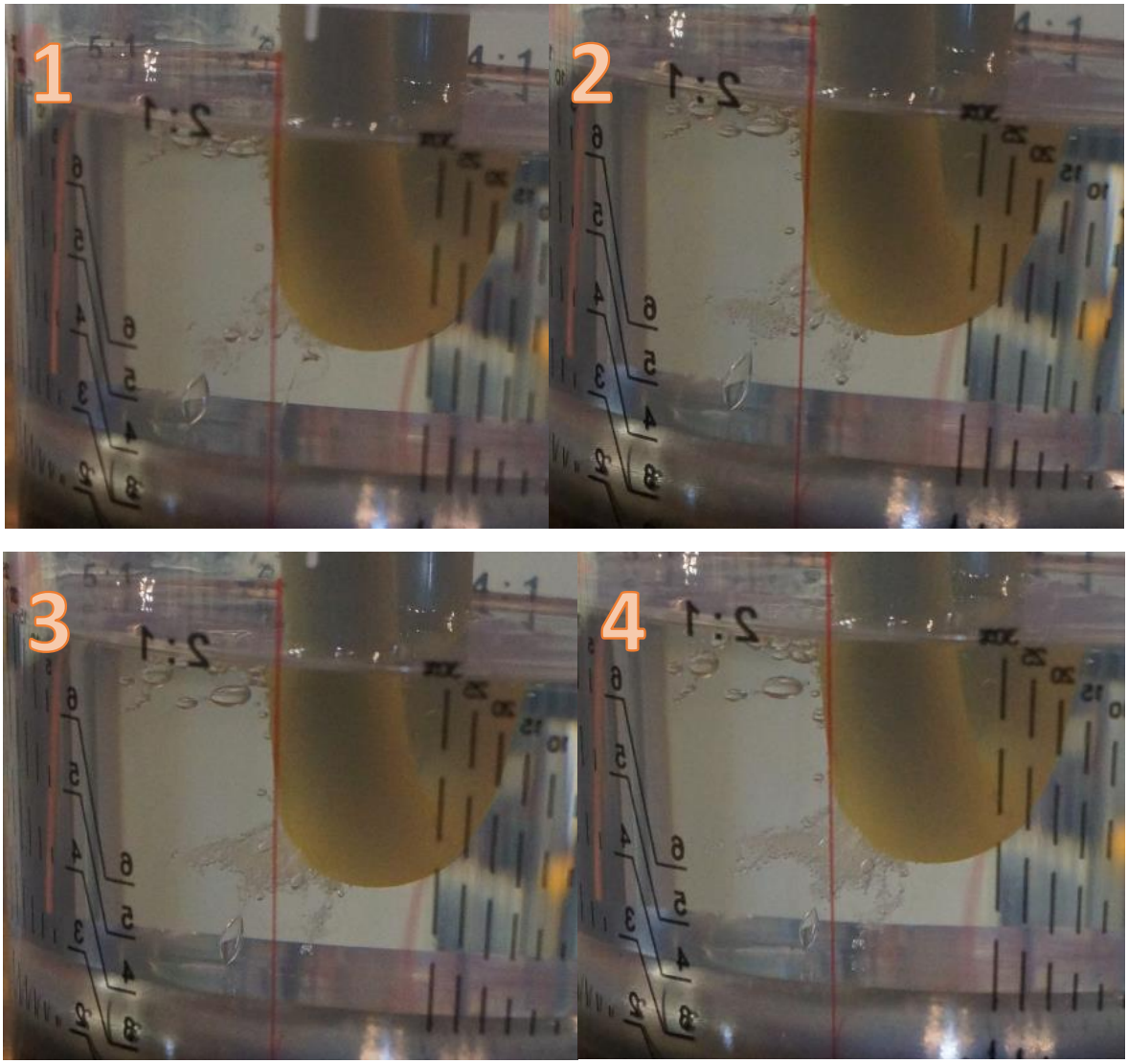

Figure 107: Relating PD activity to physical activity

The pictures were taken every 30 seconds as shown in Fig. 107, and are labelled from 1-4. As visible in the picture, elongation occurred, which created dispersion. It could be said that the recorded PD observation represented this physical activity.

5.11 Comparison of Small Scale PD Results

Comparison of PD results were done, to see the impacts from different types of moisture content and electrode material.

5.11.1 Comparison of PD Results between Dispersed and Free Water, Electrode

PD inception voltage of 5 kV for dispersed water at 40ºC was similar to 1 ml free water. The PD magnitude was dissimilar, the dispersed water had approximately 3 pC, while the free water had approximately 1000 pC. The PD pattern was similar for both cases, which was not unexpected. It should be noted that for both conditions, breakdown occurred once the voltage exceed 5 kV. Depending on the moisture condition within the oil, breakdown could occur slightly after a reading of 3 pC or after 100 pC. This gave the oil an unpredictable behaviour.

5.11.2 Comparison of PD Results with Free Water, between Electrode and Cable

PD inception voltage of the cable was at 15 kV, 10 kV higher than the electrode in the similar condition. The PD magnitude was approximately 1000 pC for the electrode, and approximately 1.5 pC for the cable setup. With a largely similar electric field, the electrode configuration had higher PD activity because there was no blockage of electron movement. However, the insulator might be exposed to irreversible internal degradation. The PD pattern was similar for both cases. Clipping was involved in both cases.

5.11.3 PD Results over a Temperature Range, Climate Chamber, Electrode

Figure 108: Left to right, 60°C, 50°C, 40°C, 30°C

As shown in Fig. 108, it could be clearly seen that with the decreased in temperature, the dispersion of moisture content was increased.

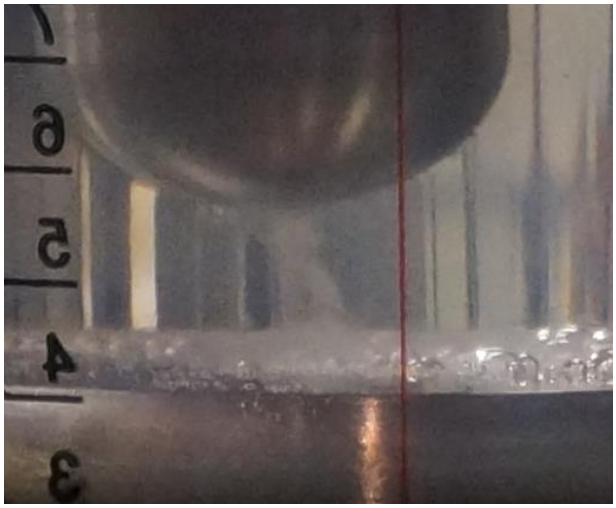

Figure 109: Water channel between the electrode at 60°C

As shown in Fig. 109, when a water channel is formed between electrodes, this allowed electron movement and PD activity was recorded.

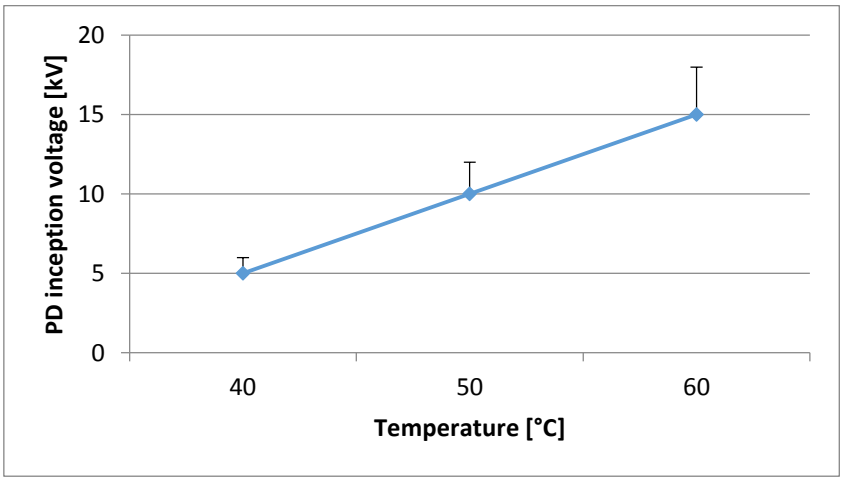

Figure 110: PD inception voltage of the oil sample at different temperature

As shown in Fig. 110, PD inception voltage occurred at different voltages for different temperatures. This variation could be attributed to the increased dispersion of water molecules in the oil, when the temperature decreased; a phenomenon that was well explained at the start. The PD patterns from the variations were largely similar and resembled an internal cavity.

5.12 Full Scale Partial Discharge Test

The goal of the experiment was to ascertain on a realistic scale, the information and knowledge obtained in previous chapters. The experiment was also to further understand the behaviour between the oil and water droplets under actual load conditions.

Figure 111: Full scale setup

As shown in Fig. 111, the full scale cable termination setup comprised of a piece of medium voltage cable as shown on the right. The cable was connected to a regular cable termination on one end and to a glass container on the other end for observation purposes. High voltage was applied through the transformer on the left and PD measurements were observed through a Haefely PD detector. Approximately 70 kV was applied during this test as this was similar to field conditions and to simulations used in previous chapters. Two sets, spaced 20 seconds apart, of water droplets approximately 1 ml in volume was dripped with PD and physical activities observed.

Figure 112: Placement of water droplets of approximate 1 ml, no applied voltage

As shown in Fig. 112, the first set of water droplets were released and was kept spherical through surface tension with the oil. There was no voltage applied. As known from previous chapters, the stress cone is the area of interest as the field enhancement is the highest.

Figure 113: Elongation and dispersion observed (left), Degradation on an elongated water droplet whilst getting dragged down by gravity (right)

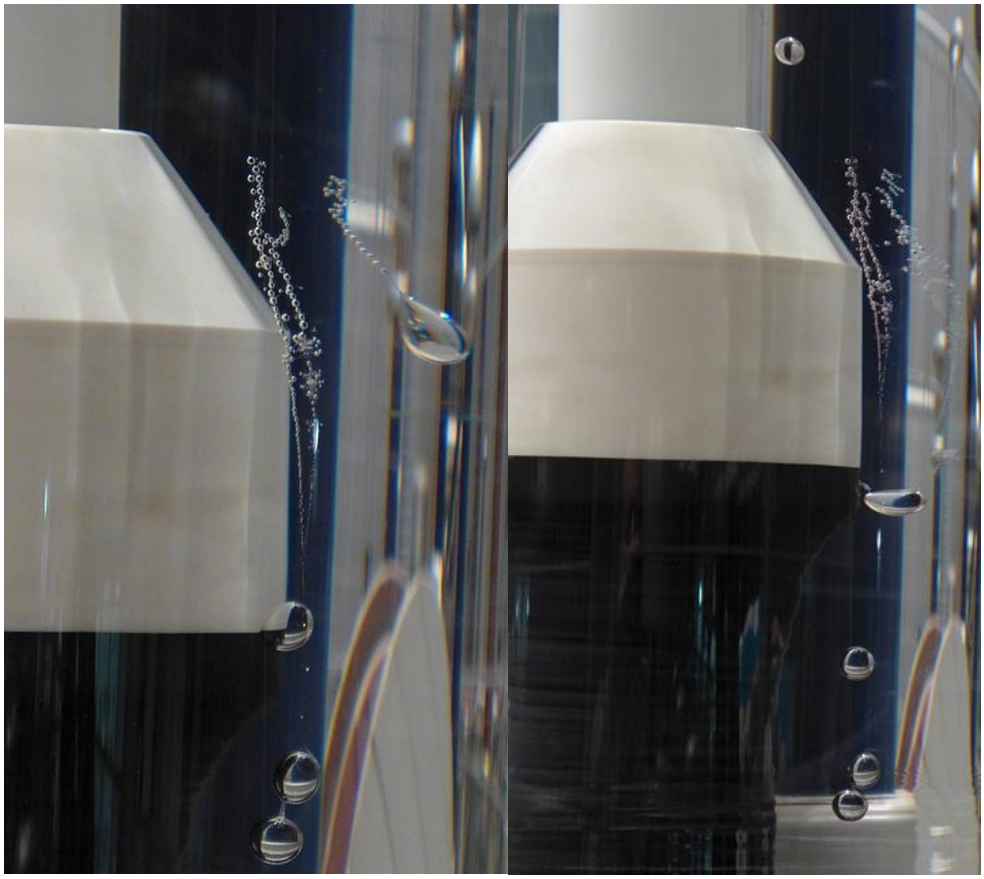

Figure 114: Close-up of dispersion faced (left); Halt of dispersion after water droplet leaves area of high stress (right)

As shown in Fig. 113 on the left, the water droplet was exposed to the electric field and though unable to be attracted in entirety, it was elongated and dispersion occurred when the critical field strength at the tip was met. As shown in Fig. 113 on the right, despite the main body of water droplet leaving the field of high concentration, dispersion continued at the tip of the droplet through field enhancement of a trail of tiny droplets.

As shown in Fig. 114 on the left, a cloud of smaller water droplet was attracted to the area of higher field strength after the main droplet body sunk due to gravity. As shown in Fig. 114 on the right, the trail of tiny droplet creation stopped after main droplet was no longer affected by the field enhancements.

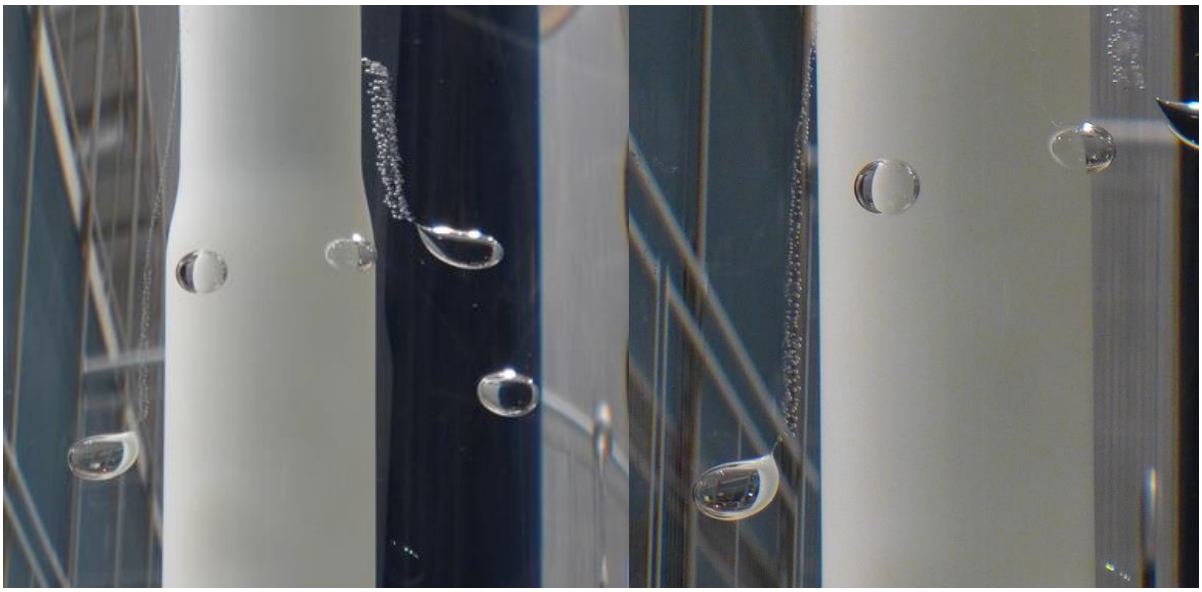

Figure 115: Degradation occurring at top (left); Clear evidence of larger radius resulting in smaller critical field strength (right)

As shown in Fig. 115 on the left, a second set of water droplets were released and immediately degradation of a larger droplet was observed as soon as the droplet entered a region of elevated field strength.

As shown in Fig. 115 on the right, droplets of water with a smaller radius was not affected by roughly the same field strength as the radius was smaller which resulted in a higher critical field strength. However, smaller droplets do not guarantee inactivity because if the droplet was smaller enough, it would be physically attracted and suspended in mid-air, where further coalesces and emulsion activities could take place.

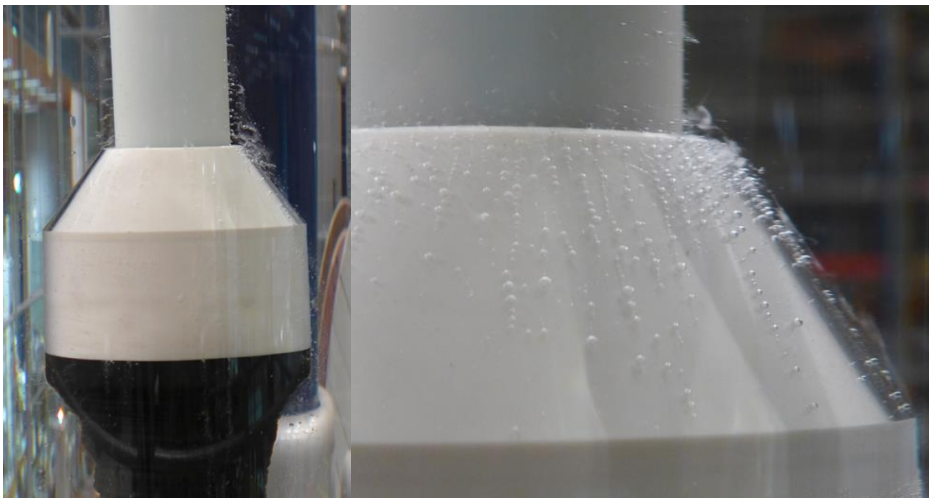

Figure 116: Remnant of attracted dispersed water droplet (left); Close-up of dispersed water around stress cone (right)

As shown in Fig. 116 on the left, the tiny water droplets were attracted to the stress cone and exposed to repetitive emulsion and coalesce. These water droplets were small enough to not sink and were polarised by the electric field. This resulted in a fine mist around the stress cone as shown in the close-up picture on the right of Fig. 116. As proved in previous chapters, the water droplets would be attracted to each other, further dispersed into smaller portions and continuously repeated.

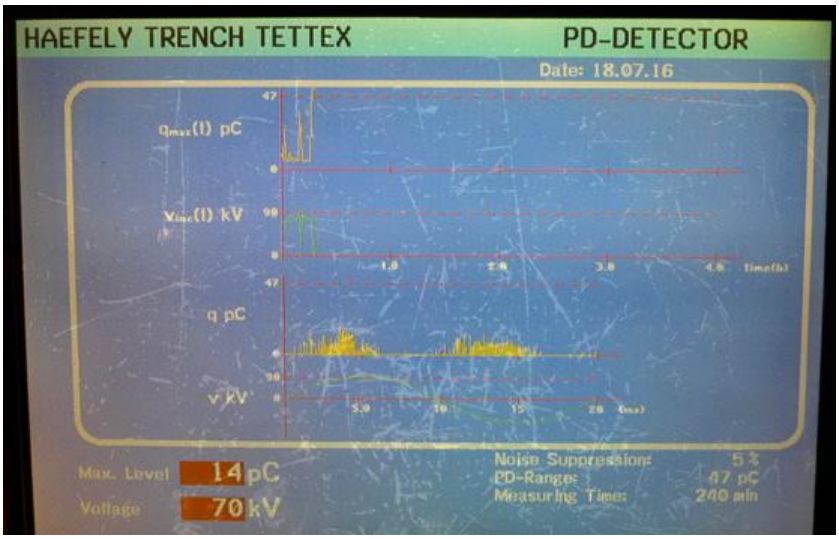

Figure 117: PD activity observed

As shown in Fig. 117, the elongation of water droplets and later dispersion was directly related to PD activity – this observation is consistent to previous chapters. Magnitude of 14 pC was observed, with an average of 7 to 8 pC, which was similar to previous recorded PD activities. The PD patterns obtained were largely similar, with a mixture of internal and surface discharge, but was more inclined towards internal discharge. As proven in previous chapters and shown in this experiment, the deformation of water droplets can be healthily indicated by an internal discharge PD pattern.

5.13 Discussion of Partial Discharge Test

Through the range of small scale experiments, it can be seen that PD activity can be attributed to the elongated and disintegration of water droplets. As shown in the experiments, PD inception voltage occurred at different voltages for different temperatures due to the difference in dispersed water content. The PD patterns observed from the varying experiments were largely similar and resembled an internal cavity.

Through the full scale PD measurement, it can be seen that the results and knowledge obtained from the small scale test was verified on the full scale setup. With elongation and deformation of water droplets relating to PD activity. It can be said that any elongation and deformation of water droplets are the cause of PD activity.

6 Conclusion and Future Work

6.1 Non-intrusive Diagnostic Methods with Performed Experiments

The main intention was to gather all the known diagnostic techniques and produced a method that could provide knowledge of polluted terminations during operating conditions. This is more cost efficient and would allow continued operations, which is desired.

Samples taken to check for moisture content, permittivity and breakdown values reveal sufficient information, but fall under the intrusive category and are thus not suitable.

Tan delta test produced favourable results, but the complexity of the operation makes it impossible on operational terminations. The tan delta test requires isolation of the test object to ascertain the quality of the cable insulation but the cable is intrinsically linked to the system and the required isolation is not possible.

Partial discharge is the only non-intrusive method possible for such a diagnosis, as clearly proven in the chapters leading up. However, the limitations are that presence of PD activity can only provide a signal of water content around areas of field strength. There exist a possibility of water content at the base of the termination whilst showing no PD activity. As shown before, unless the field strength at the tip of the water droplet exceeds the critical level, the water droplet will not disintegrate and not provide any information.

As shown in Chapter 2, when the sample is heated up, it would cause water to gain energy and rise, this movement when passing the areas of higher field strength would translate into PD activity.

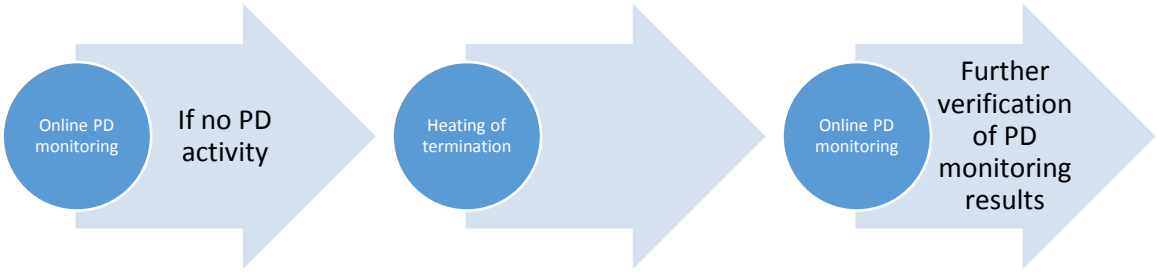

Figure 118: Order of Verification

Therefore, for a comprehensive verification, PD monitoring should be conducted initially and a second time when the sample is heated up as shown in Fig. 118. Dry conditions will return little to no results, whereas contaminated samples will produce significant PD activity. Such a test is safe, as it will not lead to breakdown due to the quick processing time. It is also physically viable, as the termination was filled with hot oil initially and sealed, causing it to be pressurised when the oil cools down, heating of the oil will return the conditions to the initial stages.

6.2 Conclusion

Moisture content in oil-filled cable termination is harmful. It degrades the dielectric properties, causes partial discharge activity and can lead to ageing of insulation, and in severe cases, breakdown. More often than not the presence of moisture content is not immediately felt, but over time contributes significantly.

As shown through the breakdown test conducted, the breakdown strength of the oil decreased exponentially with the introduction of moisture, with a critical point of roughly 100 ppm. The breakdown strength is also affected by a sufficiently large water droplet due to a reduction in critical field strength as a result of a larger radius.

In general, the dielectric constant of the oil was not considerably affected with the introduction of moisture, but the dielectric loss had a more prominent result. When exposed to change in temperature, regions of 40^{o}C to 60^{o}C have the most activity for dielectric constant and loss. This temperature region is also the range physically faced by the termination, as the large amount of volume in the termination affects the convection rate.

Heat is also a parameter of concern as it changes the viscosity and conductivity of the liquids involved. Heat reduces the viscosity of the oil which helps with movement, but causes the conductivity of water to increase which is undesirable. Cooled oil will greatly retard the migration of water droplet to regions of high stress, but will also greatly contribute to retention of water droplet to regions of high stress if present.

Water content can also have the potential to go undetected at the base of the termination, only to rise again during temperature cycling. This could be provide untrue results if just a partial discharge measurement was performed. To attain optimal results and insight, combination of heating and partial discharge measurements would provide adequately strong results.

6.3 For Future Work

As it is evident that partial discharge is indicative of water content within a termination at the areas of field strength, though knowledge of potential water content at the base is lacking. Research could be performed for a sensor to be designed and placed at the base of the container that provides information of free water content. The sensor should be able to monitor not only locally, but the entire base. This approach coupled with online PD monitoring will provide sufficient information to identify possible contaminated terminations.

- Further identification of PD patterns
- Installation of online PD monitoring
- Research into sensor that observes entire base of tank for free water
- Coordination between PD monitoring and free water sensor to provide optimal detection

References

[1] F. H. Kreuger, Industrial High Voltage - Volume I, Delft: Delft University Press, 1991.

[2] C. W. G. B1-29, *Guidelines for maintaining the integrity of XLPE cable accessories.*

[3] K. B. Liland, A. K. Bjorke, S. Hvidsten, H. Faremo and E. Bjerkan, "Failure Modes and Condition Assessment of High Voltage Oil Filled XLPE Termination," in *IEEE Electrical Insulation* , 2009.

[4] G. Birkenes, *Examinations of Water Induced Electrical Breakdown in Oil-Filled Terminations,* MSc Thesis, 2010.

[5] E. Ildstad, *Water Migration and Water Treeing in Cross-Linked Polyethylene Cables,* PhD Thesis, 1985.

[6] S. B. Sample, B. Raghupaty and C. D. Hendricks, "Quiescent Distortion and Resonant Oscillations of a Liquid Drop in an Electric Field," *International Journal of Engineering Science,* vol. 8, no. 1, pp. 97-109, 1970.

[7] M. H. Davis, "Two Charged Spherical Conductors in a Uniform Electric Field," RAND Corporation, 1964.

[8] G. Taylor, "Disintegration of Water Drops in an Electric Field," *Proc. R. Soc. Lond.,* vol. 146, pp. 383-397, 1964.

[9] G. Berg, L. Lundgaard, M. Becidan and R. Sigrnond, "Instability of Electrically Stressed Water Droplets in Oil," in *Dielectric Liquids,* 2002.

[10] J. D. Sherwood, "Breakup of Liquid Droplets in Electric and Magnetic Fields," *J. Fluid Mech.,* vol. 188, pp. 133-146, 1988.

[11] A. Pedersen, E. Ildstad and A. Nysveen, "Forces and Movement of Water Droplets in Oil Caused by Applied Electric Field," in *Annual Report Conference on Electrical Insulation and Dielectric Phenomena,* 2004.

[12] F. Mauseth, S. Hvidsten and G. Birkenes, "Water Ingress in High-Voltage Cross-Linked Polyethylene (XLPE) Cable Terminations," *IEEE Electrical Insulation Magazine,* vol. 28, no. 5, 2012.

[13] F. Mauseth, S. Hvidsten and G. Birkenes, "Surface Degradation of XLPE Insulation at Oil-Water Interfaces," in *Electrical Insulation and Dielectric Phenomena,* 2011.

[14] M. Connecticut, "Town of Mansfield," [Online]. Available: https://www.mansfieldct.org/Schools/MMS/staff/hand/atomsheat_files/image004.jpg.

[15] M. H. P. Suwarno, "Effects of Water Content on Dielectric Properties of Mineral Transformer Oil," *International Journal of Electrical, Computer, Energetic, Electronic and Communication Engineering,* vol. 9, no. 10, 2015.

[16] J. P. Crine, R. Grob and J. G. H. Casanovas, “Influence of Water and Silanol Contents on Some Electrical Properties of Silicone Oil,” *IEEE Transactions on ELectrical Insulation,* Vols. EI-21, no. 2, 1986.

[17] K. B. Liland, K. Eidnes, K. Bjorneklett and S. Hvidsten, “Measurement of Solubility and Water Content of Insulating Oils for HV XLPE Cable Terminations,” in *Electrical Insulation*, 2008.

[18] T. Andritsch, *Epoxy Based Nanocomposities for High Voltage DC Applications. Synthesis, Dielectric Properties and Space Charge Dynamics.,* Delft: Delft University of Technology, 2010.

[19] Novocontrol, “Novocontrol Technologies,” [Online]. Available: http://www.novocontrol.de/.

[20] F. H. Kreuger, Industrial High Voltage - Volume II, Delft : Delft University Press, 1992.

[21] K. B. Liland, S. Hvidsten, G. Birkenes and F. Mauseth, “Development of a Simple Method for Condition Assessment of Oil Filled XLPE Terminations,” in *8th International Conference on Insulated Power Cables*, Paris-Versailles, 2011.

[22] PETROTECH, “PETROTECH Analytical Company,” [Online]. Available: http://en.petrotech.ru/en/equipment/Q/2/835/.

[23] CENELEC, *EN60270,* European Standard, 2001.

[24] P. H. F. Morshuis, Partial Discharge Mechanisms, Delft: Delft University Press, 1993.

Appendix

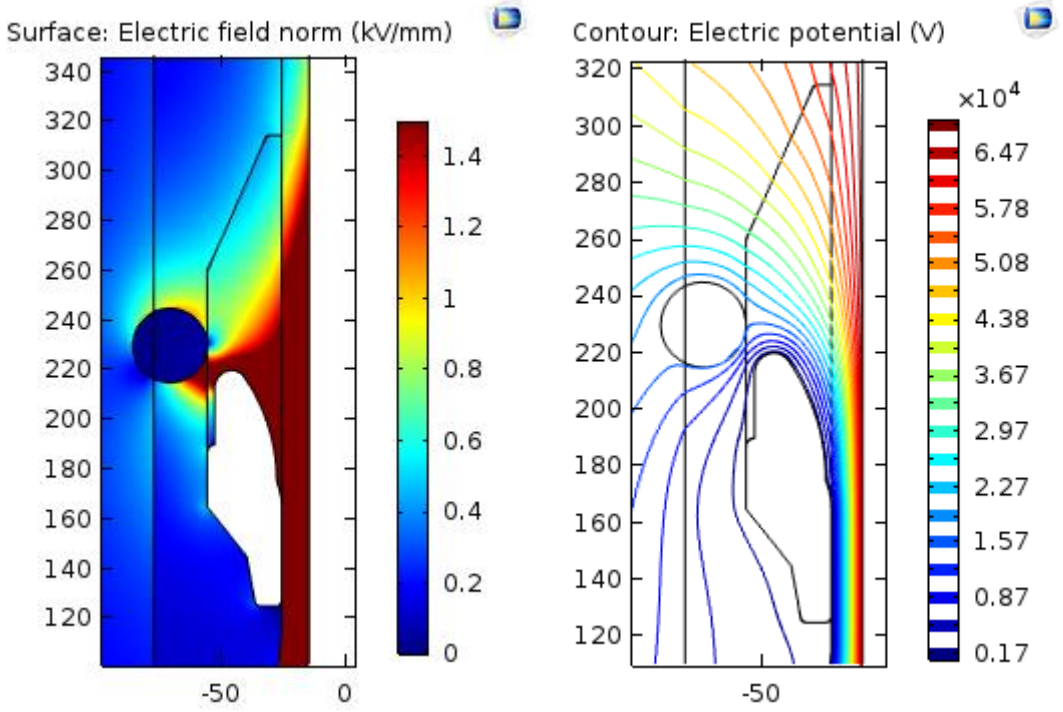

Fig. 119: 0.5 ml water droplet attached to stress cone

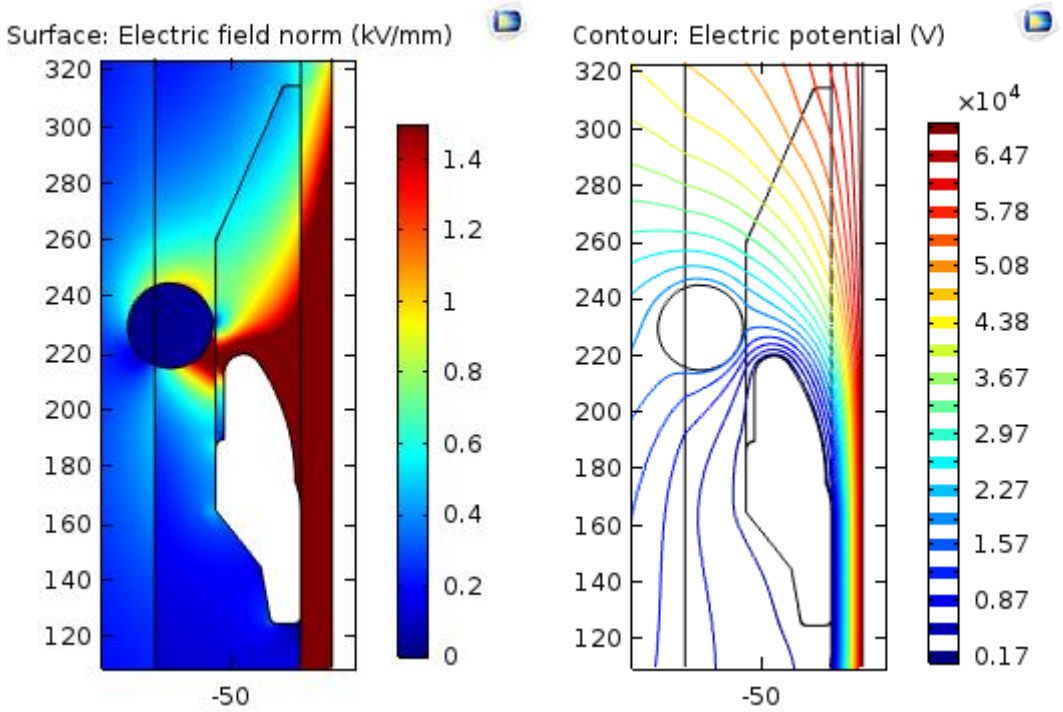

Fig. 120: 0.5 ml water droplet 1 mm from stress cone

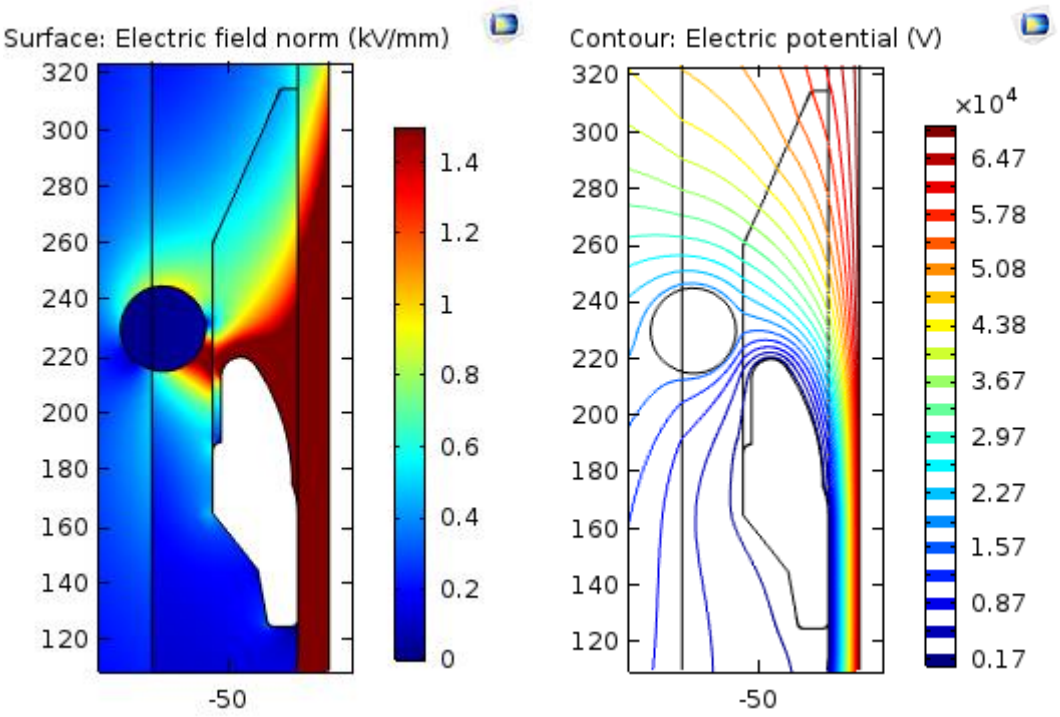

Fig. 121: 0.5 ml water droplet 2.5 mm from stress cone

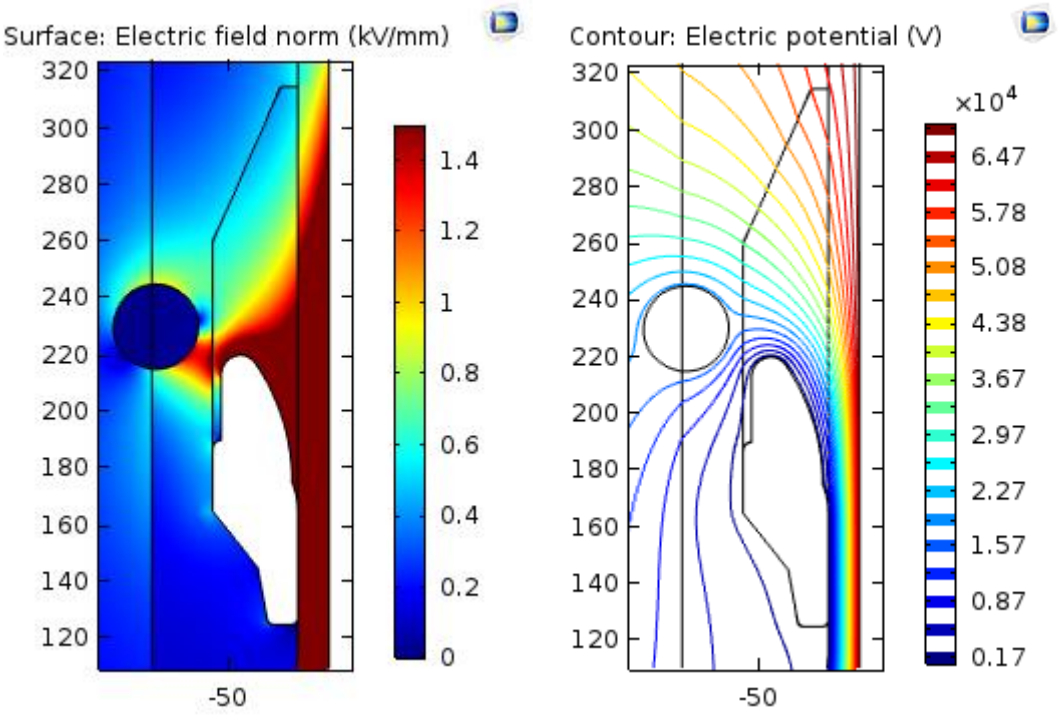

Fig. 122: 0.5 ml water droplet 5 mm from stress cone

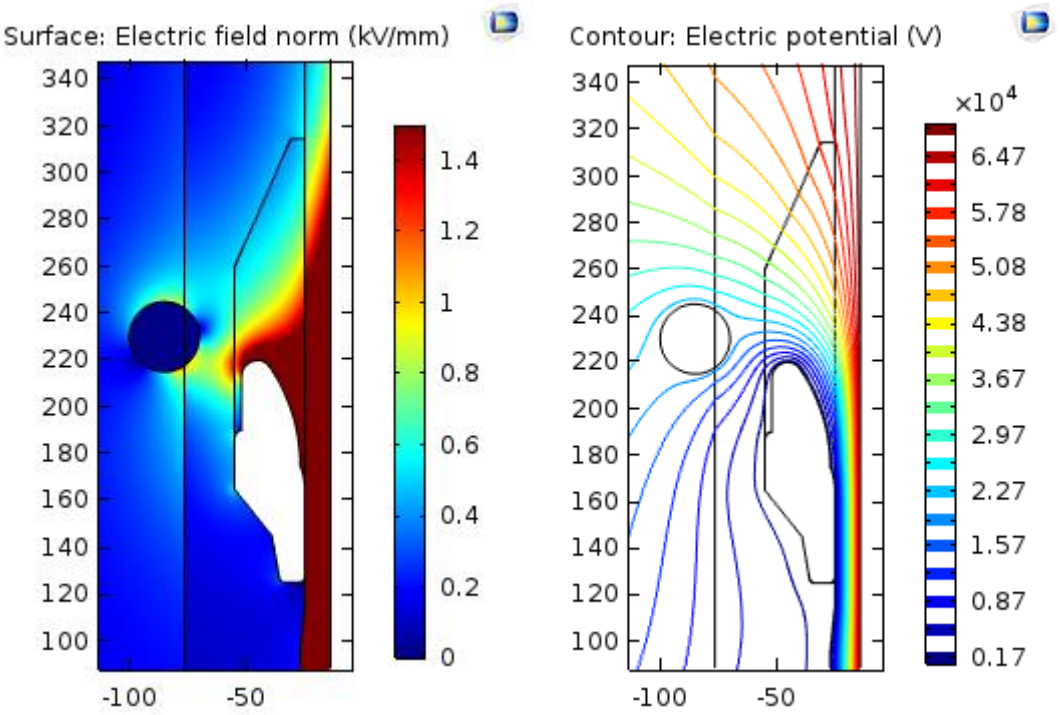

Fig. 123: 0.5 ml water droplet 15 mm from stress cone